personal buildup for

Force Motors Limited Library

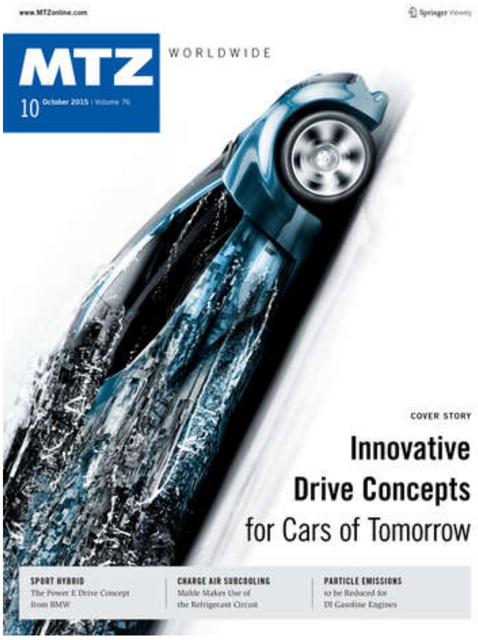

mtzw 10/2015, as epaper released on 31.08.2015
http://http:www.mtz-worldwide.com

content:

page 1: Cover. p.1

page 2: Contents. p.2

page 3: Editorial. p.3

page 4: Power_e_drive. p.4-9

page 10: LPG_Downsizing. p.10-15

page 16: eBooster_borg. p.16-21

page 22: Sechszylinder_BMW. p.22-29

page 30: BMEP. p.30-35

page 36: Ladeluftunterkuehlung. p.36-41

page 42: Imprint. p.42

page 43: Peer_review. p.43

page 44: Gleitlager_Koeffizienten. p.44-51

page 52: Partikelanzahl. p.52-57

www.MTZonline.com

Springer Vieweg

MTZ WORLDWIDE

10 October 2015 | Volume 76

COVER STORY

Innovative Drive Concepts for Cars of Tomorrow

SPORT HYBRID
The Power E Drive Concept from BMW

CHARGE AIR SUBCOOLING
Mahle Makes Use of the Refrigerant Circuit

PARTICLE EMISSIONS
to be Reduced for DI Gasoline Engines

CONTENTS

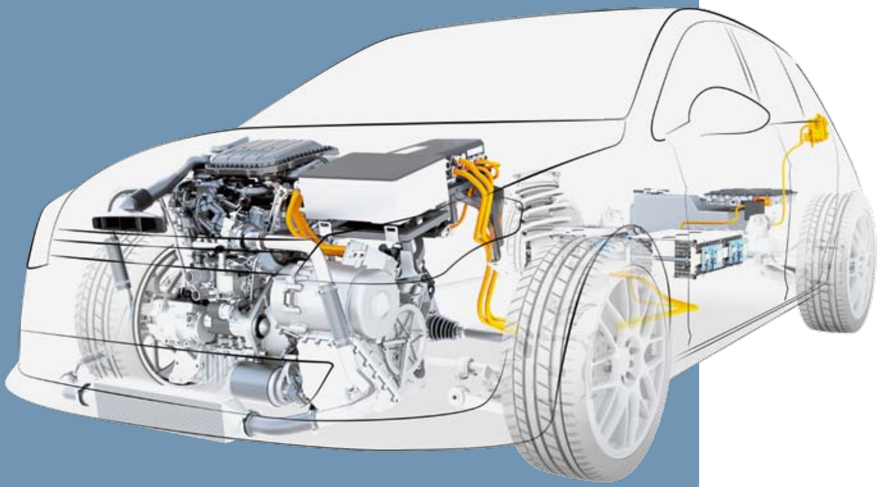

COVER STORY

Innovative Drive Concepts for Cars of Tomorrow

2020 has become synonymous with the biggest challenge facing the automotive industry. In order to comply with the CO_2 limit of only 95 g/km which will come into force then, a great deal of innovation is needed, in particular in relation to powertrains. There has never been such a wide variety of different concepts under consideration as there is today. Amongst others, electrification and engines designed for alternative fuels are certain to play an important role.

4 The BMW Power E Drive Concept's Drivetrain
Marcus Bollig, Nicolai Ardey, Martin Sautter [BMW]

10 LPG Fuel Direct Injection for Turbocharged Gasoline Engines
Javier Ariztegui, Jaime Gutierrez [Repsol], Alois Fürhapter, Hubert Friedl [AVL]

DEVELOPMENT

SUPERCHARGING
16 Application and Design of the Electrically Driven Compressor from BorgWarner
Hermann Breitbach, Dietmar Metz, Sascha Weiske, Gerd Spinner [BorgWarner]

GASOLINE ENGINES
22 The New BMW Inline Six-cylinder Gasoline Engine
Christian Landerl, Wolfgang Mattes, Markus Rülicke, Bodo Durst [BMW]

COMBUSTION
30 Development of a Natural Gas Combustion System for High Specific Power
Bertold Hüchtebrock, José Geiger, Harsh Sankhla [FEV], Avnish Dhongde [RWTH Aachen]

THERMAL MANAGEMENT
36 Refrigerant-based Charge Air Subcooling
René Dingelstadt, Peter Wieske, Andreas Eilemann, Jürgen Stehlig [Mahle]

RESEARCH

43 Peer Review

FRICTION
44 Modelling and Verification of Practice-relevant Journal-bearing Properties
Hardwig Blumenthal, Hubert Schwarze [TU Clausthal]

INJECTION SYSTEMS
52 Reduction in Particle Emissions with Gasoline Engines with Direct Injection
Helge Dageförde [Bosch], Markus Bertsch, Heiko Kubach, Thomas Koch [KIT]

RUBRICS I SERVICE

3 Editorial
42 Imprint, Scientific Advisory Board

The Moment of Truth

Dear Reader,

the Vienna Motor Symposium in May revealed the latest trends in engine and powertrain technologies. But the "moment of truth" will come at the International Motor Show (IAA) in Frankfurt from 17 to 27 September. When the manufacturers unveil their new models at the most prestigious motor show in the world, everyone will find out which powertrains and solutions have made it into volume production. And, most importantly, in which vehicle segments.

It has become clear in the run-up to the show that the pressure to reduce fleet fuel consumption is having an impact across brands, models and segments. Downsizing is no longer solely being applied to individual engines or vehicle classes. For example, at the launch of the latest Astra (generation K), Opel will be offering a choice of only three engines. Alongside the 1.0 l and 1.4 l gasoline engines, there is also a 1.6 l diesel. This covers all the necessary performance levels. Even Porsche will be supplying all its 911 models with turbochargers in future, with the exception of the GT3. And, please note, that's not just the top-of-the-range engine, but a standard feature. This means that the 3.4 and 3.8 l engines have been replaced with 2.7 and 3.0 l equivalents, which represents almost a paradigm shift in the sports car world.

With the premiere of the new A4, Audi is offering its 2.0 l four-cylinder gasoline engine for the first time with a more advanced form of the Miller cycle. Toyota opted for alternative valve timing in its first Prius model and is now presenting the fourth generation of the full hybrid. It is clear that OEMs and suppliers are focusing on developing innovative drive concepts, as we have highlighted on our cover story. Both volume production models and concept studies, such as the Power E Drive from BMW, demonstrate that there are many different ways of achieving what is required. Professor Küçükay's remarks on special hybrid powertrains are equally interesting. We are looking forward to finding out more in Frankfurt, as I'm sure you are too.

Dr. Alexander Heintzel
Editor in Chief

The BMW Power E Drive Concept's Drivetrain

BMW combines the vehicle dynamics of a high-performance electric drive with the road capability of an internal combustion engine in its Power E Drive concept vehicle. Depending on speed, load and the battery's state of charge, the operating strategy brings the three-cylinder engine into operation.

EXTENSION OF ELECTRIC DRIVING

Social and political demands worldwide require technological measures to reduce CO_2 and exhaust pollutant emissions for individual mobility within the next years. Compliance with these legal requirements can only be accomplished through the increased electrification of drivetrains. Crucial factors for the sustainable development and roll out of electrified powertrains are the suitability for daily use, competitive costs and the desirability of the electrified vehicles from the customers' point of view.

Driving range and fill-up/charging time are the biggest challenges facing electric drivetrains. At present, electric vehicles are already attractive offers in the urban environment. But costs and weight of the required batteries increase proportionally for large, luxurious cars and long-distance driving. Plug-in hybrid vehicles provide electric driving in urban areas already. Therefore, the key motivation for the development of the Power E Drive concept was the significantly extent of electric driving without compromises in daily use.

THE DRIVETRAIN CONCEPT

The objective of the Power E Drive concept, **FIGURE 1**, is to combine the advantages of electric motors regarding driving dynamics with the everyday-usability of internal combustion engine drivetrains. The goal is to maximise the electric driving experience far beyond the current scope of plug-in hybrid electric vehicles (PHEVs) and to increase suitability for long distance driving far beyond today's Battery Electric Vehicles (BEVs) – especially in large and heavy vehicles. In order to enhance the electric driving pleasure in comparison to a PHEV, a 200 kW electric motor is installed on the rear-axle as, for example, in BMW's rear-wheel driven BEV, the BMW i3.

To further improve electric acceleration and to realise a four-wheel drive function, another electric motor with 150 kW is used on the front-axle. In total, the electric system provides a torque of more than 700 Nm and offers maximum electric acceleration up to the traction limit.

The required electric power is provided by a high-voltage battery which is extended in size and power compared to PHEV applications. This T-shaped battery is lighter and cheaper in comparison to a BEV. It is integrated into the tunnel positioned beneath the rear bench seats, while still offering a high energy volume of 20 kWh.

Thereby average daily driven distances as well as high driving dynamics can be covered pure electrically. For long distance driving and an increase of driving

FIGURE 1 Drivetrain modes of the BMW Power E Drive concept (© BMW)

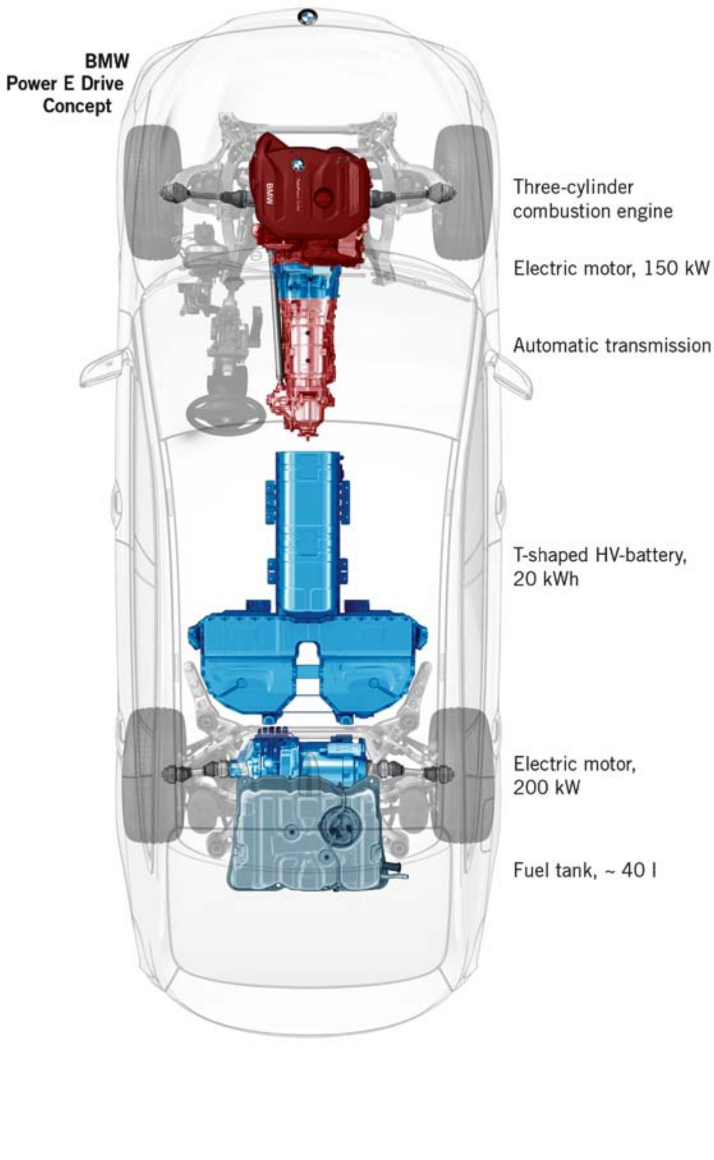

dynamics, the efficient turbocharged three-cylinder combustion engine of the BMW i8 with 170 kW is coupled with the front electric motor and the front-axle through a specially developed automatic transmission. This ensures a solid driving performance especially at high speeds even with a nearly discharged high-voltage battery or poor environmental conditions, **FIGURE 2**.

Also at low charging conditions of the battery, the vehicle provides the positive driving characteristics of a typical BEV. In this case the combustion engine covers the base load of the driving resistance and, in combination with the front electric motor, is used as a generator to provide electric energy. The generated energy is needed for battery charging and for acceleration with the electric motor positioned on the rear-axle.

The combustion engine develops power in the high speed range where the electric engine loses power and torque. Therefore the combustion drivetrain complements the positive characteristics of electric vehicles while offering high top speeds and reproducible dynamics at high speeds. These characteristics can be improved through a multi-shift transmission, **FIGURE 3**.

A tank with approximately 40 l combined with the intelligent operating system and a 20 kWh high-voltage battery together provide long-distance driving capabilities and a mostly electric driving experience. Additionally, the filling rate of gasoline of about 500 km/min tops the fastest 120 kW charging technologies of BEVs by a factor of 50.

Further development of Power E Drive is now focused on finding synergies with future PHEV and BEV drivetrains, for example through the use of standardised electric motors and transmissions. Another challenge is the cooling performance for the exhaust system and further improvements on acoustics of the combustion engine during recharge.

COHERENT INTEGRATION IN THE VEHICLE

The concept vehicle aims at four main objectives:
- validation of drivetrain integration and interaction of components in different operating modes under real driving conditions
- realisation of a measuring platform and testbed for various total vehicle subjects
- assessability of acoustical and vibration effects especially in regards to noise vibration harshness (NHV) of combustion engines
- portrayal of the subjective driving experience with focus on acceleration and operation strategy.

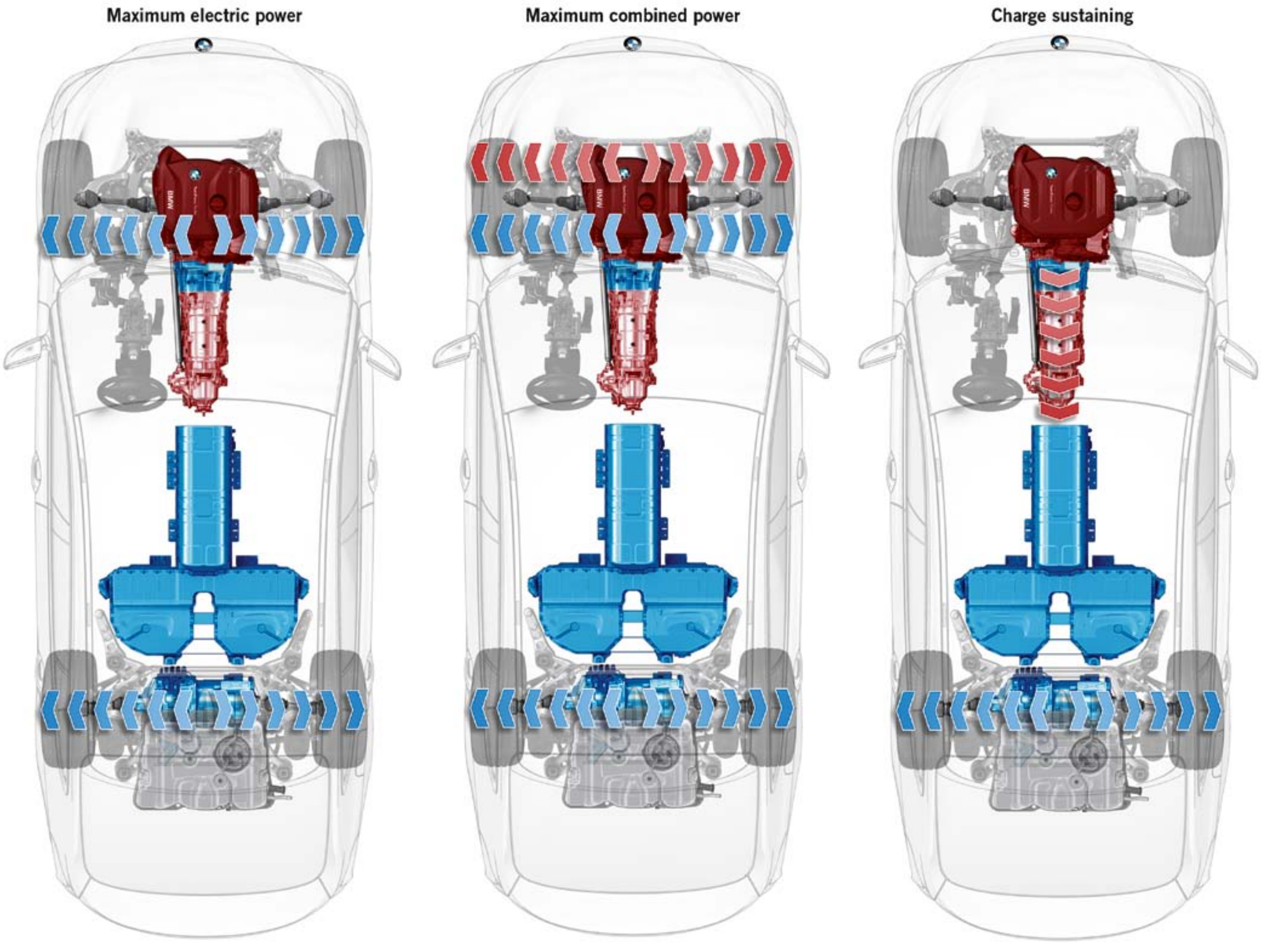

FIGURE 2 Driving modes of the BMW Power E Drive concept (© BMW)

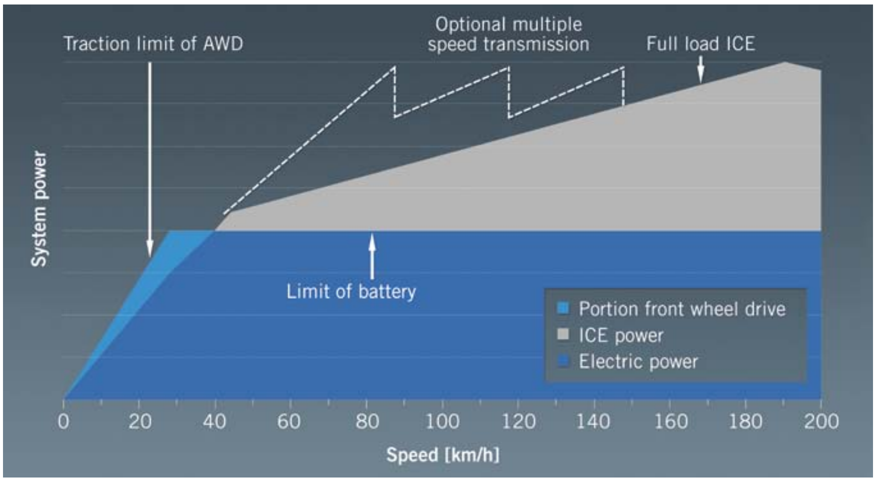

FIGURE 3 Schematic diagram of performance availability over the entire speed range (© BMW)

The BMW 5 Series GT was chosen as the basis vehicle due to its similarities to the target vehicle in regards to: vehicle segment, construction volume and weight, **FIGURE 4**. For the integration of all additional components, the underbody was modified. The rear-axles and the electric primary drivetrain were already designed for future vehicle generations, which is why the rear-end had to be changed geometrically. The high comfort, driving dynamics and acoustic characteristics of the double bedded elastic rear-axle had to be kept.

The tunnel was slightly widened and the underbody structure optimised to store the high-voltage battery. Therefore, modified seats had to be built in and interior panel, carpeting, centre console etc. had to be changed. Additionally, the quality acoustics is ensured through typical prototype insulation methods.

A special mounting solution for holding the electrified components was implemented in the front-end, which houses components exceptionally soft in a torque-roll layout. The combustion engine is supported by a pendulum bearing above and beneath the front-axle as well as through a strut brace.

Other challenges were the implementation of the electric motor, converter, combustion engine and prototype transmission as well as of the required periphery and cooling pipe systems. The high-voltage battery and electric motor both have to be cooled, therefore a large cooling surface was required. This target was achieved through a special front-end concept (analogue to the current V12 combustion engine), using outsourced radiators and a second cooling circuit.

The total vehicle weight was increased in comparison to the target production vehicle due to the prototypical vehicle construction and extensive measuring equipment. The realisation of longitudinal dynamics was ensured through compensation methods like a higher output power of the drivetrain.

The tight schedule was only realisable due to a complete pre-implementation and application of the total drivetrain on a specially designed hardware in the loop (HIL) testbed. The concept phase and setup of the vehicle including the design and production of components of the powertrain were achieved in approximately nine months.

The concept vehicle was able to confirm the expected longitudinal dynamics and the added customer value of the drivetrain. Furthermore the vehicle delivered valuable findings and measuring data for later concept developments.

Parallel to the setup and testing of the prototype vehicle results were analysed for a potential series implementation. In series production, a significant weight reduction is achievable. The experiences with the prototype vehicle proved that combining eight-cylinder driving performance with unseen fuel efficiency is possible.

OPERATION STRATEGY IS THE KEY FOR INTEGRATION

The objective of the operating strategy is to guarantee a sovereign and consistent vehicle behaviour during the entire speed range at all charge conditions of the high-voltage battery, also known as state of charge (SOC). Criteria for an optimisation of the operating strategy are: dynamics and efficiency, driving acoustics, driving stability and electric driving experience.

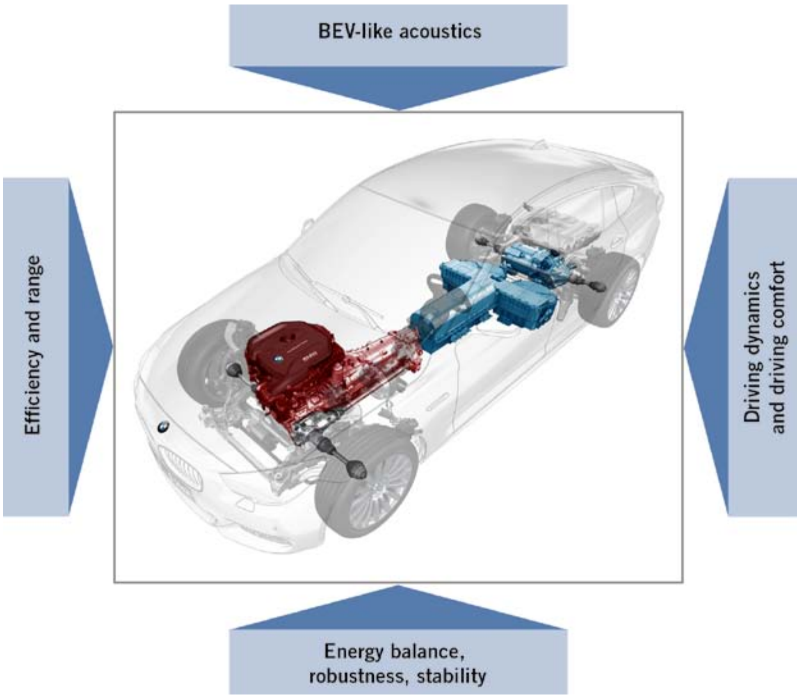

FIGURE 4 Challenges during the vehicle integration (© BMW)

Most challenging for the Power E Drive concept was to represent a driving experience for the customer that is close to the acoustics of a pure electric car while keeping the robustness and range of current combustion-driven vehicles.

The best possible solution for this conflict of interests is an operation of the combustion engine dependent on speed, load and SOC of the traction battery. The ratio of purely electric driving in "predominant BEV mode" reaches almost 100 % of the entire driving distance, **FIGURE 5**.

During the main part of operation, the customer experiences the Power E Drive concept – different to today's plug-in hybrid vehicles – as a pure electric car. The start of the combustion engine only happens at high speeds, very high accelerator pedal position or low SOC.

To solve the conflict of objectives between acoustics, energy balance and efficiency, the combustion engine covers the needed output power to overcome driving resistance at high speeds through an efficient mechanic overdrive gear. This is not noticeable acoustically due to fixed operation and stronger wind noises at high speed.

The energy saved in a traction battery is refrained for later use at lower speeds. If the state of charge is very low, the battery is charged through the combustion engine by increasing its load point and managing a neutral SOC. An acoustically noticeable combustion engine is wanted at full-load to highlight the sporty characteristics of the vehicle.

The described operating strategy can be individually customised:
- MAX EDRIVE prioritises electric driving at all states.
- BATTERY CONTROL holds the SOC of the high-voltage battery or prioritises the charging of the high-voltage battery through load point shifting of the combustion engine.
- SPORT fulfils maximum performance through additional torque of the combustion engine from the front-axle and the electric motor to the rear-axle.

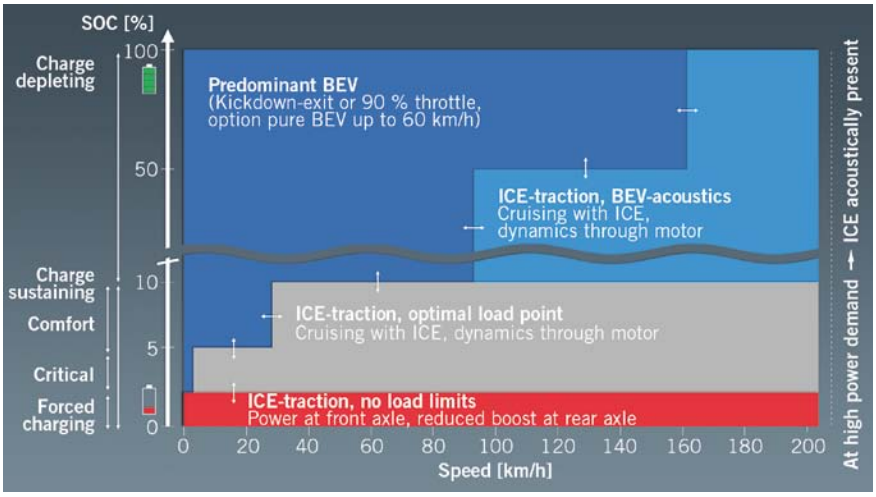

FIGURE 5 Operating strategy for balance of total vehicle characteristics (© BMW)

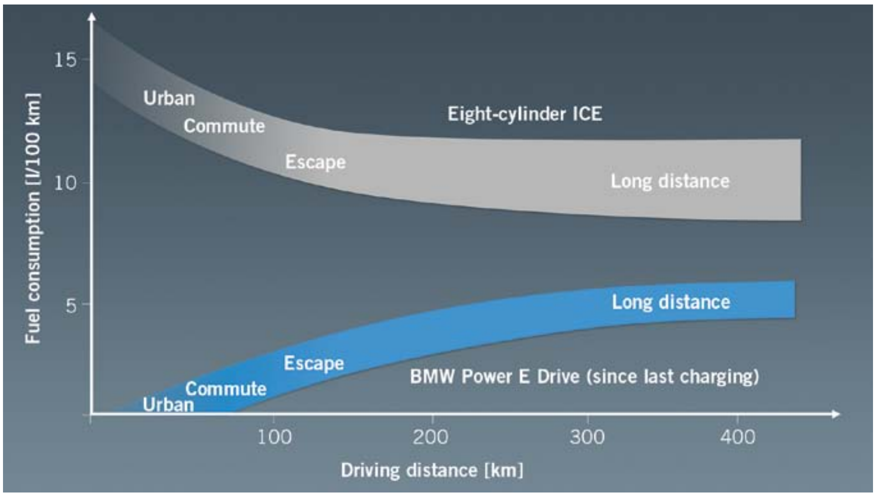

FIGURE 6 Gasoline consumption by customer profile (© BMW)

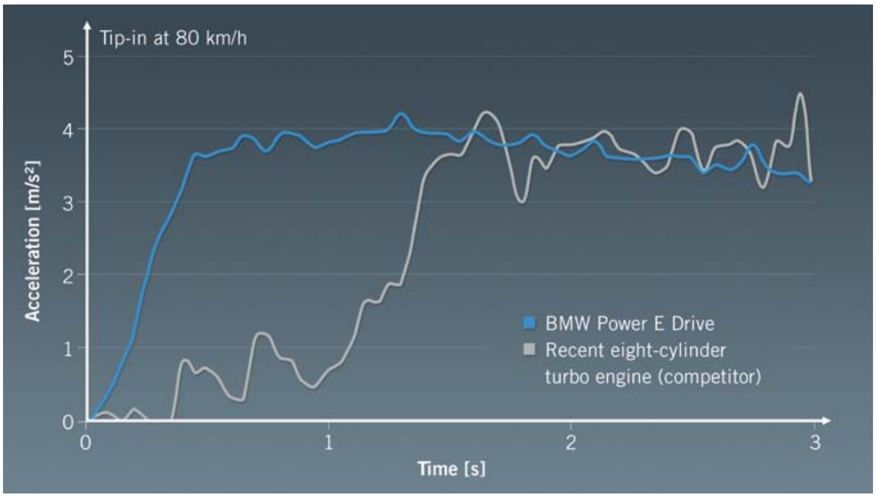

FIGURE 7 The acceleration performance compared to an eight-cylinder turbocharged engine (© BMW)

DRIVING PERFORMANCE AND FUEL EFFICIENCY

The high-voltage battery of the Power E Drive concept was designed to cover the main part of daily driving ranges of BMW customers purely electrically. The vehicle reaches an average range of 80 km in customer use. A normal average daily journey of a BMW customer has a worldwide average of only about 60 km. This average consists mostly of short-distance drives of less than 50 km and only a few long-distance journeys of more than 100 km. This typical distribution leads to a perception of a pure electric vehicle use in everyday driving, independent of customer characteristics (urban, commuter, long-distance driver). Urban customers will reach an electric driving ratio of 90 %.

The high ratio of electric driving provides a compellingly low fuel consumption, **FIGURE 6**. Customers with an urban driving profile are able to drive the Power E Drive with almost 0 l/100 km on an annual average. Commuters would have a maximum of 3 l/100 km. At long distance driving of more than 100 km, the efficient three-cylinder combustion engine works close to its optimal operation point. So even very long-distance drives can be driven with less than 5 to 6 l/100 km of fuel consumption.

The subjective and perceptible dynamics of the Power E Drive vehicle are a unique selling point. The combination of the powerful electric motor with high torque and the turbocharged three-cylinder engine offer a driving experience that has been unknown until today. With a tip-in at average speeds, the maximum acceleration is reached within milliseconds. Only a few moments later the combustion engine achieves its maximum torque. It only takes 2 s until the Power E Drive vehicle beats a conventional driven turbocharged V8 vehicle by the length of one car, **FIGURE 7**. This acceleration is followed by the continuous development of power delivery of the combustion engine at increasing speeds – which is provided constantly in comparison to a pure electric drivetrain. Therefore, the Power E Drive concept offers sports car performance even at high speed.

CONCLUSION

The Power E Drive concept car has proved that an almost complete electrification of everyday driving is possible without loss in usability. Efficiency and driving dynamics can be combined in one vehicle. Therefore, BMW believes that the Power E Drive concept vehicle will replace current plug-in hybrids in the long run. Pure electric cars will be established especially in urban use within the next decades. However, the Power E Drive concept is the ideal offer for ambitious customers of premium segments in middle-sized to luxury class cars. These customers typically do not like to accept compromises on their frequent long-distance journeys.

LPG Fuel Direct Injection for Turbocharged Gasoline Engines

Repsol and AVL have carried out tests on a turbocharged direct-injection 1.4-l gasoline engine that was converted from gasoline fuel to monovalent LPG operation. As the test showed, this fuel is suitable not only for meeting the required CO_2 targets but also for complying with the forthcoming RDE legislation in a simple way with conventional exhaust aftertreatment technology. A 15 % reduction in fuel consumption, related to the NEDC, was measured in the vehicle.

AUTHORS

Dr.-Ing. Javier Ariztegui
is Senior Technologist at the Technical Centre of Repsol S.A. in Mostoles (Spain).

Jaime Gutierrez, M. Sc.
is Technical Director in Energy for Transportation at the Technical Centre of Repsol S.A. in Mostoles (Spain).

Dipl.-Ing. Alois Fürhapter
is Lead Engineer in the Department Development Gasoline Engines at the AVL List GmbH in Graz (Austria).

Dr.-Ing. Hubert Friedl
is Product Manager for Business Unit Gasoline Engines at the AVL List GmbH in Graz (Austria).

ADVANTAGES WITH DIRECT INJECTION

Forthcoming legislation is increasing pressure to reduce CO_2 as well as emissions for WLTP (World Harmonized Light Duty Vehicle Test Procedure) and for RDE (Real Driving Emissions) [1]. Liquified Petroleum Gas (LPG), commercially known as Autogas offers a vast potential to reduce CO_2 emission and to meet Euro 6c PN (particle number) limits for gasoline engines.

The scope of this article describes the technical solution and the results of an Autogas direct injection (LPG-di) application in a compact class passenger car. Within this LPG monofuel prototype development, the ambitious targets for CO_2 and PN emission reduction have been achieved without changing the base engine geometry. Using engine geometry modifications and the higher octane rating of the fuel, LPG would even offer additional efficiency potential.

LPG is an alternative fuel recognised as such by the European Union prepared from a mixture of propane and butane (hydrocarbons with three and four carbon atoms) and substantially different to either compressed natural gas (CNG), cryogenic liquefied natural gas (LNG) or compressed biogas (CBG), which mainly contain methane (a hydrocarbon with one carbon atom). A distinctive characteristic of LPG is that under moderate pressures (typically 300 to 1000 kPa depending on composition) and at ambient temperature, it is a liquid with similar properties to gasoline. Thus the fuel may be stored in liquid phase in the vehicle tank, enabling a range similar to that of gasoline. Even more importantly, Autogas in liquid phase may be used in modern direct injection gasoline engines with a similar injection hardware as that used for gasoline. With the injection settings adjusted to the properties of the fuel, the engine may operate normally. In addition, the engine may be started directly with Autogas since this system does not require a prior vaporisation of the fuel.

AVAILABILITY OF LPG

When analysing the availability of LPG, several production routes should be considered. Worldwide, there are three main sources of LPG:
- oil refining processes
- LPG associated with crude oil production
- LPG produced in natural gas wells together with methane (accounting for up to 7 % of production).

FIGURE 1 shows the historical production of these routes [2]. It should be noted that alternative routes to oil refining accounted for 61 % of the total production in 2013.

Looking ahead to the potential to provide an extra LPG for automotive use in the future, four main sources arise:
- declining residential and commercial demand of LPG in Europe
- natural gas wells
- production of hydrotreated vegetable oil (HVO)
- conventional refining processes.

According to **FIGURE 1**, production of LPG from natural gas wells has experienced a

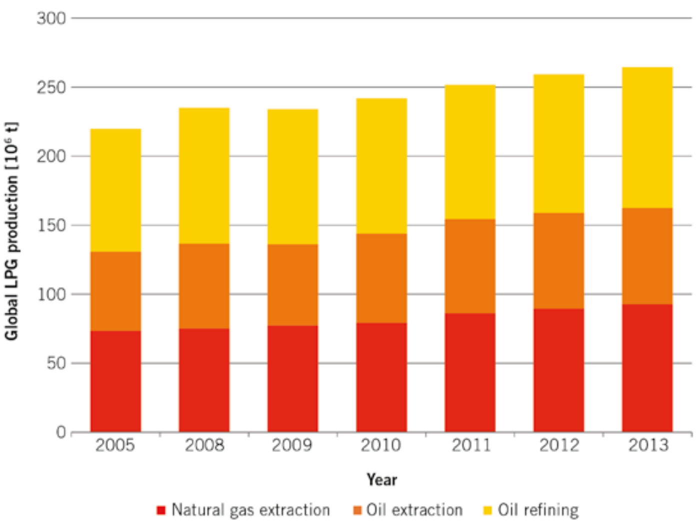

FIGURE 1 Historical evolution of worldwide LPG production (© Repsol)

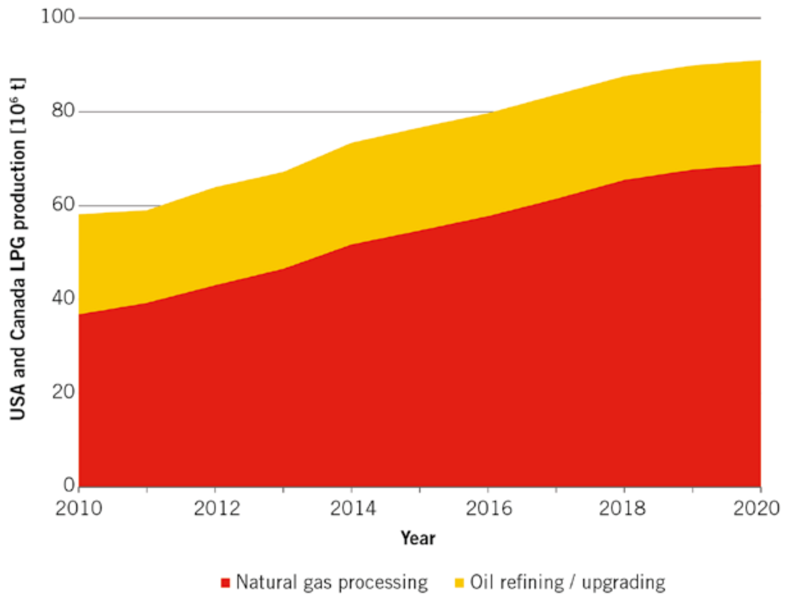

FIGURE 2 Prognosis of USA and Canada LPG production in horizon 2020 (© Repsol)

vigorous growth since 2010. This trend is expected to continue in the future caused by the shale gas expansion in North America, as **FIGURE 2** shows [3]. According to the latest estimates, USA and Canada will increase LPG production by 30 × 10^6 t/year in the period from 2010 to 2020 due to additional natural gas processing. This extra production alone represents 11 % of the total European (EU-27) fuel demand for automotive use (light-duty and heavy-duty) in 2015.

HVO is a biofuel produced by hydrogenation of the molecules contained in oils. Its production has experienced an uptake in last years with industrial plants growing around the world. During the hydrogenation process, approximately 5 % of the oil mass processed ends up as propane, creating a bio-LPG.

SUPPLY INFRASTRUCTURE

Autogas is the more widespread alternative fuel in Europe. However, the supply grid for the final user is very asymmetrical with some countries with thousands of dispensing points and others with just some dozens [4]. Despite these exceptions, in general, there exists a minimum infrastructure to support the initial phase of a potential massive use of Autogas.

As may be seen in **FIGURE 3**, Autogas dispensing units coexist with the rest of the fuels in the same rack at the service station. The dispensing nozzle has a design similar to that of conventional fuels. Also, the supply process takes

FIGURE 3 Service station with Autogas dispenser (© Repsol)

a similar time to that of conventional fuels. These characteristics guarantee a seamless introduction of Autogas for the final user.

Even more important is the possibility of a future growth of the grid. The addition of Autogas to conventional service stations does not require massive investments, with total costs below 100,000 Euro and a standardised hardware.

OBJECTIVES FOR THE PROTOTYPE DEVELOPMENT

As a base for the prototype development, a standard VW Golf 7 with 1.4-l TSI gasoline engine (EA211, maximum power 103 kW and maximum torque 250 Nm) with a six-speed manual transmission was chosen. The targets for the Autogas development were:

- same performance, same transient response as base vehicle
- Euro 6 emissions (including particles for Euro 6 c) in NEDC
- efficiency optimisation for Autogas operation
- demonstration of CO_2 benefit compared to base vehicle.

Before the start of the development, the vehicle was carefully investigated to have an accurate assessment of base engine and vehicle performance for later comparison.

The modifications of the fuel system were accomplished with relative little effort and cost. For the fuel storage and supply system commercially available components were used. The fuel lines and high pressure (HP) pump were carried over from the base vehicle configuration. Only the direct injection injectors (provided by Delphi) were changed to approximately 30 % higher flow rate to compensate the lower density of Autogas.

The engine control was completely transferred into a rapid prototyping engine management system (RPEMS). This RPEMS allowed full control for optimisation of engine maps as well as recalibration of vehicle operation with Autogas. The base mapping data from the original gasoline EMS was acquired by screening tests on a chassis dynamometer.

For engine and vehicle testing during development, a defined LPG formulation with approximately 50 vol. % propane, 25 vol. % isobutane and 25 vol. % n-butane was chosen. This fuel formulation (in accordance to European Specification EN 589) reflected a central point of the European specification.

RESULTS FROM STEADY-STATE ENGINE OPERATION

The favourable mixing behaviour of Autogas allows a calibration of the engine for best efficiency without being compromised by soot and particles. Due to the better combustion stability, higher internal residual gas contents can be applied by optimised cam-timing in part load operation. This way, up to 5 % better engine efficiency may be reached with Autogas settings.

Particle emissions with Autogas are orders of magnitude lower compared to gasoline operation, **FIGURE 4**, despite the base gasoline application representing an already Euro 6 optimised status with up to three injections per cycle. With Autogas direct injection a particle filter will not be necessary for future emission legislations such as RDE. In fact, as **FIGURE 5** shows, the reduction in PN emissions is equivalent to the efficiency required for a particle filter.

Due to the higher octane rating of Autogas compared to gasoline, full load operation advantages may be gained. Autogas direct injection provided the same full load performance with stoichiometric mixture and a significantly reduced knock limitation, which additionally delivered substantial fuel consumption and CO_2 reductions in this condition.

RESULTS FROM TRANSIENT ENGINE OPERATION

Essential for Euro 6 compliance is an emission-optimised engine cold start and an efficient catalyst heating phase to reach a fast catalyst light-off. With Auto-

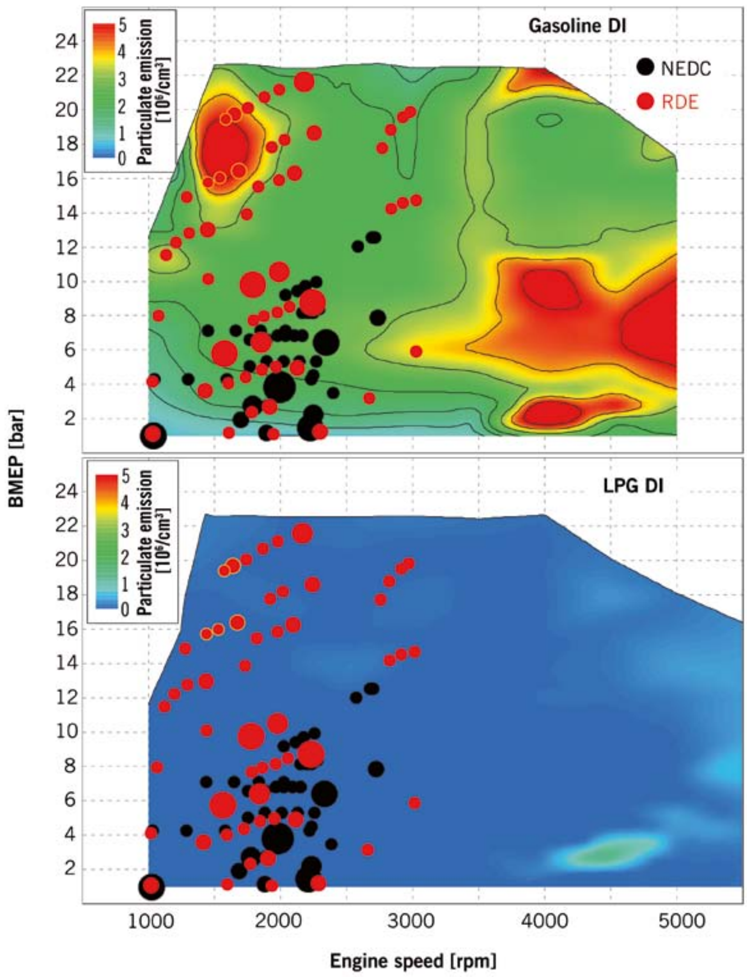

FIGURE 4 Comparison of PN emission maps for gasoline and Autogas (© AVL)

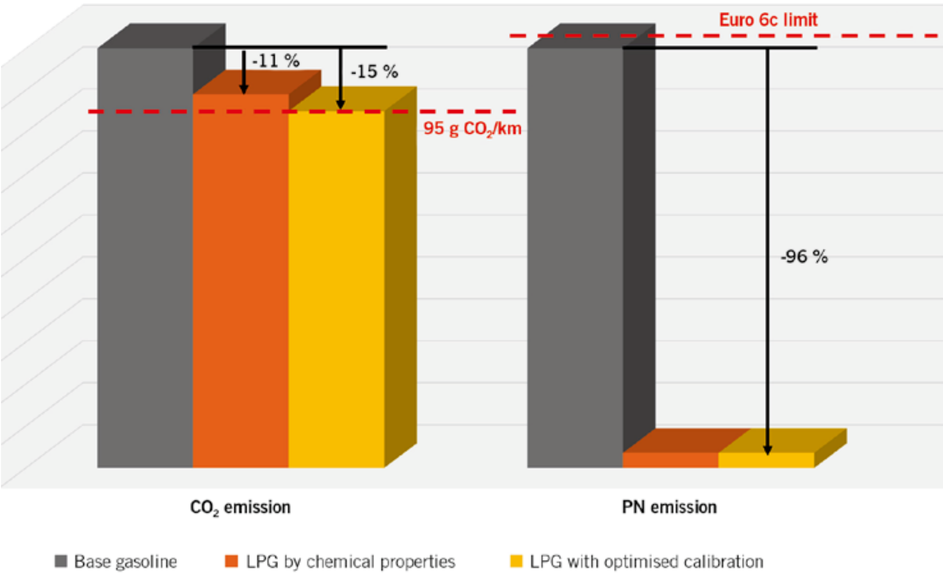

FIGURE 5 Advantages of Autogas versus gasoline fuel for CO_2 and PN emissions in NEDC (© AVL)

gas, cold start and catalyst heating calibration is significantly easier compared to gasoline operation and thus more robust. A full catalyst heating calibration was developed for Autogas and emissions as well as combustion stability proved to be better compared to gasoline.

FUEL ECONOMY EVALUATION FOR NEDC

After refinement of vehicle driveability and emission calibration, the vehicle was tested on the chassis dyno. The positive impact from Autogas, was finally proved and a 15 % CO_2 reduction compared to gasoline operation was achieved at full Euro 6c compliant emissions in a cold NEDC test. As **FIGURE 5** shows, this improvement can be attributed to the fuel chemical properties (11 %) and to the enhanced Autogas combustion calibration (4 %). The test procedure was performed with fixed shifting points of the manual gearbox and without start/stop system. A further reduction of the absolute CO_2 level down to 95 g CO_2/km (EU 2020 target) was predicted by simulation utilising the additional benefits from cylinder deactivation, start/stop (base vehicle configuration) and a double clutch gearbox for free shifting points, without cost-intensive hybridisation.

CHALLENGES FOR VEHICLE APPLICATION

For stabilised operation conditions on the engine test bed no significant difficulties related to Autogas were experienced. However some challenges arose in vehicle application due to the specific physical properties of LPG.

CHALLENGES – INJECTION CONTROL

Autogas has a significantly greater density variation by pressure and temperature than gasoline. Especially the liquid-gas phase transition is in the typical temperature range of a warm engine, thus great density changes were expected. To cope with this, the standard gasoline injection pre-control functionality was extended by a temperature correction model which compensates the density differences in case of fuel cut-in after fuel cut-off and for hot start.

CHALLENGES – HOT START

Due to the high volatility of Autogas, restart after a hot soak proved to be challenging. "Vapour lock" in the high pressure pump prevented fuel to be delivered to the HP rail. A logical solution is to purge the high pressure chamber of the pump with cold, liquid fuel from the tank. For this purpose, a modified HP pump with a separate purging valve would be a solution.

CONCLUSIONS

The use of Autogas in direct injection engines demonstrates potential advantages as an automotive fuel:
– availability of LPG resources
– established refilling infrastructure and moderate cost for new points
– beneficial combustion parameters with respect to cold start as well as full load
– substantial CO_2 reductions due to chemical properties and favourable engine settings
– close to zero PN emission, in line with gaseous fuels.

These advantages were demonstrated by means of a prototype compact class car with a 1.4-l turbo direct injection engine running on Autogas with monofuel operation.

A final CO_2 improvement of 15 % was achieved in NEDC with the demonstrator car, with 11 % coming from the fuel chemistry and a further 4 % gained from enhanced calibration. Autogas allowed stoichiometric operation within the complete engine map, which in turn provided substantial fuel consumption and CO_2 reductions in full load operation.

Due to excellent combustion performance and very low PN emission, Autogas offers an extremely attractive solution to meet forthcoming RDE regulations with conventional three-way catalyst technology at very moderate costs.

REFERENCES

[1] Fraidl, G.; Kapus, P.; Schöggl, P.; Krapf, S.; Vidmar, K.; Wanker, R.; Weissbäck, M.: RDE – Challenges and Solutions. 36th International Vienna Engine Symposium, 2015
[2] European LPG Association: Autogas in Europe, the Sustainable Alternative. In: An LPG Industry Roadmap, Edition 2013
[3] Hart, W. (IHS): Mind the Gap. 27th World LP Gas Forum & 29th AIGLP Congress, Miami, 2014
[4] World LPG Association & Argus Consulting Services: Statistical review of Global LP Gas 2014

Leading Aluminum.
Leading the Way.

UACJ, established by the integration of Furukawa-Sky Aluminum Corp. and Sumitomo Light Metal Industries Ltd., is the largest manufacturer of rolled aluminum products in Japan.

66th IAA Cars
Hall: 4.0
Stand: B12

Automobile Technology

UACJ Corporation

Tokyo Sankei Bldg., Otemachi 1-7-2, Chiyoda-ku, Tokyo, 100-0004 Japan
Telephone: +81-3-6202-2667, Telefax: +81-3-6202-2032
www.uacj.co.jp/english/ IAA-info@uacj-groupweb.jp

Application and Design of the Electrically Driven Compressor from BorgWarner

With an electrically assisted compressor, the eBooster, BorgWarner supplements conventional turbocharging concepts improving boost pressure and transient engine behaviour for low engine speeds. This will both provide engine power increase, as well as a fuel consumption advantage due to the lower back pressure at high load and less need for fuel enrichment at full load.

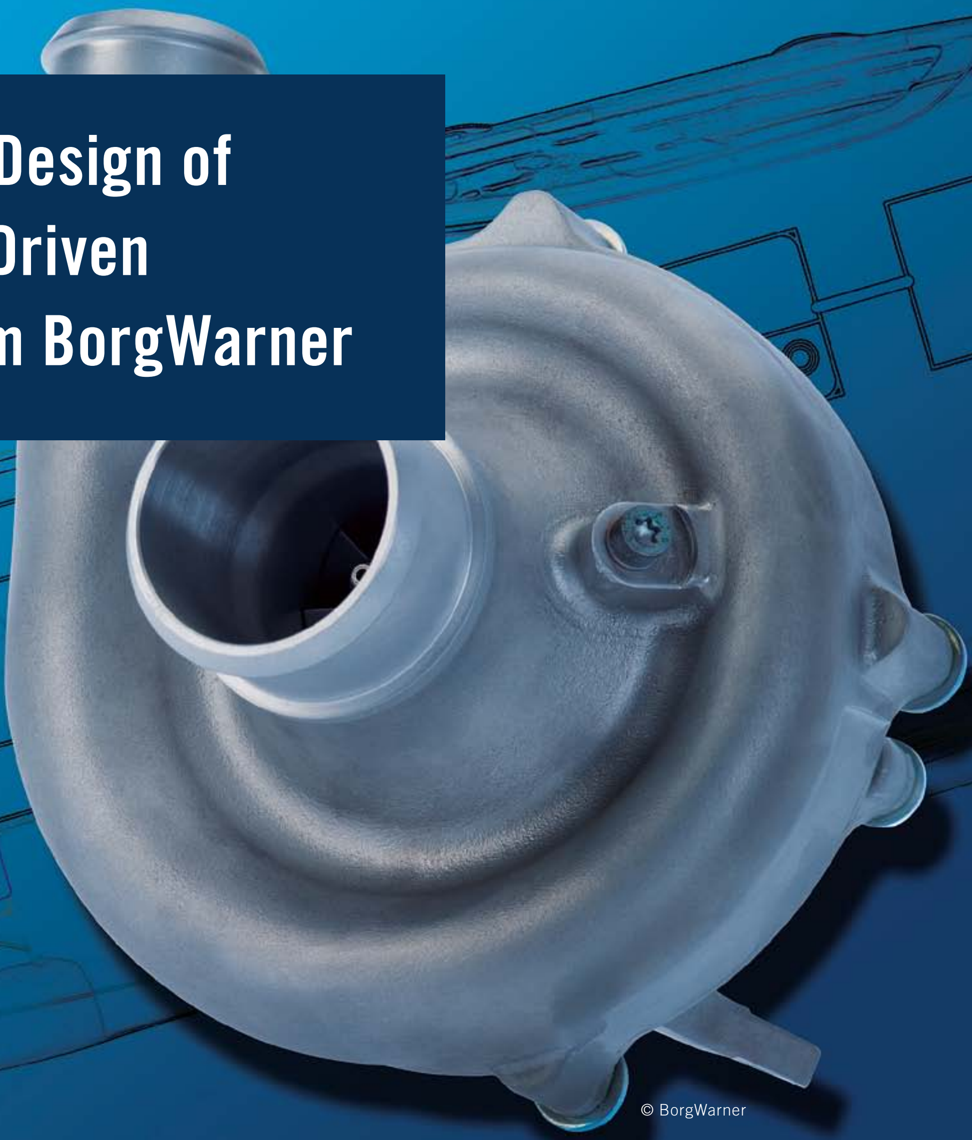

ELECTRICALLY ASSISTED BOOSTING BECOMES ATTRACTIVE

Since the 1960's, serial production turbochargers for automotive applications were developed, first for gasoline engines, later very successfully for diesel engines. Significant increase in torque and power were key enablers for engine downsizing and down-speeding. With that, turbo response became an increasing challenge. Besides continuous improvement of turbochargers, several new concepts were evaluated, like combining turbocharger and mechanical compressor, using multiple turbochargers in parallel or serial configuration or using electrically assisted turbochargers [1].

Electrically assisted boosting systems have repeatedly been investigated, starting in the 1990's. At 12 V, with state-of-the-art power electronics and microprocessors at the time, boost assist power around 2 kW was realised [2]. With the inertia of turbine, compressor and available electro motor technology, drive power of electrically assisted turbocharges in transient operation was almost used up to accelerate the rotating assembly, before significant boost pressure was generated. At the same time, the available electrical power and energy from the vehicle system was significantly lower than it is today.

With increasing vehicle electrification, significant progress in power electronic parts, compact electric motors and microprocessors for motor control, power levels of 2.5 kW at 12 V and 5 kW at 48 V seem feasible, and electrically assisted boosting becomes attractive again. Especially electrically driven compressors look promising because without turbine, rotor inertia can be kept low [3].

BENEFITS OF AN ELECTRICALLY DRIVEN COMPRESSOR FOR A COMBUSTION ENGINE

BorgWarner developed an electrically assisted compressor, the eBooster, to improve boost pressure and transient engine behaviour for low engine speeds without impact on the engine gas exchange, since without additional turbine, there is no backpressure increase. This is a significant advantage, especially with gas engines susceptible to engine knock. The independence of the eBooster from exhaust gas allows more flexible packaging, leaves, as compared to multistage turbochargers, more exhaust heat for the after treatment system, and causes less heat flux into the engine compartment.

The preferred position for the eBooster is downstream from the turbo compressor. Due to the lower boost pressure ratio, the power consumption is lower as well as the required compressor map width. Thus, electrical boosting can be extended over a larger engine speed range. Positioning upstream of the turbo compressor would effectively lower the usable turbo compressor map width, since the higher air density would shift the compressor operating point towards the surge limit.

The eBooster can improve transient behaviour, maintaining engine output with conventional turbo matching. Alternatively, transient response can be kept constant, and a larger turbine with lower back pressure can be used. This will both provide engine power increase, as well as a fuel consumption advantage due to the lower back pressure at high load and less need for fuel enrichment at full load.

The following analysis shows the potential of a 12-V eBooster with 2 kW power on a diesel engine, with focus on emission cycle operating range [3]. Basis is a 2.0-l engine with single stage variable turbine geometry turbo (VTG). Compared are two equal power 1.6-l engines, one with VTG turbo combined with eBooster and one with a regulated two stage system (R2S), **TABLE 1**.

The turbocharger matching has been optimised for every case, **FIGURE 1**. The

		2.0-l	1.6-l
Rated power (at 4000 rpm)	[kW]	128	
Specific power (at 4000 rpm)	[kW/l]	64	80
Rated power (at 1750 rpm)	[Nm]	360	
Specific torque (at 1750 rpm)	[Nm/l]	180	225
Max. brake mean effective pressure	[bar]	23	28

TABLE 1 Comparison of engine concepts (© BorgWarner)

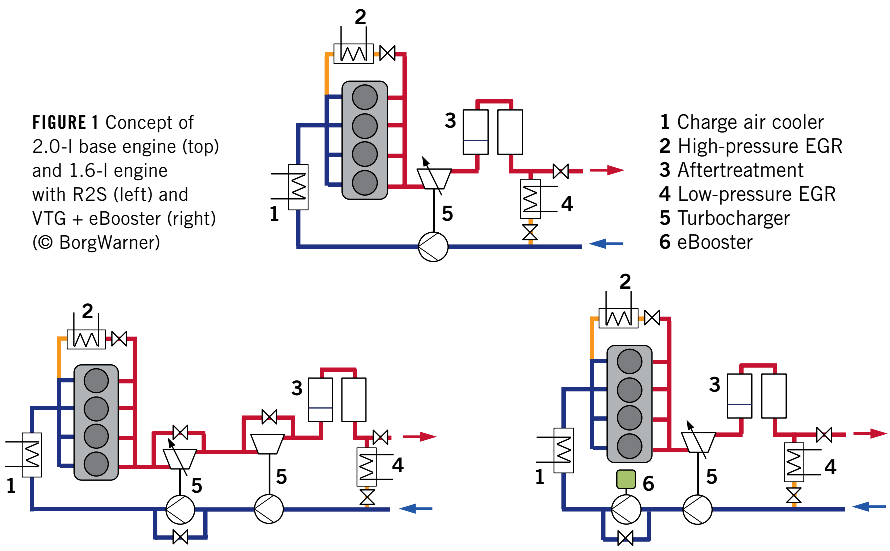

FIGURE 1 Concept of 2.0-l base engine (top) and 1.6-l engine with R2S (left) and VTG + eBooster (right) (© BorgWarner)

1 Charge air cooler
2 High-pressure EGR
3 Aftertreatment
4 Low-pressure EGR
5 Turbocharger
6 eBooster

AUTHORS

Dr. Hermann Breitbach is Director Development Turbocharger Passenger Car at the BorgWarner Turbo Systems GmbH in Kirchheimbolanden (Germany).

Dietmar Metz is Program Director eBooster at the BorgWarner Turbo Systems GmbH in Kirchheimbolanden (Germany).

Dr. Sascha Weiske works in Advanced Development Thermodynamics at the BorgWarner Turbo Systems GmbH in Kirchheimbolanden (Germany).

Gerd Spinner works in Advanced Development at the BorgWarner Turbo Systems GmbH in Kirchheimbolanden (Germany).

eBooster (6) with bypass valve is positioned behind VTG compressor (5), but before charge air cooler (1). The high pressure stage of the R2S turbo is a VTG turbine (5).

The 1.6-l engine with VTG without eBooster operation shows a significant gap in torque, **FIGURE 2** (top), since the turbocharger was adapted for higher boost pressure at full load to achieve power targets. Thus, in part load, the surge margin is limiting torque earlier. The eBooster allows compensating the torque gap, the electrical power required in the respective speed points is indicated in **FIGURE 2** (top).

FIGURE 2 (bottom) shows the increase in engine power at 1400 rpm versus the electrical power of the eBooster. An amplification factor of around seven to ten can be achieved through the increased amount of air for the combustion process. With increased air mass flow, turbine power will go up, thus, the VTG vanes can be opened further, the turbine efficiency will go up, and the air exchange losses will decrease, so overall, a better fuel efficiency will be achieved.

The R2S system also meets torque targets. However, the high pressure stage does take around a factor two more energy from the exhaust gas flow as the eBooster is consuming electrically, **FIGURE 3** (top). In case the electrical energy is coming from recuperation, the overall energy balance is advantageous for the eBooster, otherwise for the R2S system.

The transient response of the concepts was evaluated for load steps at 1500 rpm, **FIGURE 3** (bottom). The VTG remains mostly closed, only at 5 % dynamic reserve to surge line, it is slightly opened. The eBooster speed is controlled to achieve boost pressure target.

The torque curves show the initial advantage of the 2.0-l engine before boost pressure builds up. With boost pressure from the eBooster, the 1.6-l VTG engine torque gradient becomes steeper; the full load torque is achieved earlier than with the 2.0-l engine and even the R2S engine. However, the R2S system can maintain high boost pressure also in steady-state operation, where the eBooster can only deliver transient boost.

FIGURE 4 (top) shows an FTP-75 drive cycle with the power consumption of the eBooster, calculated with a dynamic drive model for a premium car with

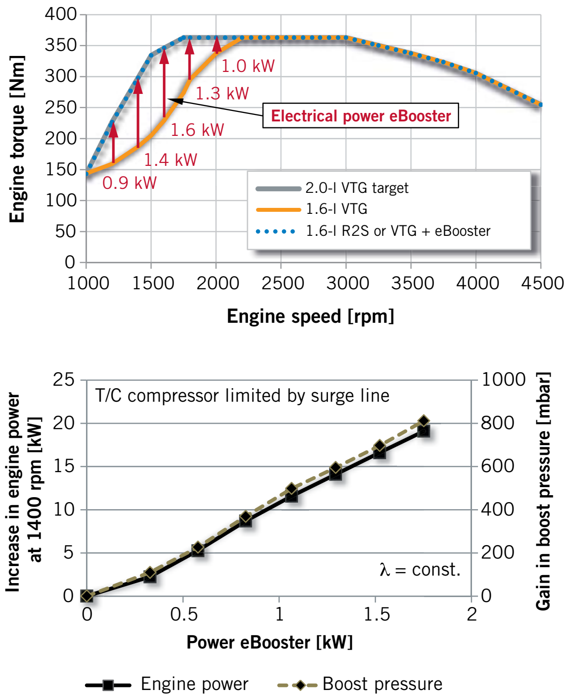

FIGURE 2 Torque curves for 2.0-l engine versus 1.6-l single-VTG and two stage concepts (top) and additional engine power achieved through electrical boosting at 1400 rpm (bottom) (© BorgWarner)

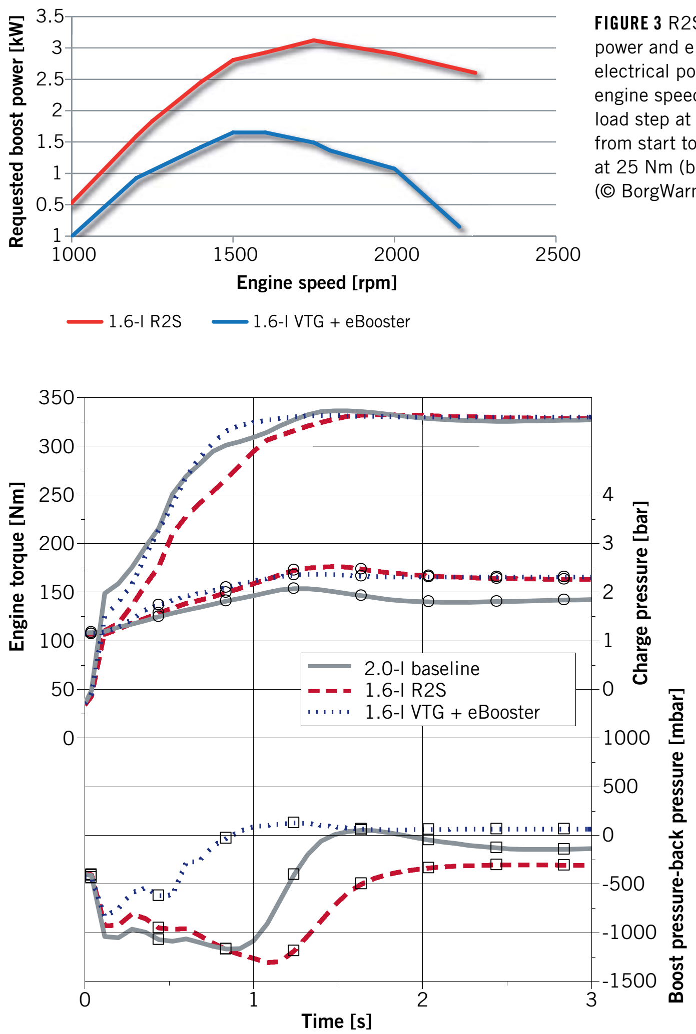

FIGURE 3 R2S turbine power and eBooster electrical power versus engine speed (top) and load step at 1500 rpm from start torque at 25 Nm (bottom) (© BorgWarner)

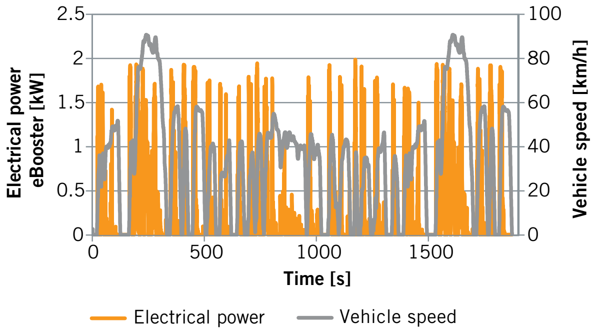

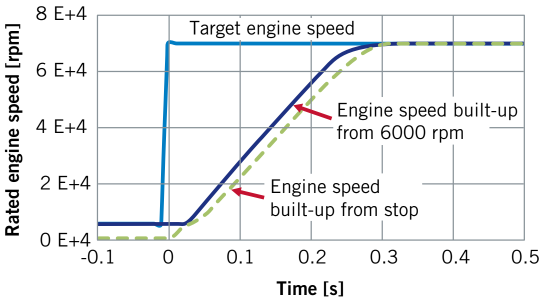

FIGURE 4 FTP75 with eBooster electrical power consumption (top) and eBooster transient acceleration from idle and standstill (bottom) (© BorgWarner)

power to weight ratio of 13 kg/kW and a six-speed transmission. The eBooster is operated with 2 kW and a minimum speed maintained of 6000 rpm. In the cycle, the average power consumption is around 210 W. The eBooster is in idle around half of the time. Switching it off would save around 13 W. With additional boost pressure from the eBooster, a higher amount of low pressure EGR can be used and gas exchange advantages can be generated. With that, around 4 % fuel efficiency increase is expected, with only slight disadvantages in NO_x emissions compared to the R2S concept. Advantages in particulate emissions are expected compared to the reference engine, since the time of the air/fuel ratio at the smoke limit decreased by 5 %.

REQUIREMENTS OF THE ELECTRICALLY DRIVEN COMPRESSOR

From the eBooster function, clear design requirements could be derived:
- the inertia of the electrical motor has to be minimised
- electrical and mechanical losses need to be minimised
- the motor has to be robust against high temperatures
- a very compact design with integrated power electronics
- very efficient power electronics (at 5 kW electrical power, every percent efficiency loss means 50 W of heat flux to be conducted away from the power board)
- eBooster variants have to be modular for 12- and 48-V variants
- NVH has to be considered in the concept.

DESIGN OF THE ELECTRICALLY DRIVEN COMPRESSOR

The design concept decisions were guided by the above key requirements. A brushless permanent magnet DC motor was selected, because it is clearly more efficient than asynchronous or switched reluctance motors. The motor has to be very robust to high temperatures to endure high on time, thus, samarium-cobalt magnets, being magnetically stable beyond 300 °C, were selected.

Also, the permanent magnet motor does not need magnetisation energy from the power electronics, which helps keeping it efficient and compact. The motor was designed such, that motor torque over motor rotation does only show low torque ripple, to minimise high frequency noise from the motor.

FIGURE 4 (bottom) shows the motor transient response to a full speed command, both starting from 6000 rpm idle speed and from a motor hold position. From idle, 90 % of maximum speed is reached after 230 ms, from motor hold in 250 ms. Electronic circuits and bearings are designed such, that the eBooster can either be run in idle continuously, or can be put in standstill.

When choosing the eBooster operating speed, it had to be considered, that the energy to accelerate a rotor is proportional to the speed squared. Thus, an optimum had to be selected between a large motor with low speed, a large compressor wheel but a very quick speed ramp and a small, very high speed motor with small compressor and longer speed ramp.

A compromise was chosen at a speed of 70,000 rpm, to achieve an overall homogeneous package with roughly similar diameter between motor, power electronic and compressor side of the eBooster. The 48-V eBooster has an overall length of only 170 mm (including the compressor inlet flange) and a diameter of only 135 mm.

Also, the stator was optimised for long on-times and high duty cycle by using a high density copper filling and designing for a good heat transfer to the housing. For low heat generation, the power electronics is using parts with lowest resistance specifications and highly efficient capacitors, the CAN interface is integrated. A good connection from electronic board to housing guarantees an efficient heat transfer.

Specification	12-V eBooster	48-V eBooster
Max. current [A]	200	130
Built-up to 90 % rated engine speed [ms]	250	230
Max. power output [kW]	2.4 (transient) 1.7 (nominal)	6.2 (transient) 5 (nominal)
Rated engine speed [rpm]	60,000	70,000
Pressure ratio [-]	1.3	1.45
Air flow [kg/h]	150	300
Switch-on time over lifetime	Appr. 50 % at rated power	Appr. 33 % at rated power
Max. time boost-event [s]	12	14
Max. on-time	60 to 80 %	60 to 80 %

TABLE 2 Key eBooster product specifications (© BorgWarner)

Both air and water cooling were investigated. Air cooling would be preferred from a vehicle integration standpoint. However, air cooling is only feasible for the 12-V eBooster. With the 48-V eBooster, only water cooling with good heat transfer to stator and power electronic board was feasible.

Finally, with all these design concepts, excellent specifications could be achieved for the eBooster. **TABLE 2** shows typical values, especially on-time and duty cycle are however application specific and depend on water, air and eBooster ambient temperatures in the respective vehicle application. To achieve best duty cycle values, usage of water from the low temperature circuit is recommended, however not mandatory. With favourable operation conditions, the 48-V eBooster can achieve around 2 kW permanent power.

To ensure that the eBooster is always available for boosting in the vehicle application, BorgWarner developed a simulation tool to predict temperature and eBooster availability. That can be used as basis for load management. Lower currents, and higher power for larger displacement engines and more benefits in transient performance and fuel economy are advantages of the 48-V eBooster. A simulation, using customer drive profiles and load cycles, can determine eBooster energy consumption, such that the OEM can early on check his vehicle electric system.

SUMMARY

BorgWarner's eBooster supplements the conventional turbocharger. Even at low engine speeds, boost pressure can be supplied very quickly to enhance engine transient response. With that, the eBooster offers potential to increase engine power. With respective matching of the overall system eBooster and turbocharger, both fuel efficiency improvements and, especially with diesel engines, optimisation of pollutant emissions are feasible.

REFERENCES

[1] Arnold, S. et al.: Design and Development of e-Turbo for SUV and Light Truck Applications. DEER conference, 2004

[2] Münz, S. et al.: Der eBooster – Konzeption und Leistungsvermögen eines fortgeschrittenen elektrisch unterstützten Aufladesystems. 7th Supercharging Conference, Dresden, 2002

[3] Spinner, G.; Weiske, S.; Münz, S.: BorgWarner's eBooster – the new generation of electric assisted boosting. 18th Supercharging Conference, Dresden, 2013

© BMW

The New BMW Inline Six-cylinder Gasoline Engine

The completion of the first end-to-end modular design generation of the BMW Group reaches its zenith with the simultaneous series launches of the new inline six-cylinder gasoline engine and the new inline six-cylinder diesel engine. The rigorous derivation of characteristics from the modular design system have been combined with the further optimisation of the inline six-cylinder gasoline engine with regard to efficiency, smooth performance, responsiveness, power output as well as torque build-up with low weight. The new inline six-cylinder gasoline engine was introduced simultaneously in July 2015 in the new BMW 7 Series and in the facelift of the 3 Series Sedan and Touring. There will be an introduction in other vehicle derivatives in the near future. With a power output of 240 kW, this latest generation continues the tradition of the inline six-cylinder engine which has been built at BMW since 1933.

OBJECTIVE

The main objectives for the inline six-cylinder gasoline engine were a further increase in efficiency as a result of reduced consumption with simultaneous gains in power output and torque, a further weight reduction, development of the unsurpassed smooth performance, and a further enhancement in responsiveness while preserving outstanding low-end torque. Over and above this, it was vital to comply with the strictest exhaust emission standards worldwide as well as to ensure vehicle integration without difficulty for all BMW vehicle series with longitudinally installed engines. Integration into the existing production network was also an integral part of the requirements specification.

CONCEPTION

The rigorous derivation of characteristics from the three-cylinder and four-cylinder modular transverse engines was obligatory. In addition, with the longitudinal engines, the next step in the enhancement of the modular engines was initiated in spring 2015. The basic configuration of the cylinderset was not changed and the components of the valve gear were adopted. The implementation of the new demanding objectives was achieved essentially by optimising the gas exchange, de-throttling the air flow by means of the charge air cooling integrated in the intake system, enhancement of the heat management with the introduction of a heat management module (HMM), and the implementation of various friction measures.

BASIC ENGINE

Building on the three-cylinder and four-cylinder modular engines already in series production, the basic engine of the six-cylinder engine was newly designed in comparison with its predecessor, **FIGURE 1**. The crankcase is designed as a permanent mold cast aluminium deep-skirt construction, enabling synergies in the casting process with the six-cylinder diesel engine as regards core design and associated tool variants. The so-called LDS layer (Lichtbogen-Draht-Spritzen) made of a sprayed-on iron alloy, which is already familiar from the modular engine family, is used as liner material. The crankshaft has been optimised with regard to weight and now provides a once more improved degree of balance with lower weight. The prove multi-component bearings are used as the main bearings; the connecting rod bearings are polymer-coated on the rod side and designed with a conventional two-material bearing on the cap side.

In the crankshaft drive, both the stroke/bore ratio and the connecting rods were adopted from the modular design system. The rise in compression in comparison with the predecessor from 10.2 to 11.0 was achieved with pistons from the modular design system. To reduce friction, the LDS layer made it possible

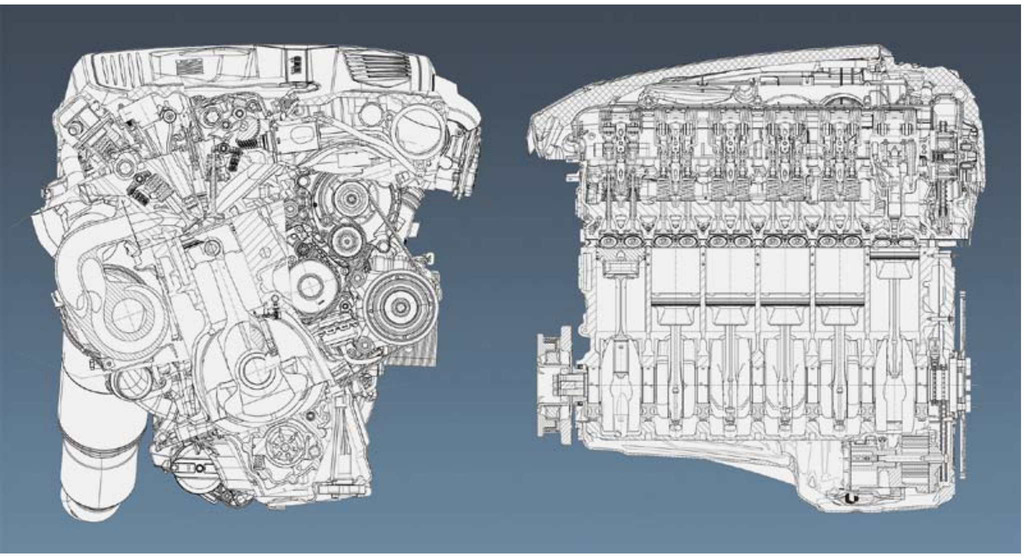

FIGURE 1 Longitudinal and cross sections (© BMW)

AUTHORS

Dipl.-Ing. Dr. techn. Christian Landerl is Head of Development Gasoline Engines at the BMW AG in Munich (Germany).

Dipl.-Ing. Wolfgang Mattes is Head of Engineering Design Gasoline Engines at the BMW AG in Munich (Germany).

Dipl.-Ing. Markus Rülicke is Head of Modular Design Gasoline Engines Projects at the BMW AG in Munich (Germany).

Dr.-Ing. Bodo Durst is Head of Development Exhaust Systems and Combustion for Gasoline Engines at the BMW AG in Munich (Germany).

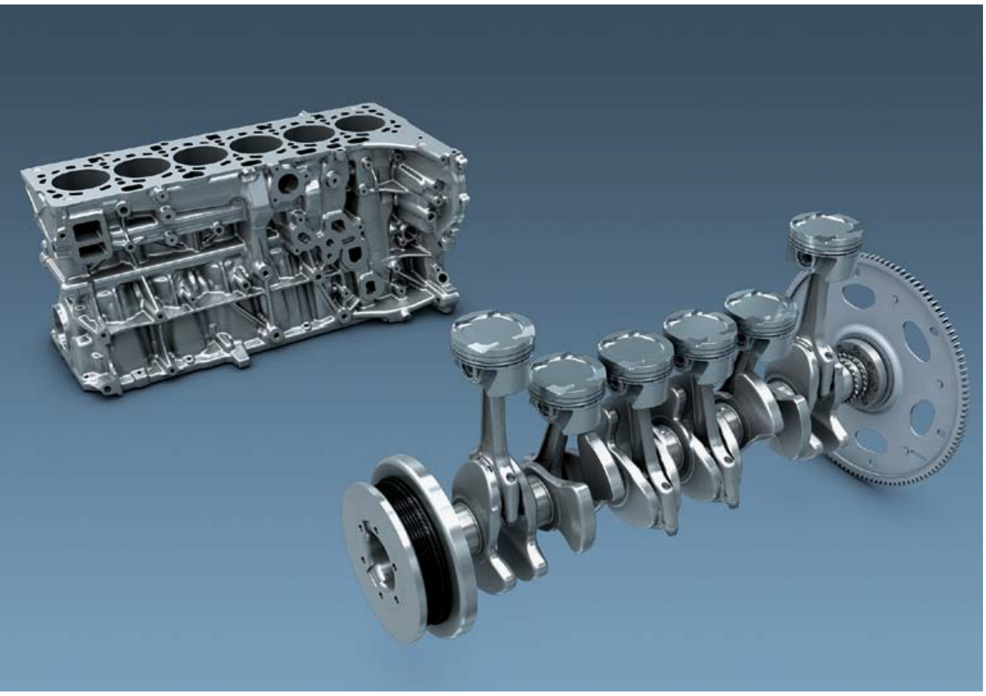

FIGURE 2 Crankcase and crankshaft drive (© BMW)

TABLE 1 Key specifications and main dimensions (© BMW)

Key specification	Unit	Six-cylinder
Maximum power (corresponding rpm)	kW at rpm	240 at 5500-6500
Maximum torque (corresponding rpm)	Nm at rpm	450 at 1380
Maximum engine speed	rpm	7000
Specific power	kW/l	80.1
Specific torque	Nm/l	150.1
Maximum specific work	kJ/l	1.88
Basic measurement		
Piston displacement	cm^3	2997.6
Bore	mm	82
Stroke	mm	94.6
Stroke/bore ratio	–	1.15
Volume per cylinder	cm^3	499.6
Connecting rod length	mm	148.2
Connecting rod ratio	–	0.319
Cylinder distance	mm	91
Piston		
Compression height	mm	33.2
Top ring land	mm	7.8
Piston pin		
Diameter	mm	22
Lenght	mm	52
Valves		
Diameter inlet / exhaust	mm	30.1 / 28.5
Stem diameter inlet / exhaust	mm	5.0 / 6.0
Compression ratio	–	11

to further optimise the tangential forces of the piston rings. **FIGURE 2** shows the crankcase and the crankshaft drive; the technical data are shown in **TABLE 1**.

The cylinder head was derived from the base dimensions of the transverse modular design system; the Vanos units are positioned on the transmission side and are driven via a two-piece chain drive with support point used in the diesel engine to drive the high-pressure pump. The intermediate gear on the gasoline engine is rubberised for the best possible chain acoustics. In the same way as the other modular engines, the new inline six-cylinder engine is equipped with the latest generation of the Valvetronic fully variable valve gear with compact dimensions.

The oil supply is ensured by a volume-flow controlled variable flow vane pump driven by a chain. It is designed to work in tandem with the vacuum pump and is positioned in the oil sump of the oil pan. The implementation as a tandem pump is the best possible solution with regard to package and weight. A characteristic map control valve fitted in the crankcase activates the volume control in the oil pump. An oil pressure sensor in the main oil gallery serves as the reference variable for the control operation. Control of the oil pressure during warm-up to below 3.5 bar achieves a characteristic-map-controlled shutdown of the piston spray nozzles to reduce particulate emissions. The reduction of the pump drive power this involves leads to a reduction in the fuel consumption in many characteristic-map ranges. Thanks to the standardised vehicle architecture, a standardised oil pan can be used for derivatives with standard drive units from the 3 Series to the 7 Series. Oil level measurement takes place automatically during operation, without contact via a packaged ultrasonic level sensor (Puls). The oil filter module with filter and oil-to-water heat exchanger, which is standardised for this diesel engine, is arranged directly at the crankcase.

The deployment of active crankcase ventilation reduces condensate as well as fuel and combustion residues in the engine oil. In conjunction with the increased volume flow rate of the ventilation, the register arrangement of the oil separators enables a significant increase in the degree of separation in partial load. The recirculation of cleaned

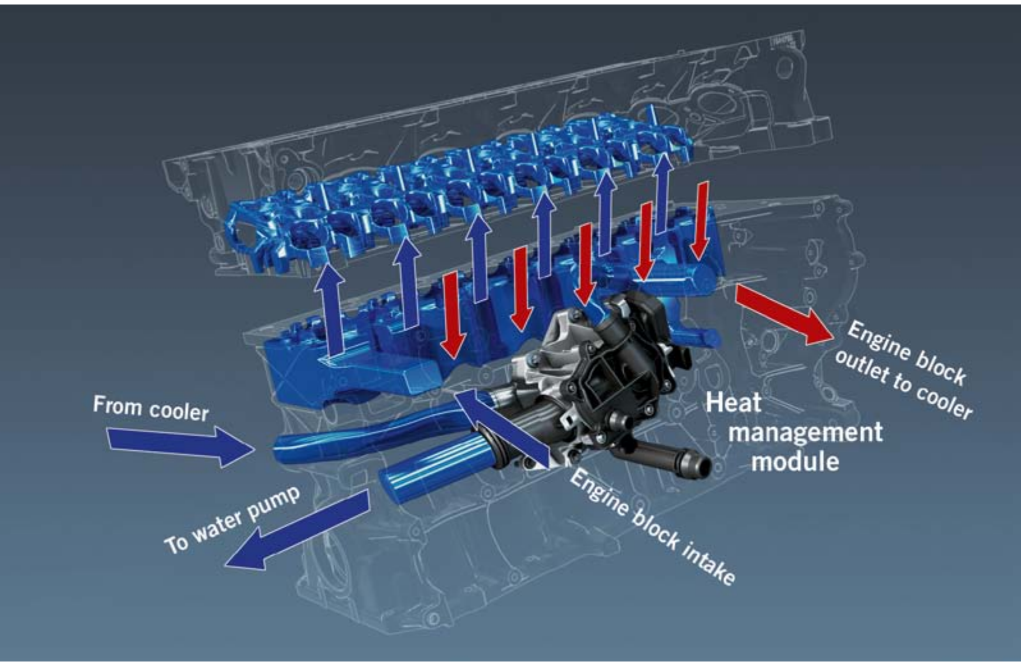

FIGURE 3 Coolant circuit, cylinder head and crankcase, including heat management module (© BMW)

blow-by gases in partial load avoids external lines within the cylinder head cover and leads directly into the inlet ports; in charged operation, the gases are routed through an externally heated line upstream of the compressor.

To optimise consumption in the warm-up range and to quickly regulate the coolant temperature, the cooling circuit has been revised and a heat management module deployed for control instead of a thermostat. **FIGURE 3** shows the heat management module, including the coolant distribution in the crankcase and cylinder head.

High-precision injection of the 2nd generation with a central coil injector is used in the direct fuel injection. The maximum system pressure of 200 bar is provided by means of a high-pressure fuel pump driven by a triple cam on the exhaust camshaft. As is the case for all modular gasoline engines, a direct rail is used in the six-cylinder engine. The fuel injectors being bolted directly to the rail via retaining bridges means that no additional lines and connecting elements are necessary. Here, in consistent modular design approach, the six-cylinder engine uses two three-cylinder rails. In combination with the central spark plug position, this system is an essential basis for achieving the functional objectives.

PERIPHERALS AND DME

The untreated air intake, including intake muffler with integrated air filter, is arranged on all derivatives on the exhaust side, thus leading to a short feed path into the exhaust turbocharger. In the same way for all derivatives, the clean air line which introduces the crankcase ventilation gases is routed upstream of the engine directly into the throttle valve. The throttle valve is designed for all longitudinal engines as a common part and the cooling of the clean air in the intake system means it is configured for the higher air temperatures. To enable a compact package that is compatible in all model series and also to reduce the pressure loss in the air intake system, the charge air cooler has been designed as indirect and integrated into the intake system. The newly developed indirect charge air cooler is inserted from the rear into the plastic intake system. As a result of the design of the intake system and cooler, there is no need for additional internal sealing despite the extensive length. **FIGURE 4** shows the arrangement

FIGURE 4 Intake system with indirect charge air cooler (© BMW)

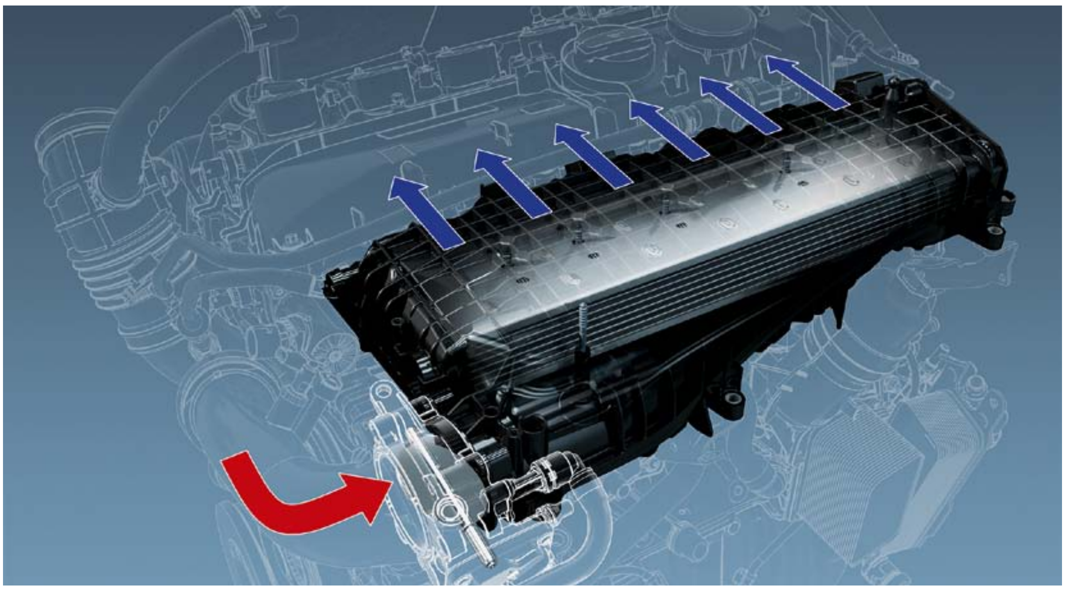

of the charge air cooler in the intake system, including the air path. Cooling takes place through a low-temperature circuit supplied by an electric water pump.

The six-ribbed belt drives the alternator, water pump, and air-conditioning compressor. The arrangement of the tensioner on the alternator has enabled the belt layout to be configured in such a way that the functionality is ensured even with lowered initial tension, thus raising the consumption potential and implementing a standardised belt for all longitudinal engines.

A newly developed platform with a multi-core processor implemented for the first time is used in the engine management system. Depending on the requirements and with the corresponding deployment of three to twelve cylinders, it enables all variants, including diesel. In order to take account of the enhanced requirements from the vehicle architecture, the new control unit is based on a processor with multi-core architecture (2 × 300 MHz, 1 × 200 MHz, 8 MB flash), providing all standard interfaces for communication with FlexRay, CAN, LIN, and SENT. The modular design logic makes use of a standardised connector system (254 pins), a standardised housing with the options of air and water cooling, and common software modules up to a uniform programme status.

The platform development was a major step in gaining control of the increasing complexity and variety of versions within the engine control systems, but also of the application. This reduces what used to be complex engine-specific individual functionalities, creating advantages with regard to flexibility, applicability as well as testability of the entire engine management system, for gasoline and diesel engines, and hybrid drive systems.

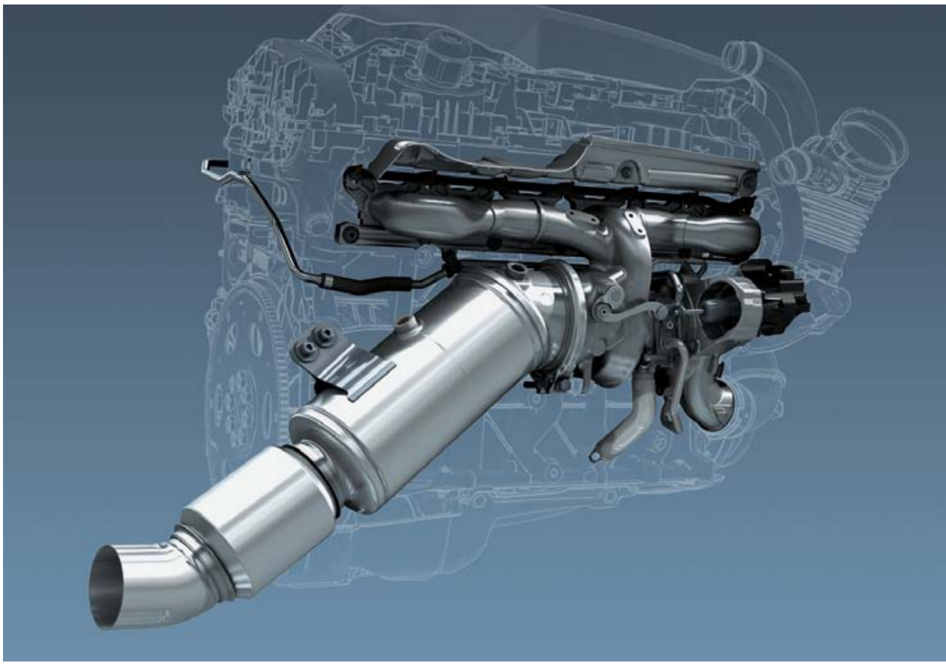

FIGURE 5 Hot end (© BMW)

CHARGING

The newly developed TwinScroll turbocharger shown in **FIGURE 5** is designed as an integral solution of charger housing and manifold for cylinders 3 and 4. The manifolds of cylinders 1 and 2 as well as 5 and 6 are cast parts and permanently fixed onto the central integral component. The advantage of this arrangement is not only the simplification of the interfaces, but also the option of being able to retrofit manifold cooling. To ensure the well-known excellent response characteristics, the exhaust flows from cylinder bank 1 (cylinders 1 to 3) and cylinder bank 2 (cylinders 4 to 6) are consistently routed as separate up to the turbocharger. The manifold is mounted by means of the clamp/slide strip concept that has been established in the modular design system. In order to achieve optimal catalytic converter heating, the electrically operated wastegate has a maximum opening angle of 54°. Thanks to application measures, an air diverter valve is not necessary. The engine-proximate catalytic converter arranged directly behind the exhaust turbocharger is designed as a common part for all derivatives. The arrangement close to the engine means that it reaches operating temperature very quickly, thus enabling the elimination of an underbody catalytic converter.

THERMAL MANAGEMENT

In order to achieve the lowest fuel consumption in driving modes that are relevant to the cycle and the customer, intelligent engine heat management is of major significance. This is achieved for the described drive system by means of various measures discussed below.

The coolant flows via a pump that is flange-mounted directly onto the crankcase into the coolant jacket of the engine. Initially, the coolant flows through the crankcase longitudinally on the exhaust side. Subsequently, the coolant enters the cylinder head, where it is distributed by a transverse flow to defined positions of the cylinder head with high thermal loads. The intake side serves to return the coolant into the crankcase and forward it into the heat management module, an electrically actuated ball valve with various integrated switch positions (e.g. to block the heating circuit during the engine warm-up phase). The selected cooling concept achieves on the whole a more uniform temperature level as well as a reduction in the maximum component temperatures in the cylinder head.

The belt-driven mechanical water pump has a blocking element with an integrated bypass that is precisely coordinated with regard to through-flow. In combination with a powerful engine-oil-to-water heat exchanger, this achieves optimal distribution of the heat in both the structure and fluids during the warm-up phase of the drive unit, thus minimising friction losses. The full oil-side through-flow of the engine-oil-to-water heat exchanger also enables maximum feedback during the warm-up as well as comparatively low engine oil temperatures during vehicle operation with high load. In addition, a further reduction in friction could be achieved, in particular at low engine oil temperatures, using a highly modern engine oil of viscosity class 0W-20.

In the engine warm-up phase, a generously dimensioned coolant jacket around the exhaust ports recovers more waste heat and contributes to the implementation of stoichiometric combustion in the entire characteristic-map range.

The deployment of a component temperature sensor positioned near the exhaust port in the cylinder head in combination with a coolant-temperature sensor arranged at the engine outlet enables temperature control that is optimised for every operating mode, with its familiar positive influence on friction and consumption.

As a result of its fast controllability and short reaction time, the heat management module flange-mounted at the engine outlet also permits an increase in the coolant temperature during normal vehicle operation to leverage further potentials for the minimisation of friction, as this enables a reduction of the on-hand cooling output to the required minimum.

COMBUSTION PROCESS

The combustion process of the new inline six-cylinder engine corresponds to the combustion system of the BMW modular gasoline engines described in [1] and is based on the TwinPower Turbo combustion process familiar from the predecessor engines. The reduction in size of the bore by 2 mm to 82 mm as well as the increase in the compression ratio to 11.0 leads to an increase in efficiency. The greater stroke/bore ratio of 1.15 resulting from the reduced bore represents an optimum with regard to thermodynamics and friction. The spark position of the spark plug could be drawn approximately 2 mm further out of the combustion chamber, which leads to a significant reduction in the stresses to which the spark plug is exposed.

Despite the smaller bore, a significantly wider piston recess shape has been chosen compared to the predecessor combustion process. It was possible to considerably improve the mixture homogenisation by means of a spray configuration that is also widened, using multi-hole injectors with reduced through-flow. Together with the greatly increased charge movement as a result of specific optimisation of the inlet port, this leads to significantly faster combustion.

In order to comply with foreseeable stricter general emission conditions, major features of the multi-hole injectors were optimised. The reduction in the nominal through-flow has considerably reduced the penetration depth of the spray. By optimising the spray pattern using individual-hole volume and direction distribution, a very good compromise between the requirements in the catalytic converter heating (stratification capability) and operating temperature was found. That also led to a reduction of the wall moistening of the piston and cylinder liner as well as the intake valve moistening to a minimum. The so-called CVO (controlled valve operation) functionality of the 2nd generation ensures that another area of the characteristic curve of the injector can be used for the injection of tiny volumes. In total, these measures have an extremely positive effect, i.e. an again significantly reduced number of particulates in the entire characteristic-map range.

FIGURE 6 shows the course of the indexed specific fuel consumption against the indexed load at a speed of 2000 rpm. It can be seen clearly that the improvements in the combustion process development made it possible to achieve a reduction in the fuel consumption in many load ranges. In the area of rated power, the new modular engine is operated under normal ambient conditions with a stoichiometric air ratio.

VEHICLE INTEGRATION

The integration of the new inline six-cylinder engine in conjunction with the vehicle and drive system measures have enabled the demanding objectives

FIGURE 6 Specific effective fuel consumption BMW TwinPower Turbo gasoline engine in comparison with predecessor engine: Best point in the characteristic map and partial load at n = 2000 rpm; w_e = 0.2 kJ/l (© BMW)

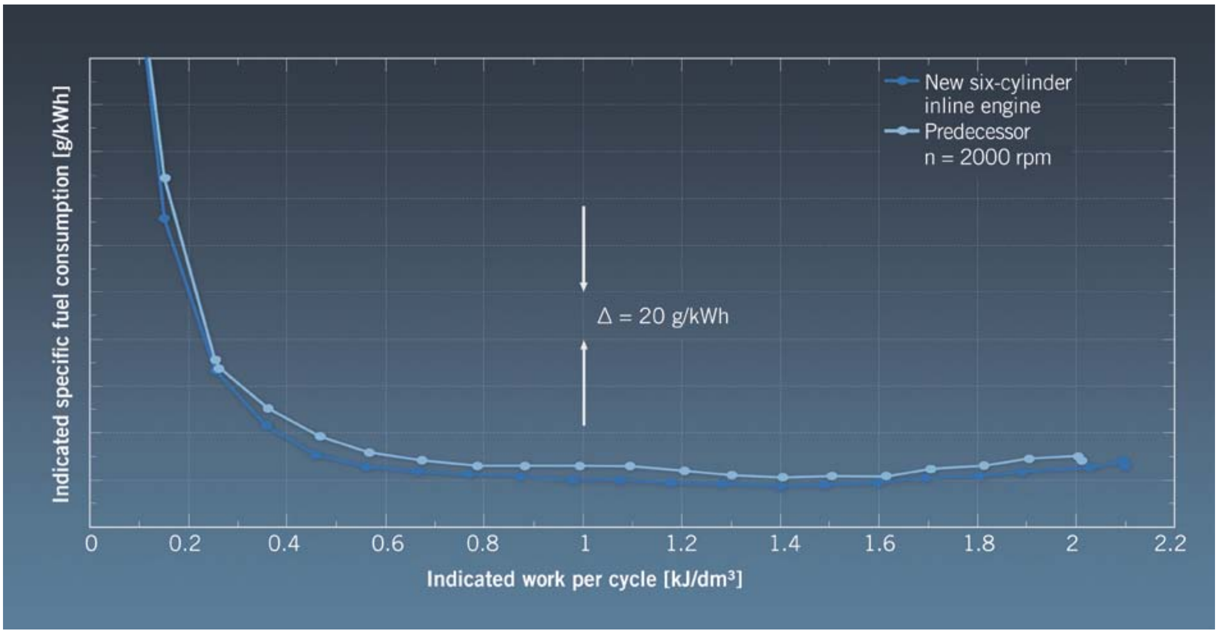

with regard to comfort, dynamics, and efficiency to be achieved. Ensuring standardised interfaces for the engine/vehicle for all relevant model series enables integration of the modular engine into the various vehicle plants in the production network of the BMW Group without any difficulty.

FUEL CONSUMPTION

The measures in warm-up, friction, and thermodynamics have enabled a 6 % reduction in the consumption of the engine in comparison with the predecessor. In conjunction with the vehicle measures, this results in a reduction in fuel consumption in the NEDC for the 740i of 16 % to 6.6 l/100 km and thus in a CO_2 emission of 154 g/km. **FIGURE 7** shows fuel consumption and vehicle performance of the new 740i in comparison with the predecessor and competitors.

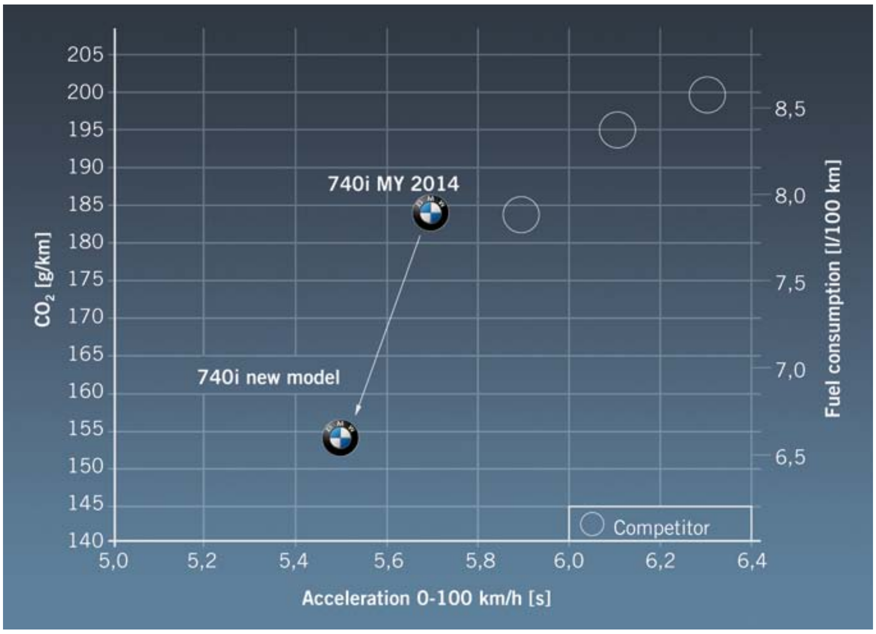

FIGURE 7 Fuel consumption and vehicle performance of BMW 740i in comparison with competitors (© BMW)

POWER OUTPUT AND TORQUE

In comparison with the predecessor, the power output was moderately raised to 240 kW. The further enhancement of the responsiveness of the engine was achieved by means of a more ample total power output and torque profile. The maximum power output is available in the engine speed range of 5500 to 6500 rpm; the maximum engine speed is 7000 rpm. The maximum torque of 450 Nm is already available as of 1380 rpm and with the revised eight-speed automatic transmission also provides the basis for efficient dynamics in the low engine speed range. The torque and power output curves of the new inline six-cylinder engine are applied in **FIGURE 8** in comparison with the predecessor.

EMISSIONS

The new inline six-cylinder engine complies with the Euro 6 emission standard and the US emission standards up to ULEV70. If required, SULEV requirements can be met with the concept shown.

ACOUSTICS

The basis for the further improved engine acoustics of the inline six-cylinder engine is a steel crankshaft with intelligent mass balance as well as the main bearing connection of the oil deflector. In conjunction with the

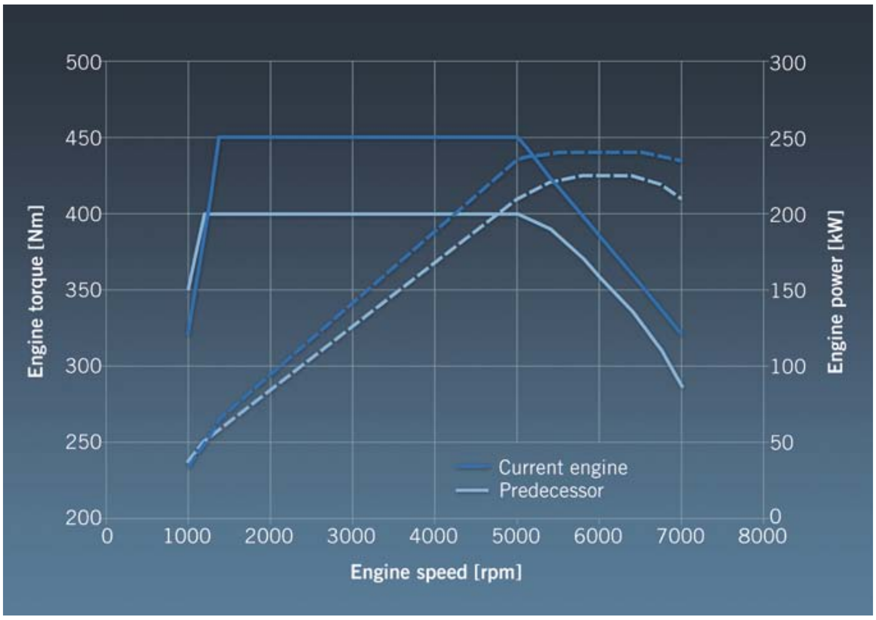

FIGURE 8 Full-load curve in comparison with predecessor engine (© BMW)

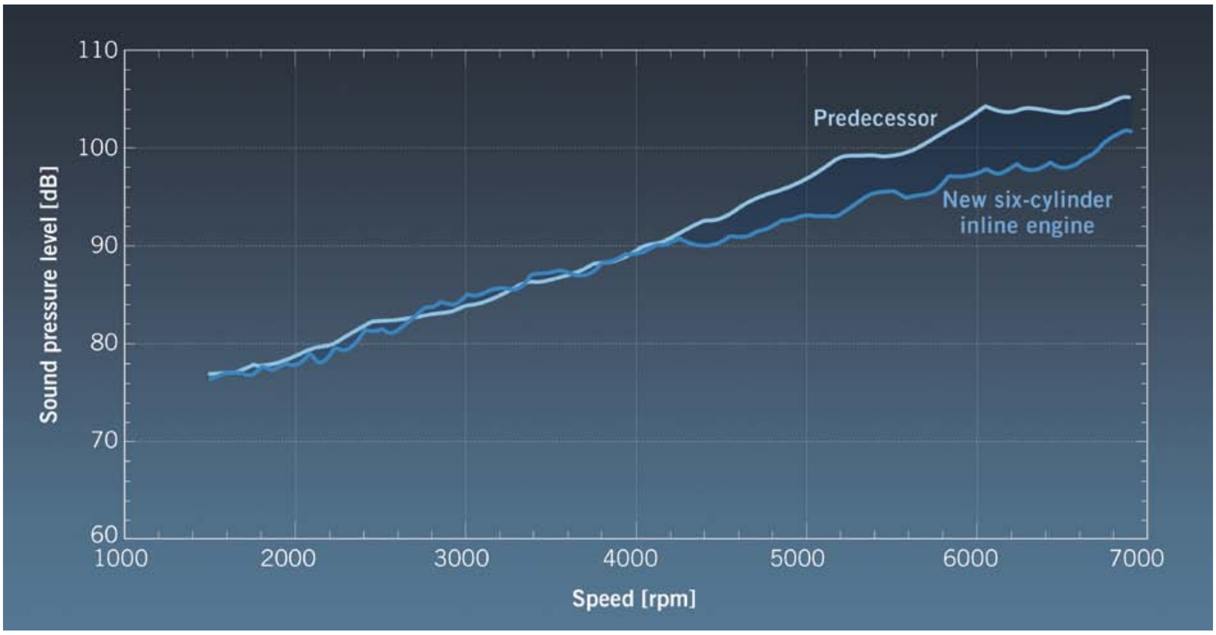

FIGURE 9 Degree of balance in acoustic pattern in comparison with predecessor engine (© BMW)

crankcase, this ensures high overall rigidity of the basic engine. Despite enhancement of torque and performance, the internally B58 called engine is quieter than its predecessor as of 4000 rpm. This has further improved the smooth running of the inline six-cylinder engine and reinforced the typical BMW core features. **FIGURE 9** contains a comparison of the full-load airborne noise emission of the new inline six-cylinder engine with its predecessor.

To improve the overall vehicle acoustics and heat configuration, an engine-proximate capsule is used additionally. The acoustic shielding close to the source has also enabled a further reduction in the overall vehicle weight by optimising the acoustic measures in the vehicle.

WEIGHT

Despite the added functions with regard to power output, acoustic pattern, and integration and/or modular design requirements, it was possible to reduce the weight of the engine by another 2 kg in comparison with its predecessor. The basis for this was a rigorous lightweight design approach for the crankcase, cylinder head, and the crankshaft drive as well as an intelligent configuration of the mounting and retainer elements.

SUMMARY

The BMW inline six-cylinder TwinPower Turbo gasoline engine has been rigorously derived from the modular design kit and meets the increased demands in the requirements specification for a BMW inline six-cylinder engine of the latest generation in full. The major objectives for the new engine such as a significant reduction in the fuel consumption while simultaneously increasing the torque and power output, compliance with worldwide exhaust emission legislation, an improvement in the acoustic pattern while simultaneously optimising the weight were achieved using the modular design approach.

The new BMW inline six-cylinder TwinPower Turbo gasoline engine with Valvetronic in the new BMW 740i in conjunction with vehicle measures in the NEDC achieves a reduction in fuel consumption of 16 % to 6.6 l/100 km and thus a CO_2 emission of 154 g/km. The engine complies with Euro 6 and/or ULEV II exhaust emission legislation and its successful series launch took place in July 2015 in the revised 3 Series Sedan and Touring simultaneously. The latest six-cylinder generation thus effortlessly keeps its promise with regard to driving pleasure and efficient dynamics.

REFERENCE

[1] Steinparzer, F.; Schwarz, C.; Brüner, T.; Rülicke, M.: Die neuen Drei- und Vierzylinder-Ottomotoren von BMW. In: MTZ 75 (2014), No. 6

Development of a Natural Gas Combustion System for High Specific Power

Due to ecological as well as economic reasons large size gas engines, especially within the medium speed range, are gaining increasing interest. Besides the already established power generation application, these types of engines are gaining importance for marine as well as rail propulsion. In the near future, the reachable power density will be the dominating driver for further extension. Besides the obligatory fulfillment of the stringent emission legislation, the achievable fuel efficiency level and the corresponding operation costs are key factors for the final customer. This article presents the development of a pre-chamber combustion system with the feasibility of high specific load at FEV. The use of efficient simulation tools allowed a target-oriented preliminary layout so that the experimental validation and detailed optimisation on the engine test rig required only few hardware variants.

BASE ENGINE

Base for the development was a medium speed diesel engine with a displacement of approximately 16 l, which is available as a single cylinder variant for experimental investigations. The focus of the conversion to gas operation was the cylinder head design. The diesel injector was replaced by a pre-chamber, composed of multiple parts. The upper part of the assembly was equipped with a top-feed gas supply with a mechanical passive check valve, a spark plug and a bore for the pressure indication. The pre-chamber was positioned in the lower part. The main gas supply was realised by a solenoid gas valve positioned close to the intake port. The compression ratio was decreased to 11.5:1. The exhaust valve timing was conventional, for the intake a moderate Miller timing (IVC 10 °CA bBDC) was chosen.

DEVELOPMENT STEPS

Compared to the combustion in an open – i.e. unseparated – combustion chamber, the pre-chamber engine allows a significant control over the process both by the design and by the operation mode of the pre-chamber. Therefore, it requires a specific combustion system layout which can be separated into two main steps [1].

The first step concentrates on the definition of the pre-chamber volume and the cross section of the nozzle orifices. Both are depending primarily on the engine size and the planned operation mode. Compared to the pre-chamber operated with stoichiometric mixtures, the operation of a pre-chamber with air

AUTHORS

Dipl.-Ing. Bertold Hüchtebrock
is Technical Specialist for Gas Engines in the Business Unit for Industrial, Commercial and Large Engines at the FEV GmbH in Aachen (Germany).

Dr.-Ing. José Geiger
is Manager in the Business Unit for Industrial, Commercial and Large Engines at the FEV GmbH in Aachen (Germany).

Dipl.-Ing. Avnish Dhongde
is Research Assistant for Thermodynamic Simulation at the Institute for Combustion Engines at the RWTH Aachen University (Germany).

Dipl.-Ing. Harsh Sankhla
is Team Leader for Thermodynamic Simulation in the Business Unit for Industrial, Commercial and Large Engines at the FEV GmbH in Aachen (Germany).

excess (lean pre-chamber) demands a larger pre-chamber volume. This is required to compensate the reduced energy density in the pre-chamber. The cross section of the nozzle orifices has to be chosen in a way that a sufficient over-pressure compared to the main chamber is generated during the pre-chamber combustion. Too high pressures would cause high thermal loads with additional negative impact on the energy balance by the increased heat transfer and flow losses. A too low pre-chamber pressure level on the other hand would increase the burn duration of the pre-chamber charge, induce possible cyclic variations and significantly reduce the turbulence transfer into the main chamber.

The second step includes the fine tuning of the pre-chamber. Within this task the crucial characteristics of the main chamber combustion can be modelled by an adapted orientation of the nozzle orifices. By tuning the combustion speed and the speed gradient respectively, the centre of combustion can be adjusted to the requirements and consequently, the knock sensitivity can be influenced.

The characteristic numbers required for the first step can be achieved by zero-dimensional simulation tools with relatively small effort. However, up to now the fine tuning of the nozzle orifice configuration needed much higher effort, and was generally done with extended test bench investigations. In order to use simulation tools to understand these complex process interactions, FEV and VKA developed a simulation process called CMD (Charge Motion Design) [2, 3], which shall be described in detail in the following section.

CMD PROCESS

The schematic diagram, **FIGURE 1**, shows an overview of the involved simulation tools as well as the interlinking of the simulation results. After the estimation of the combustion process in the pre-chamber as well as the main chamber with the 0-D tool, a 1-D gas-exchange process simulation supplies the necessary transient low pressure curves at the intake and exhaust ports. These curves are the starting point of the 3-D CFD flow and turbulence calculation in the main chamber. The 3-D CFD simulation delivers the distribution of the macroscopic and the microscopic kinetic energies as well as their interaction, which plays an important role in the combustion process. As no combustion model like ECFM, G-equation, Shell/CTC or reaction kine-

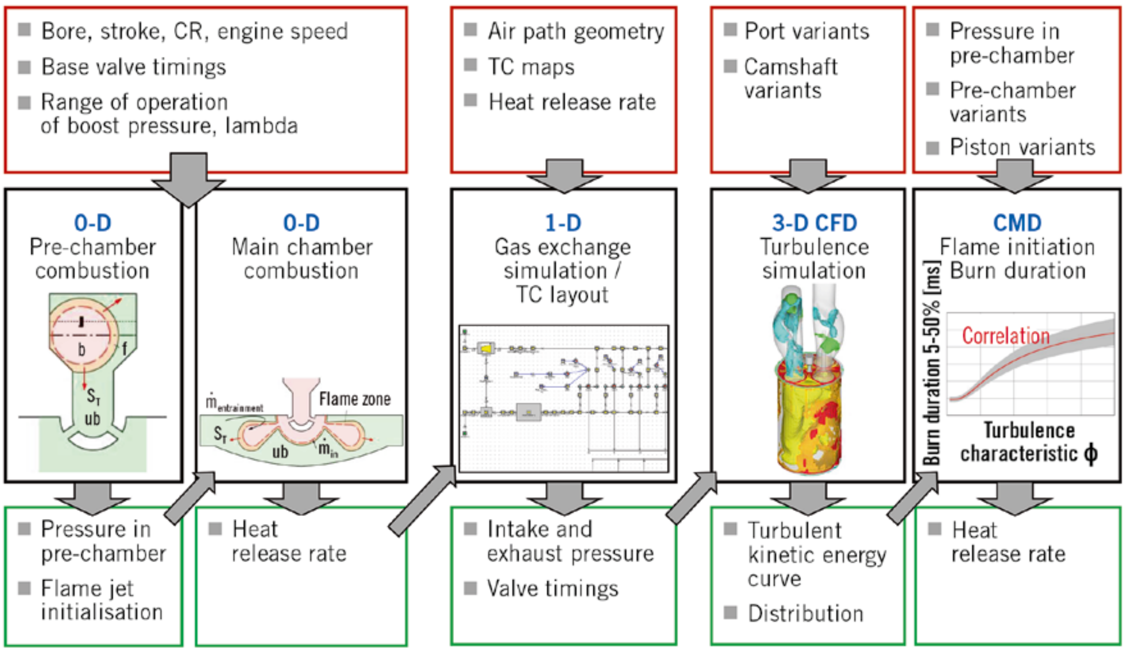

FIGURE 1 Overview simulation tools (© FEV)

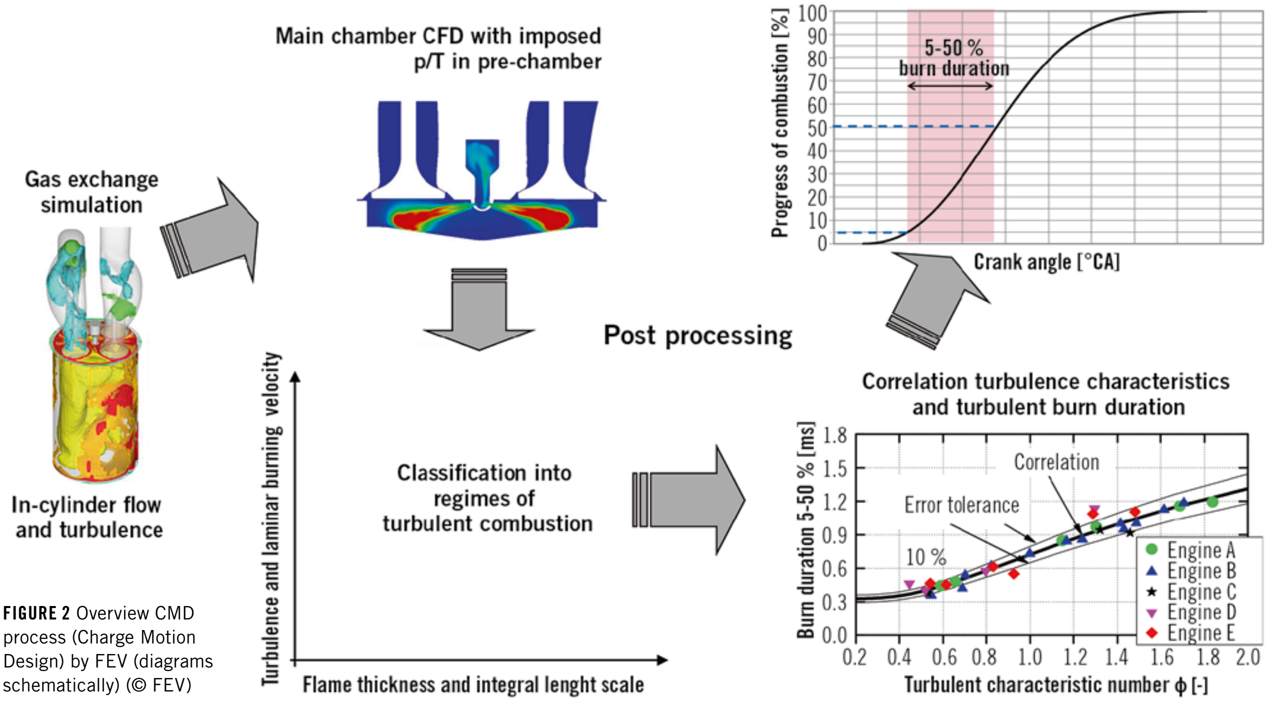

FIGURE 2 Overview CMD process (Charge Motion Design) by FEV (diagrams schematically) (© FEV)

tics with detailed chemistry is used, this approach is very quick and efficient [6]. This is followed by the CMD process as seen in **FIGURE 2**.

The CMD process was originally developed for gasoline engines with open combustion chamber and has now been transferred to pre-chamber natural gas engines [4, 5]. In this process, a turbulent characteristic number (Φ) based on physical models is defined based on the pressure, temperature, air/fuel ratio, rest gas and turbulence level in the combustion-relevant crank angle interval. An estimation of the burn duration is possible using a correlation with this characteristic number. The turbulence calculation takes into consideration the intake and the compression stroke as well as the „turbulent ignition jets" coming out of the pre-chamber. These jets are calculated by imposing the pre-chamber combustion (pressure and temperature), which is calculated by the 0-D code.

The simulation results of the CMD process are summarised in **FIGURE 3**. The 5 to 50 % burn duration estimated from the CMD correlation is compared with the burn duration received from the engine measurements. Engine 1 represents a pre-chamber engine with larger displacement than engine 2, which is the engine considered in this article for further investigations. For the optimisation of the parameters of the correlation function, different pre-chamber designs as well as operating points (load, air/fuel ratio, start of ignition) have been considered. The figure shows a good correlation between the measurement and the simulation results.

PRELIMINARY DESIGN OF THE COMBUSTION SYSTEM

With respect to the CMD-based preliminary design of the pre-chamber, the simulation results of three variants at a high load point have been shown in **FIGURE 4**. The pre-chamber A corresponds to a relatively small pre-chamber volume. Pre-chambers B and C have a bigger volume corresponding to state-of-the-art designs and differentiate themselves in the orientation of the pre-chamber holes. The turbulent characteristic number Φ is the result of the combustion jets coming out of the pre-chamber for an unchanged intake and compression stroke. The correlated 5 to 50 % burn duration is calculated from the characteristic number. The pre-chamber C shows significant advantages in the burn duration over the other two variants.

A higher turbulence level with the pre-chamber C is evident in **FIGURE 5** from the pictures of the turbulent kinetic

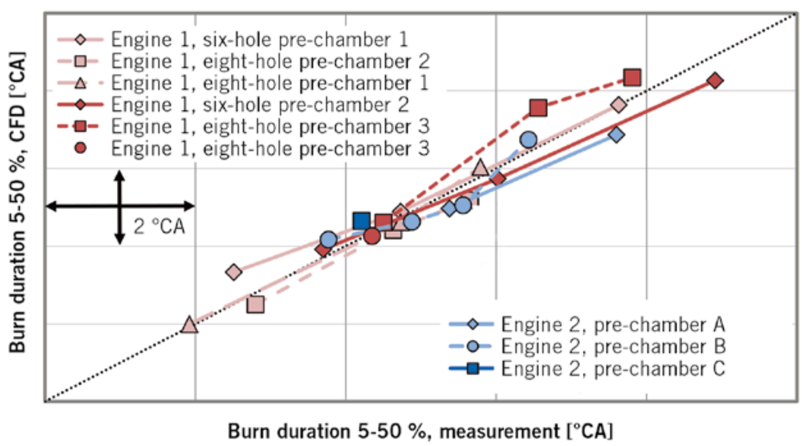

FIGURE 3 Validation of the CMD process (© FEV)

energy at different crank angles in the CFD simulation. A greater volume with higher turbulent kinetic energy can be observed with the bigger pre-chamber in the first 10 °CA interval itself, which corresponds to the ignition delay in the main-chamber. The differences in turbulence level remain during the progress of combustion which leads to a reduction in the correlated burn-duration.

On the basis of the results of the described simulation tools, different pre-chamber layouts were tested on the engine. The important results are described in the next section.

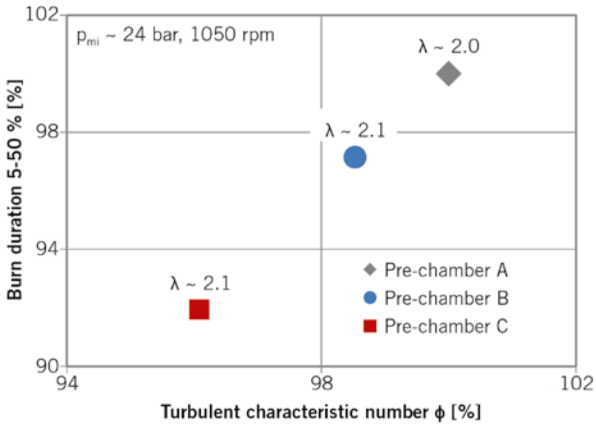

FIGURE 4 CMD evaluation of pre-chamber variants (IMEP ~ 24 bar, n = 1050 rpm) (© FEV)

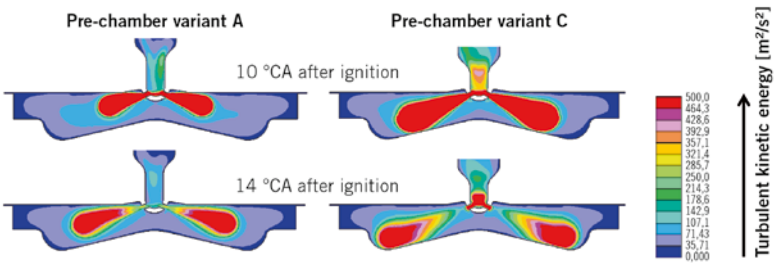

FIGURE 5 CMD evaluation of pre-chamber variants (© FEV)

PRE-CHAMBER VOLUME VARIATION

FIGURE 6 shows the experimental results for the two pre-chambers A and C at an engine speed of 900 rpm and indicated mean effective pressure (IMEP) of 20 bar. The relative air/fuel ratio in the main-chamber was 2.2 while the pre-chamber air/fuel ratio was varied by changing the injection (scavenging) pressure. With an assumption of a realistic scavenging efficiency, the relative air/fuel ratio in the "saturated" pre-chamber is estimated to be around 0.9 (scavenging pressure > 200 mbar for pre-chamber C). In the non-scavenged case ($\Delta p_{Scavenge} \rightarrow 0$), the air/fuel ratio is nearly equal to the (leaner) air/fuel ratio in the main chamber. The start of ignition was fixed so that the influence of the volume can be demonstrated. Ignition time was adjusted such that in the case of a completely scavenged pre-chamber a combustion peak pressure location of 13 °CA aTDC was achieved.

The performance of the bigger pre-chamber C shows a clear dependence on the scavenging pressure. The combustion peak pressure and its location are correlated well with the air/fuel ratio in the pre-chamber till the "saturation point" is reached. The shift of the combustion peak pressure can be attributed to two interdependent effects. Firstly, the ignition delay in the pre-chamber is itself reduced due to enrichment in the pre-chamber. On the other hand, there is a rise in the energy content in the pre-chamber and correspondingly in the ignition energy for the lean mixture in the main chamber.

The NO_x emission behaviour deserves a special mention as many operation strategies aspire for a lean mixture in the pre-chamber in order to reduce the significant emissions from the relatively rich pre-chamber and to keep the deciding total NO_x emissions below the emission limits. In this case, the NO_x emissions for the "saturated" pre-chamber C are five times higher than for the non-scavenged case.

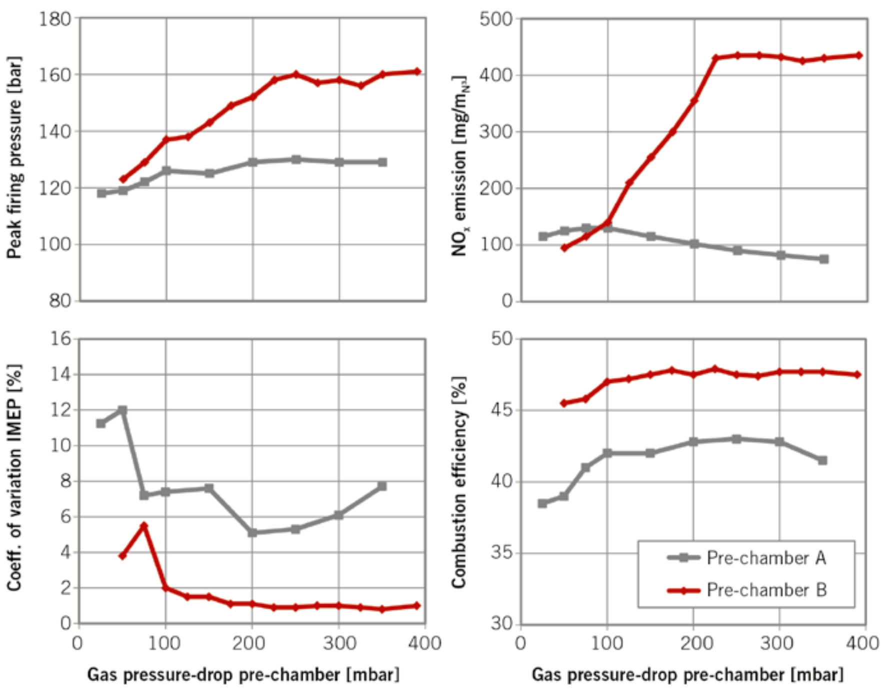

FIGURE 6 Variation of pre-chamber gas scavenging pressure (n = 900 rpm, IMEP = 20 bar, rel. $AFR_{main-chamber}$ = 2.2) (© FEV)

In both cases, however, the TA Luft emission norms (500 mg/m_N^3) are fulfilled.

In comparison with the pre-chamber C, the pre-chamber A shows no direct, observable influence of the air/fuel ratio in the pre-chamber (in fact some opposite trends are visible). With a minimum value of 5 % for the coefficient of variation of IMEP, the cyclic fluctuations are considerably larger and the operation is evaluated as being unsuitable. The bigger pre-chamber C shows a low coefficient of variation (~ 1 %) in a "partly scavenged" operation mode (100 mbar) itself [6].

The influences are reflected clearly in the indicated efficiency. The pre-chamber C has a value of 47 % over most of the region which is an advantage of 5 % points over pre-chamber A. The drop in efficiency for pre-chamber A can be correlated with the significant HC-emissions (not shown here).

On the background of the strongly different smoothness of engine operation, 50 consecutive cycles are plotted in **FIGURE 7** for both the pre-chambers with a scavenging pressure difference of 200 mbar. It is clearly visible that with pre-chamber A considerable fluctuations occur in the combustion in the pre-chamber itself. On the other hand, the reproducibility with pre-chamber C can be considered very good. Moreover, the picture draws another important conclusion – at the same mixture quality (pre-chamber air/fuel ratio), the volume-related higher energy in pre-chamber C leads to a higher over-pressure in the pre-chamber and consequently, a better ignition in the main-chamber. The thermodynamic conditions of pressure and temperature influence the combustion behaviour during the pre-chamber burn duration.

The optimal performance of the engine with pre-chamber C was confirmed with more experiments. The impressive combustion stability allows operation with leaner air/fuel ratios, fulfilling the NO_x emissions according to TA Luft with simultaneous low HC emissions. Thus, the suitability of the pre-chamber C for the high load investigations was substantiated.

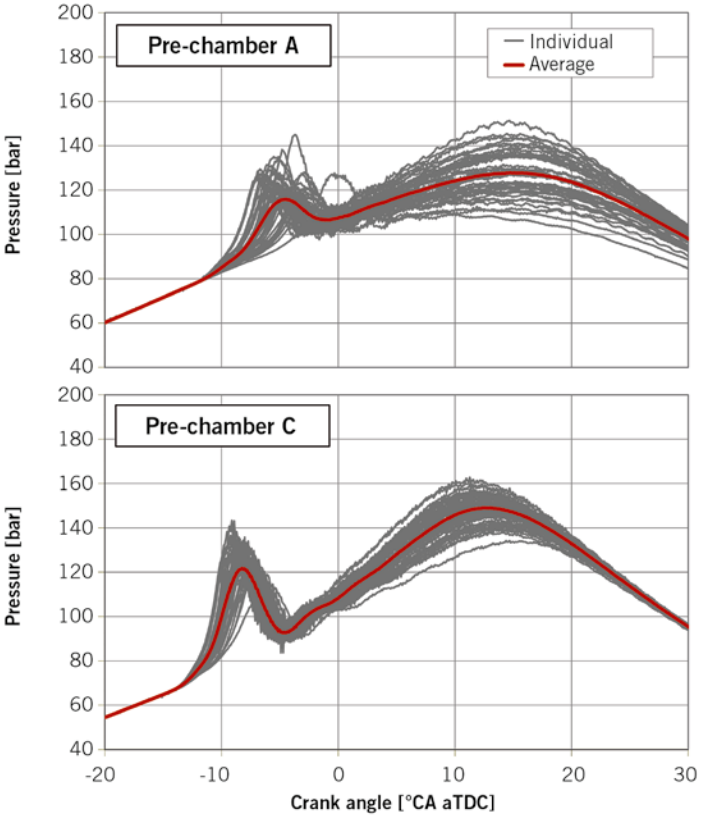

FIGURE 7 Pre-chamber pressure traces (900 rpm, IMEP = 20 bar, rel. $AFR_{main\text{-}chamber}$ = 2.2) (© FEV)

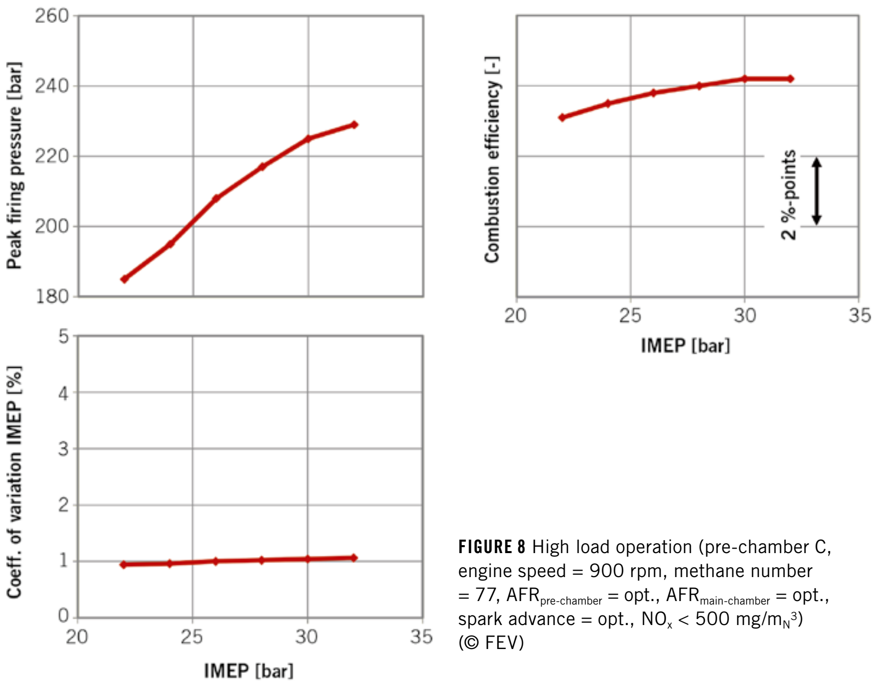

FIGURE 8 High load operation (pre-chamber C, engine speed = 900 rpm, methane number = 77, $AFR_{pre\text{-}chamber}$ = opt., $AFR_{main\text{-}chamber}$ = opt., spark advance = opt., NO_x < 500 mg/m_N^3) (© FEV)

HIGH LOAD

As an example **FIGURE 8** shows a load variation at an engine speed of 900 rpm. The IMEP was limited to 32 bar due to the peak pressure limitation of the base engine. The variation fulfilled the NO_x limit of the TA Luft legislation and shows the impressive capacity of the developed combustion system. Inspite of a relatively low methane number and the NO_x limit, high values for the efficiency could be realised. There was still potential through leaner operation, however, the peak pressure needed to be increased over the allo-

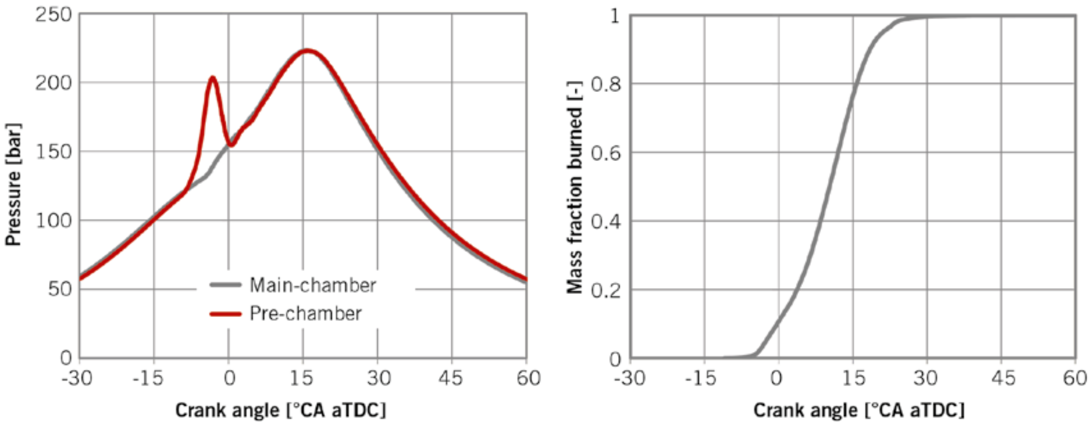

FIGURE 9 Pressure analysis (n = 900 rpm, IMEP = 32 bar) (© FEV)

wed limit. The earlier described excellent combustion stability could be achieved throughout the entire load range.

The (cycle-averaged) pressure trace for the main-chamber and the pre-chamber for the point with maximum load (IMEP = 32 bar) has been shown on the left in **FIGURE 9**. On the right, the burn-rate, which is a result of the pressure analysis, has been plotted. For this analysis, the averaged pressure trace was used.

As a result of the near stoichiometric combustion in the pre-chamber, the burn duration in the pre-chamber amounts to around 11 °CA with a maximum overpressure of about 65 bar. The center of combustion (α_{x50}) lies at 10.6 °CA aTDC. This correlates to a near optimum burn rate in the main-chamber. With a burn duration of 12 °CA for the interval of 5 to 50 %, a high combustion speed could be achieved. The result that the succeeding interval from 50 to 95 % requires only 11.4 °CA, adds to the advantage of the combustion system layout.

CONCLUSION

On a single-cylinder natural gas engine with scavenged pre-chamber, an efficient combustion system was developed at FEV. The cylinder displacement of about 16 l is valid and attractive for different applications (stationary (CHP), locomotive, marine).

In order to reduce the number of hardware variants (pre-chamber designs) to be investigated on the engine test bench, FEV's simulation tool-chain called CMD (Charge Motion Design) was utilised to guide the project. This process considers the complex dependency of the combustion on the turbulence of the cylinder change. The accuracy of the simulation was confirmed by comparing it to the measurements. The usage of the CMD process allows for a significant reduction in time and effort and leads to an overall efficient development path.

An excellent engine operation was achieved with the application of an optimised pre-chamber, whose volume equals state-of-the-art designs. Very high specific power density could be achieved with the developed combustion system owing to its high combustion stability. An IMEP of 32 bar combined with emission-fulfilling values of NO_x and HC emissions could be realised in the engine experiments.

REFERENCES

[1] Umierski, M.: Analyse des Brennverlaufes für stationäre Gas-Ottomotoren mit geteiltem und ungeteiltem Brennraum. Thesis, RWTH Aachen, 1999

[2] Wiese, W.; Pischinger, S.; Adomeit, P.; Ewald, J.: Prediction of Combustion Delay and -Duration of Homogeneous Charge Gasoline Engines based on In-Cylinder Flow Simulation. SAE Technical Paper 2009-01-1796, 2009, doi:10.4271/2009-01-1796

[3] Wiese, W.; Adomeit, P.; Ewald, J.: Charge Motion Development for the Realization of Robust SI Combustion Systems. 11th Conference „Der Arbeitsprozess des Verbrennungsmotors", 2007

[4] Dhongde, A.; Morcinkowski, B.; Deppenkemper, K.; Franzke, B.; Pischinger, S.: Durchgängiger Simulationsprozess zur Verbrennungsvorhersage anhand des Strömungszustands im Zylinder für Otto, Diesel und Gasmotoren. 16th MTZ Congress VPCplus, Hanau, 2014

[5] Franke, M.; Geiger, J.; Lierz, K.; Heuser, P.; Jagodzinski, B.; Schlemmer-Kelling, U.: Development strategies for gas engines in high- and medium-speed applications. ASME 2014 Internal Combustion Engine Division Fall Technical Conference, Columbus, IN, USA, 2014

[6] Umierski, M.; Pleimling, H.; Hüchtebrock, B.: Zyklische Schwankungen des Arbeitsprozesses von Gasmotoren. 3rd Dessauer Conference for Gas Engines, 2003

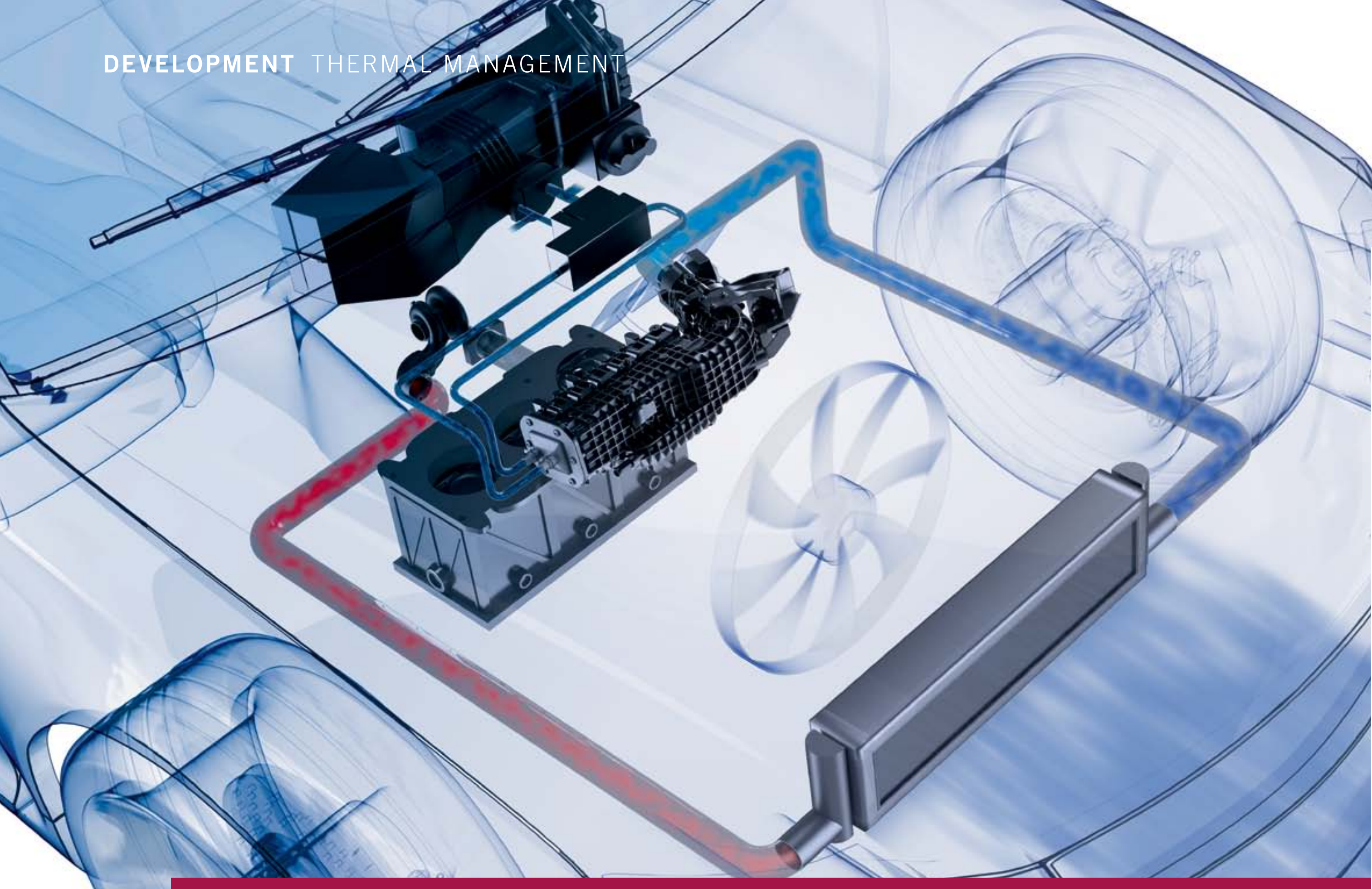

Refrigerant-based Charge Air Subcooling

Downsizing combined with turbocharging is considered as an essential aspect of the on-going development of gasoline engines. Due to the principle involved, the required charge air cooling was previously limited to temperatures above the ambient level. With charge air subcooling, Mahle has undercut this barrier by cooling charge air even further and thereby opening up new potential for longitudinal vehicle dynamics and lower fuel consumption.

GAINING NEW POTENTIAL

Turbocharging brings the improvement of longitudinal vehicle dynamics back into the spotlight, because smaller displacement typically reduces the instantaneous torque response. In order to improve the drivability of smaller, more powerful engines, the responsiveness of the engine at low speeds is critical. In recent years, Mahle has presented air intake modules with integrated indirect and cascaded indirect charge air cooling, two methods for cooling charge air as effectively as possible. With refrigerant-based charge air subcooling below ambient temperature, the company opens up new potential for longitudinal vehicle dynamics and efficiency.

BASIC PRINCIPLES OF CHARGE AIR SUBCOOLING

Charge air that has been heated due to compression is detrimental to combustion, causing higher susceptibility to knocking and thermal loads on engine components. The density of the charge air also falls as the temperature rises, thus

AUTHORS

René Dingelstadt
is Project Manager in the Corporate Advanced Engineering at the Mahle International GmbH in Stuttgart (Germany).

Dr.-Ing. Peter Wieske
is Head of System and Concepts in the Corporate Advanced Engineering at the Mahle International GmbH in Stuttgart (Germany).

Dr. Andreas Eilemann
is Director Predevelopment Engine Cooling Light Vehicles at the Mahle Behr GmbH & Co. KG in Stuttgart (Germany).

Jürgen Stehlig
is Director Global Development Air Intake Modules and Cylinder Head Covers at the Mahle Filtersysteme GmbH in Stuttgart (Germany).

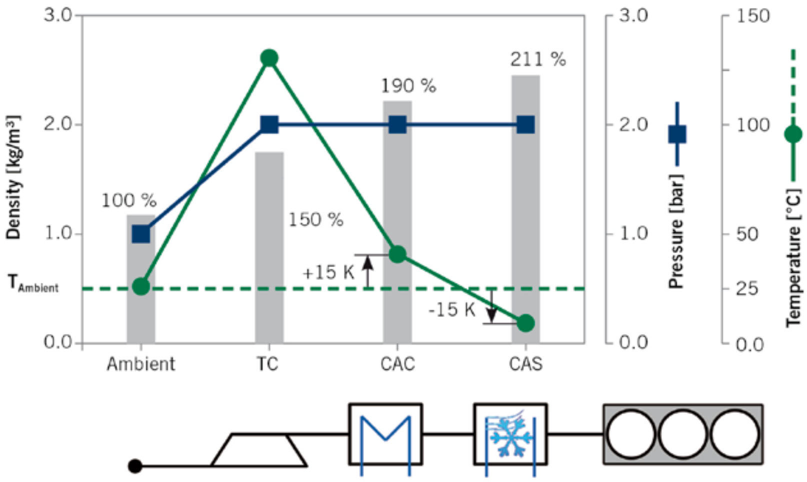

FIGURE 1 Change in charge air density and temperature due to turbocharging (TC), charge air cooling (CAC) and charge air subcooling (CAS) (© Mahle)

reducing the maximum quantity of oxygen allowed in the combustion chamber. Based on ambient conditions, a turbocharger doubling the pressure results in an increase in charge air density of only 50 %, due to the higher temperature caused by the compressor. The downstream cooling of the charge air to about 15 K above ambient temperature increases its density by another 40 %, which means that the turbocharger and charge air cooler each contribute a similar amount to the increase in intake air density. Subcooling the charge air, for example to 15 K below ambient temperature, would increase the charge air density by another 21 % which is equivalent to raising boost pressure by 200 mbar, **FIGURE 1**.

Charge air can be subcooled by tapping the surplus cooling performance of the air conditioning circuit available after initial cooling the passenger compartment. The air conditioning circuit is generally designed to cool off the passenger compartment quickly when outside temperatures are high. Afterwards, it uses less of its capacity to maintain the climate. For a typical mid-size vehicle – depending on the ambient conditions and humidity – the excess cooling performance after initially cooling down a compartment in Europe can be assumed to be 3 to 5 kW [1, 2].

SYSTEM DESCRIPTION

FIGURE 2 shows the schematic design of an indirect charge air subcooling system integrated in the air intake module (iCAS). In comparison with the non-inte-

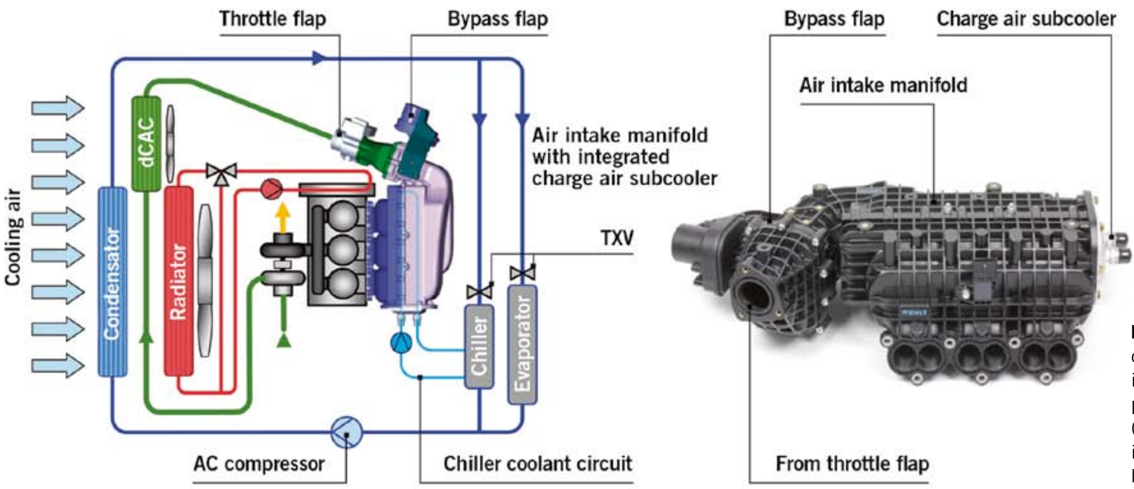

FIGURE 2 Schematic diagram of the applied iCAS system (left) and prototype hardware (air intake module with integrated iCAS and bypass, right) (© Mahle)

grated "add-on" variant, the integrated solution has clear advantages in transient responsiveness owing to the shorter charge air paths [2]. For the integrated charge air subcooling system, both the bypass and the indirect heat exchanger are incorporated in the air intake module. In addition, a chiller (refrigerant/coolant heat exchanger) with an expansion valve (TXV) is connected in parallel with the cabin evaporator of the A/C-system. The two thermal expansion valves are switchable, so that the chiller and/or the cabin evaporator can be cut off from the refrigerant flow. The chiller feeds subcooled coolant to the heat exchanger integrated in the iCAS air intake module via an intermediate circuit.

When evaluating charge air subcooling, the additional power consumption associated with the air conditioning compressor must be considered. The climate conditions in particular will affect the benefit that can be achieved with respect to responsiveness or fuel savings. Measurements show that the ratio of power gained from subcooling to the power consumption of the air conditioning compressor is over 4:1 at an ambient temperature of 25 °C and relative humidity of 50 %. The optimised design, with an intermediate coolant circuit (indirect system), can utilise the thermal inertia of the intermediate circuit to separate the loading and unloading of the system in time and to further increase the ratio to above 5:1 [2]. The bypass valve integrated in the intake module can be used to invoke the subcooling function as needed. This allows the system both to be pre-conditioned for rapid load demands on the combustion engine and to run without subcooling when under partial load.

UTILISING THE HUMIDITY CONDENSATE

The humidity of the intake air condenses when the temperature falls below the dew point. A relative humidity of 100 % at an air temperature of 10 °C and absolute boost pressure of 2 bar limits the relative humidity of the intake air at an ambient pressure of 1 bar and 25 °C to 20 %. If the humidity of the intake air is greater, condensation will occur. Due to this condensation, the required cooling performance increases by the amount of the heat of condensation of the water that is condensed, **FIGURE 3**.

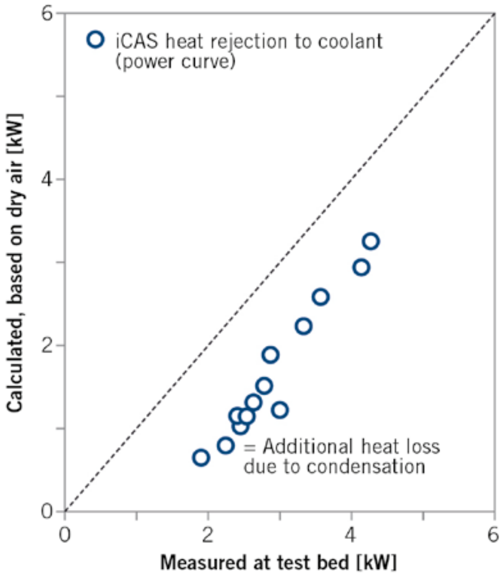

FIGURE 3 Measured vs. theoretical charge air cooling performance required for condensation-free dry air; full-load curve of a turbocharged 1.0 l engine (© Mahle)

FIGURE 3 shows the required cooling performance for the charge air with 15 K subcooling, as derived from the coolant balance, in comparison with the cooling performance needed for dry air. The measurement points are on the full-load curve of a turbocharged 1.0 l engine, intake air has a temperature of 25 °C and relative humidity of 50 %, and absolute boost pressure ranges between 1.8 and 2.0 bar. As the measurements show, due to the condensation of air humidity, the required cooling performance is always greater than the theoretical required cooling performance for dry air. Below the dew point, the ratio of air charge gain to the required cooling performance is indeed worse than at operating points without condensation. However, the advantages of introducing water into the combustion chamber are well known [3] and are the subject of current studies [4, 5]. **FIGURE 4** shows the influence of condensed intake air humidity on the spark angle that can be applied in knock-limiting operation. Starting from a condensation-free operating point (30 °C charge air, ambient air at 25 °C and 50 % relative humidity), dropping the charge air temperature to 10 °C allows the spark angle to be advanced by 2 °CA. Increasing the relative humidity from 50 to 90 % allows the ignition angle to be improved by another degree, and thus a good half a degree earlier MFB 50. The condensate drops that enter the combustion chamber do not directly influence the air temperature at first.

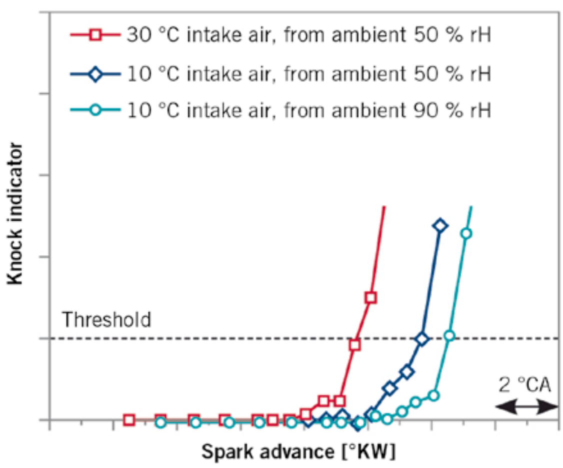

FIGURE 4 Influence of charge air temperature and humidity on the applicable ignition angle (© Mahle)

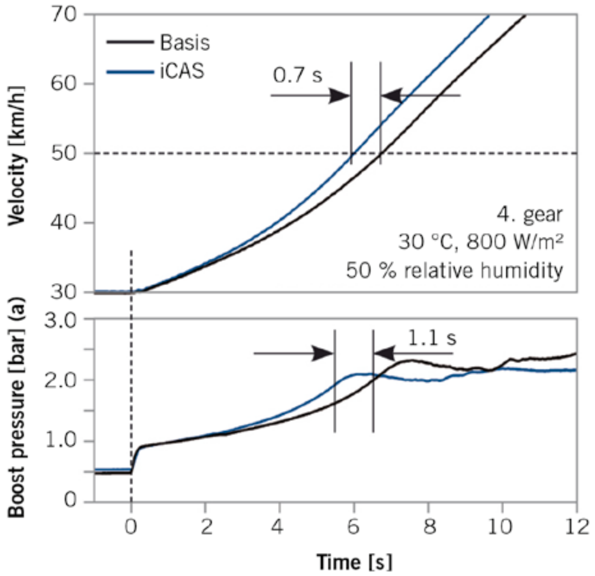

FIGURE 5 Results – acceleration behaviour with iCAS (© Mahle)

During the compression stroke, when the drops evaporate again, do they ultimately contribute to lower temperatures in the combustion chamber at the start of combustion.

The flow guidance in the air intake module is designed to prevent the accumulation of large amounts of condensate and to ensure that occurring condensate is distributed as evenly as possible among the individual cylinders. The bypass feature of the iCAS in particular ensures that the charge air subcooler only operates with large mass air flows.

VEHICLE RESULTS: ACCELERATION BEHAVIOUR

Mahle has installed the air intake module with integrated iCAS in a compact-class demonstrator vehicle in order to verify the gain in longitudinal vehicle dynamics, to investigate the effects of parallel operation of the cabin evaporator and the chiller, and to determine the potential of a recuperative loading strategy [2]. For the test, an acceleration of 30 km/h to 50 km/h was performed in fourth gear at 30 °C ambient temperature, 50 % relative air humidity, and 800 W/m² simulated solar load in a climatic wind tunnel, **FIGURE 5**. The air conditioning compressor is disengaged during acceleration in both cases. In the case of iCAS, the thermal inertia of the charged iCAS intermediate circuit ensures charge air subcooling. For the iCAS variant, the bypass valve is switched at the beginning and the charge air is fed through the subcooling path. The charge air at the cylinder inlet is thus cooled down by 25 K.

As the measurements show, boost pressure builds up more quickly due to the increased density and simultaneous reduction in charge air temperature. The time needed to reach 90 % of the steady-state full scale value is reduced by 1.1 s in comparison with the baseline. Overall, the vehicle reaches the target speed 0.7 s earlier than the variant without iCAS.

Both variants are applied such that they use the same effective torque once the torque plateau is reached. The increased dynamics are thus limited to the lower speed range with the wastegate closed. An additional torque increase seems entirely possible, however, based on the previously unused engine potential with respect to boost pressure and peak pressure level as well as to protect components.

VEHICLE RESULTS: RECUPERATION OF BRAKING ENERGY

Especially in order to demonstrate the potential of braking energy recuperation via the air conditioning compressor, and thus into the iCAS, a hypothetical driving profile was run in the climatic wind tunnel. The vehicle accelerated from 30 to 130 km/h, **FIGURE 6**. After driving at this speed, the vehicle braked down to 30 km/h again. The air conditioning compressor is disengaged from the engine during the entire acceleration phase. Performing this test thus simulates the maximum heat input to the iCAS intermediate circuit. The temperature of the intermediate coolant circuit thus rises from 10 to 20 °C. Nevertheless, the charge air can be subcooled by 20 °K throughout the entire acceleration process. During the subsequent phase at constant speed, the charge air subcooling system is switched off and the charge air is fed through the bypass. When the brake pedal is actuated, the air conditioning compressor is fully engaged and the iCAS intermediate circuit is subcooled again. The results of this test show that the energy absorbed during the acceleration phase can be discharged from the system again for braking deceleration up to about -2 m/s² via the air conditioning compressor engaged at maximum power. At higher heat input levels or greater braking deceleration, of course, only part of this energy can be recuperatively removed from the system. By storing the subcooling energy in the iCAS intermediate circuit, the heat input and output are separated in time. The heat output shifts from the acceleration phase into the braking phase, which reduces the required cooling performance during the acceleration phase. Even if the potential for recuperative support of cabin air conditioning is limited for reasons of comfort, the combination of the chiller and the thermal mass of the intermediate circuit are an ideal recipient for recuperative cooling performance.

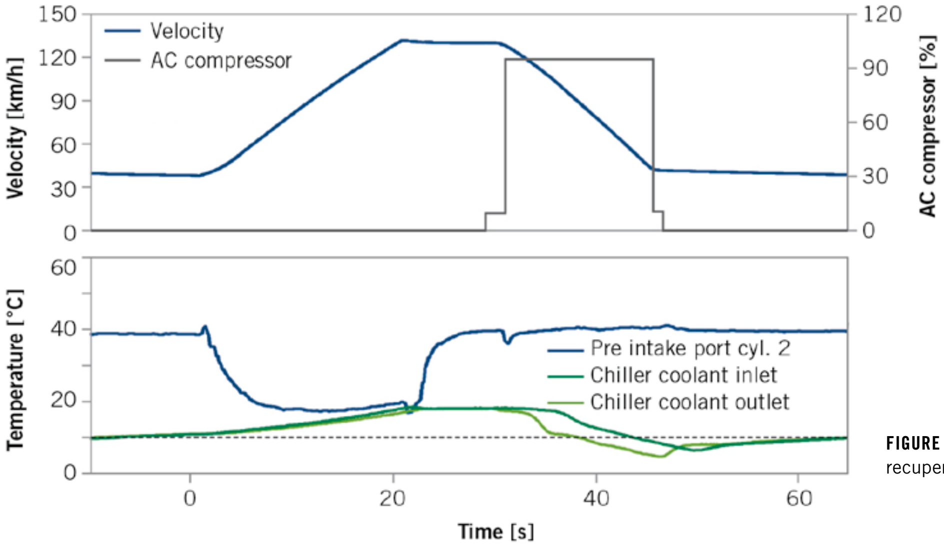

FIGURE 6 Results – vehicle measurements with recuperation of braking energy (© Mahle)

SUMMARY

Charge air subcooling can be suitable supplement to conventional charge air cooling, particularly in gasoline engines. The surplus capacity of the air conditioning system available after cooling the passenger compartment is sufficient for subcooling air mass flows up to 300 kg/h, thus improving longitudinal vehicle dynamics. iCAS is thus particularly well suited for engines with displacements between 1.0 and 1.5 l, and for larger displacement engines with appropriate adjustments to the operating range. When the temperature falls below the dew point, the intake air humidity condenses and the resulting evaporative cooling thus contributes to better conditions at start of combustion. While simultaneously providing the cooling performance required for subcooling, the power gained in the lower speed range is four times greater than the power consumed by the air conditioning compressor. A simple thermal storage system can be implemented with the intermediate circuit and the chiller, allowing charge air subcooling even when the air conditioning compressor is disengaged during acceleration, and recuperative recharging during braking phases. An air-side bypass allows the charge air subcooling to be focused on the upper load range as required.

REFERENCES

[1] Wieske, P.; Dingelstadt, R.; Warth, M.; Stehlig, J.; Eilemann, A.; Tremble, P.: Improvement of transient response with charge air subcooling: An Integrative Approach, 23rd Aachen Colloquium
[2] Eilemann, A.; Wieske, P.; Warth, M.; Stehlig, J.: Charge Air Subcooling – enabler for improved drivability and fuel economy, Vienna Motor Symposium 2015
[3] Wassereinspritzung in Vergasermotoren, MTZ 2 (1940), No. 4, p. 134
[4] „Official Car of MotoGP™“: BMW M startet mit innovativer Technologie in die Saison 2015; BMW press release, 03/30/2015,
[5] Bulander, R.: Powertrain optimization using a comprehensive systems approach, Vienna Motor Symposium 2015

IMPRINT

MTZ

WORLDWIDE

www.MTZonline.com

Founded 1939 by Prof. Dr.-Ing. E. h. Heinrich Buschmann and Dr.-Ing. E. h. Prosper L'Orange

Organ of the Fachverband Motoren und Systeme im VDMA, Verband Deutscher Maschinen- und Anlagenbau e.V., Frankfurt/Main, for the areas combustion engines and gas turbines
Organ of the Forschungsvereinigung Verbrennungskraftmaschinen e.V. (FVV)
Organ of the Wissenschaftliche Gesellschaft für Kraftfahrzeug- und Motorentechnik e.V. (WKM)
Organ of the Österreichischer Verein für Kraftfahrzeugtechnik (ÖVK)
Cooperation with the STG, Schiffbautechnische Gesellschaft e.V., Hamburg, in the area of ship drives by combustion engine

10I2015 _ Volume 76
Springer Vieweg I Springer Fachmedien Wiesbaden GmbH
P. O. Box 15 46 · 65173 Wiesbaden · Germany I Abraham-Lincoln-Straße 46 · 65189 Wiesbaden · Germany

Amtsgericht Wiesbaden, HRB 9754, USt-IdNr. DE811148419
Managing Directors Armin Gross, Joachim Krieger, Dr. Niels Peter Thomas

Managing Director Marketing & Sales Armin Gross I **Director Magazines** Stefanie Burgmaier I **Director Production** Dr. Olga Chiarcos

EDITORIAL STAFF

EDITORS IN CHARGE
Dr. Johannes Liebl, Wolfgang Siebenpfeiffer

EDITOR IN CHIEF
(responsible for editorial content)
Dr. Alexander Heintzel
phone +49 611 7878-342 · fax +49 611 7878-462
alexander.heintzel@springer.com

DEPUTY EDITOR IN CHIEF
Dipl.-Journ. (FH) Martin Westerhoff
phone +49 611 7878-120 · fax +49 611 7878-462
martin.westerhoff@springer.com

MANAGING EDITOR
Kirsten Beckmann M. A.
phone +49 611 7878-343 · fax +49 611 7878-462
kirsten.beckmann@springer.com

EDITORS
Angelina Hofacker
phone +49 611 7878-121 · fax +49 611 7878-462
angelina.hofacker@springer.com
Dipl.-Ing. Ulrich Knorra
phone +49 611 7878-314 · fax +49 611 7878-462
ulrich.knorra@springer.com
Dipl.-Ing. Michael Reichenbach
phone +49 611 7878-341 · fax +49 611 7878-462
michael.reichenbach@springer.com
Markus Schöttle
phone +49 611 7878-257 · fax +49 611 7878-462
markus.schoettle@springer.com

PERMANENT CONTRIBUTORS
Dipl.-Ing. (FH) Richard Backhaus, Andreas Burkert, Dipl.-Ing. (FH) Andreas Fuchs, Roland Schedel, Stefan Schlott

ENGLISH LANGUAGE CONSULTANT
Paul Willin

ONLINE I ELECTRONIC MEDIA
Portal Manager Automotive
Christiane Brünglinghaus
phone +49 611 7878-136 · fax +49 611 7878-462
christiane.bruenglinghaus@springer.com
Editorial Staff
Katrin Pudenz M. A.
phone +49 6172 301-288 · fax +49 6172 301-299
redaktion@kpz-publishing.com

SPECIAL PROJECTS
Managing Editorial Journalist
Markus Bereszewski
phone +49 611 7878-122 · fax +49 611 7878-462
markus.bereszewski@springer.com
Editorial Staff I Coordination
Dipl.-Reg.-Wiss. Caroline Behle
phone +49 611 7878-393 · fax +49 611 7878-462
caroline.behle@springer.com
Christiane Imhof M. A.
phone +49 611 7878-154 · fax +49 611 7878-462
christiane.imhof@springer.com

PROJECT MANAGEMENT I ASSISTANCE
Yeliz Konar
phone +49 611 7878-180 · fax +49 611 7878-462
yeliz.konar@springer.com
Martina Schraad
phone +49 611 7878-276 · fax +49 611 7878-462
martina.schraad@springer.com

ADDRESS
Abraham-Lincoln-Straße 46 · 65189 Wiesbaden
P. O. Box 1546 · 65173 Wiesbaden, Germany
redaktion@ATZonline.de

ADVERTISING

SALES MANAGEMENT
(responsible for advertising)
Volker Hesedenz
phone +49 611 7878-269 · fax +49 611 7878-78269
volker.hesedenz@best-ad-media.de

MEDIA SALES
Frank Nagel
phone +49 611 7878-395 · fax +49 611 7878-78395
frank.nagel@best-ad-media.de

KEY ACCOUNT MANAGEMENT
Rouwen Bastian
phone +49 611 7878-399 · fax +49 611 7878-78399
rouwen.bastian@best-ad-media.de

DISPLAY AD MANAGER
Nicole Brzank
tel +49 611 7878-616 · fax +49 611 7878-78164
nicole.brzank@best-ad-media.de

AD PRICES
Advertising ratecard from October 2014.

MARKETING I OFFPRINTS

HEAD OF MARKETING MAGAZINES + EVENTS
Jens Fischer
phone +49 611 7878-340 · fax +49 611 7878-407
jens.fischer@springer.com

OFFPRINTS
Martin Leopold
phone +49 2642 907-596 · fax +49 2642 907-597
leopold@medien-kontor.de

PRODUCTION I LAYOUT
Heiko Köllner
phone +49 611 7878-177 · fax +49 611 7878-78177
heiko.koellner@springer.com

All persons specified may be contacted by post at the publisher's address.

SUBSCRIPTIONS
Springer Customer Service Center GmbH
Haberstraße 7 · 69126 Heidelberg · Germany
phone +49 6221 3454-303 · fax +49 6221 3454-229
Monday to Friday, 8 a.m. to 6 p.m.
springervieweg-service@springer.com
www.my-specialized-knowledge.com/automotive

ORDERING OPTIONS
The eMagazine MTZworldwide appears 11 times a year for subscribers. Ordering options and details on the subscription conditions can be found at www.my-specialized-knowledge.com/MTZworldwide.

YOUR HOTLINE TO MTZ

Editorial Staff
☎ +49 611 7878-120
Customer Service
☎ +49 6221 3454-303
Advertising
☎ +49 611 7878-395

The articles published in MTZworldwide are produced with the greatest possible care and attention. However, the editors do not accept any liability for the correctness, completeness and current accuracy of the content printed. The content of advertisements is the sole responsibility the advertiser.

Every annual subscription includes access to the online archive at Springer für Professionals. Access is available exclusively to the individual subscriber and is not transferable.

No liability can be accepted for the unsolicited submission of manuscripts, photographs or illustrations.

Springer Vieweg is part of Springer Science+Business Media.

Springer Vieweg

PEER REVIEW

Peer Review Process for Research Articles in ATZ, MTZ and ATZelektronik

STEERING COMMITTEE

Prof. Dr.-Ing. Lutz Eckstein	RWTH Aachen University	Institut für Kraftfahrzeuge Aachen
Prof. Dipl.-Des. Wolfgang Kraus	HAW Hamburg	Department Fahrzeugtechnik und Flugzeugbau
Prof. Dr.-Ing. Ferit Küçükay	Technische Universität Braunschweig	Institut für Fahrzeugtechnik
Prof. Dr.-Ing. Stefan Pischinger	RWTH Aachen University	Lehrstuhl für Verbrennungskraftmaschinen
Prof. Dr.-Ing. Hans-Christian Reuss	Universität Stuttgart	Institut für Verbrennungsmotoren und Kraftfahrwesen
Prof. Dr.-Ing. Ulrich Spicher	MOT	
Prof. Dr.-Ing. Hans Zellbeck	Technische Universität Dresden	Lehrstuhl für Verbrennungsmotoren

ADVISORY BOARD

Prof. Dr.-Ing. Klaus Augsburg
Prof. Dr.-Ing. Michael Bargende
Prof. Dipl.-Ing. Dr. techn. Christian Beidl
Prof. Dr. sc. techn. Konstantinos Boulouchos
Prof. Dr. Dr. h.c. Manfred Broy
Prof. Dr.-Ing. Ralph Bruder
Dr. Gerhard Bruner
Prof. Dr. rer. nat. Heiner Bubb
Prof. Dr. rer. nat. habil. Olaf Deutschmann
Prof. Dr.-Ing. Klaus Dietmayer
Dr. techn. Arno Eichberger
Prof. Dr. techn. Helmut Eichlseder
Prof. Dr. Wilfried Eichlseder
Dr.-Ing. Gerald Eifler
Prof. Dr.-Ing. Wolfgang Eifler
Prof. Dr. rer. nat. Frank Gauterin
Prof. Dr. techn. Bernhard Geringer
Prof. Dr.-Ing. Uwe Dieter Grebe
Dr. mont. Christoph Guster
Prof. Dr.-Ing. Holger Hanselka
Prof. Dr.-Ing. Horst Harndorf
Prof. Dr. techn. Wolfgang Hirschberg
Prof. Dr. techn. Peter Hofmann
Prof. Dr. rer. nat. Peter Holstein
Prof. Dr.-Ing. Volker von Holt
Prof. Dr.-Ing. habil. Werner Hufenbach
Prof. Dr.-Ing. Armin Huß
Dr. techn. Heidelinde Jetzinger
Prof. Dr.-Ing. Roland Kasper
Prof. Dr.-Ing. Prof. E. h. mult. Rudolf Kawalla
Prof. Dr.-Ing. Tran Quoc Khanh
Dr. Philip Köhn
Prof. Dr.-Ing. Ulrich Konigorski
Prof. Dr. Oliver Kröcher
Prof. Dr.-Ing. Peter Krug
Dr. Christian Krüger
Prof. Dr. techn. Thomas Lauer
Prof. Dr. rer. nat. Uli Lemmer
Dr. Malte Lewerenz
Prof. Dr.-Ing. Markus Lienkamp
Prof. Dr. rer. nat. habil. Ulrich Maas
Prof. Dr.-Ing. Markus Maurer
Prof. Dr.-Ing. Martin Meywerk
Ao. Univ.-Prof. Dr. Gregor Mori
Prof. Dr.-Ing. Klaus D. Müller-Glaser
Dr. techn. Reinhard Mundl
Prof. Dr. rer. nat. Peter Neugebauer
Prof. Dr. rer. nat. Cornelius Neumann
Prof. Dr.-Ing. Nejila Parspour
Prof. Dr.-Ing. Peter Pelz
Prof. Dr. techn. Ernst Pucher
Dr. Jochen Rauh
Prof. Dr.-Ing. Konrad Reif
Prof. Dr.-Ing. Stephan Rinderknecht
Prof. Dr.-Ing. Jörg Roth-Stielow
Dr.-Ing. Swen Schaub
Prof. Dr. sc. nat. Christoph Schierz
Prof. Dr. rer. nat. Christof Schulz
Prof. Dr. rer. nat. Andy Schürr
Prof. Dr.-Ing. Ulrich Seiffert
Prof. Dr.-Ing. Hermann J. Stadtfeld
Prof. Dr.-Ing. Karsten Stahl
Prof. Dr. techn. Hermann Steffan
Prof. Dr.-Ing. Wolfgang Steiger
Prof. Dr.-Ing. Peter Steinberg
Dr.-Ing. Peter Stommel
Dr.-Ing. Ralph Sundermeier
Prof. Dr.-Ing. Wolfgang Thiemann
Prof. Dr.-Ing. Dr. h.c. Helmut Tschöke
Prof. Dr.-Ing. Georg Wachtmeister
Prof. Dr.-Ing. Jochen Wiedemann
Prof. Dr. rer. nat. Gerhard Wiegleb
Prof. Dr. techn. Andreas Wimmer
Prof. Dr. rer. nat. Hermann Winner
Prof. Dr. med. habil. Hartmut Witte
Dr.-Ing. Michael Wittler

Scientific articles of universities in ATZ Automobiltechnische Zeitschrift, MTZ Motortechnische Zeitschrift and ATZelektronik are subject to a proofing method, the so-called peer review process. Articles accepted by the editors are reviewed by experts from research and industry before publication. For the reader, the peer review process further enhances the quality of the magazines' content on a national and international level. For authors in the institutes, it provides a scientifically recognised publication platform.

In the Peer Review Process, once the editors has received an article, it is reviewed by two experts from the Advisory Board. If these experts do not reach a unanimous agreement, a member of the Steering Committee acts as an arbitrator. Following the experts' recommended corrections and subsequent editing by the author, the article is accepted.

In 2008, the peer review process utilised by ATZ and MTZ was presented by the WKM (Wissenschaftliche Gesellschaft für Kraftfahrzeug- und Motorentechnik e. V./ German Professional Association for Automotive and Motor Engineering) to the DFG (Deutsche Forschungsgemeinschaft/German Research Foundation) for official recognition. ATZelektronik participates in the Peer Review since 2011.

THE SEAL OF APPROVAL FOR SCIENTIFIC ARTICLES IN MTZ.
MTZ PEER REVIEW
REVIEWED BY EXPERTS FROM RESEARCH AND INDUSTRY.

Modelling and Verification of Practice-relevant Journal-bearing Properties

For high-speed rotors in turbines, compressors, transmission gears and electric motors, fluid-film bearings are preferentially employed for ensuring high availability as well as maximal reliability during continuous operation. Exact prediction and experimental verification of the bearing characteristics are thus of vital technical importance. Consequently, a joint FVV-FVA project has been initiated at the Institute of Tribology and Energy Conversion Machinery at Clausthal University of Technology for supporting comprehensive experimental investigations on hydrodynamic bearings.

THE SEAL OF APPROVAL FOR SCIENTIFIC ARTICLES IN MTZ.
MTZ
PEER REVIEW
RECEIVED 2015-03-10
REVIEWED 2015-05-05
ACCEPTED 2015-06-25
REVIEWED BY EXPERTS FROM RESEARCH AND INDUSTRY.

AUTHORS

Dr.-Ing. Hardwig Blumenthal
is Member of the Scientific Staff at the Institute of Tribology and Energy Conversion Machinery at the the Clausthal University of Technology (Germany).

Prof. Dr.-Ing. Hubert Schwarze
is Head of the Institute of Tribology and Energy Conversion Machinery at the Clausthal University of Technology (Germany).

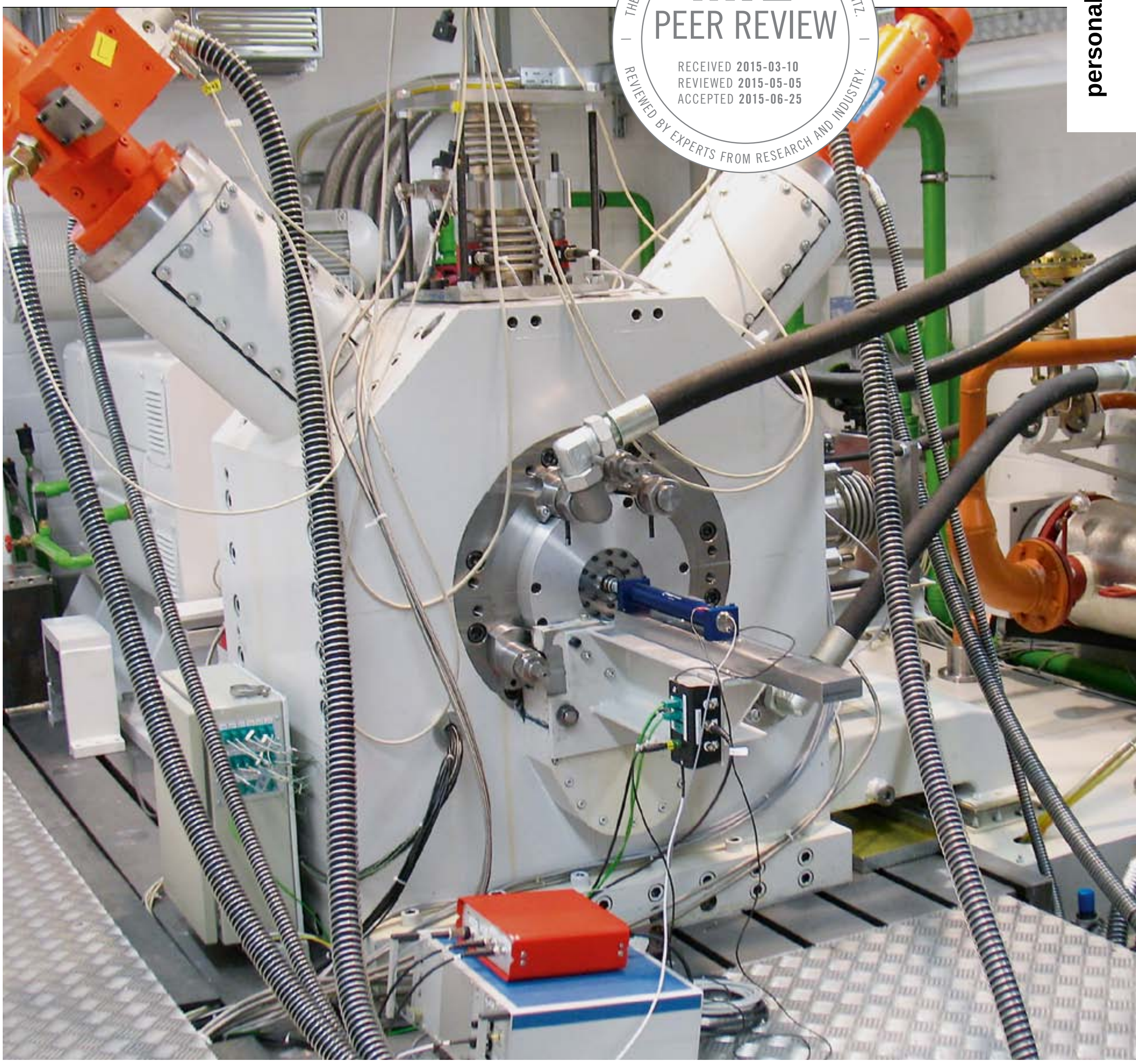

1 INTRODUCTION
2 CURRENT STATUS OF THE RESEARCH
3 DESCRIPTION OF THE TEST RIG
4 RESULTS
5 SUMMARY

1 INTRODUCTION

The static and dynamic properties of hydrodynamic radial bearings depend on the static journal eccentricity, the bearing-width ratio, and the bore profile, among other factors. In numerous research projects, corresponding characteristic curves have been determined both theoretically and experimentally for bearing bores of different shapes under various operating conditions. The effect of the journal bearing on the vibrational and stability characteristics of high-speed rotors has likewise been investigated by various methods; see for instance [1-4]. The results of these investigations indicate that the operational behaviour of rotors with journal bearings can be reliably predicted only if all conditions taken as basis for the theory have also been verified in practice.

2 CURRENT STATUS OF THE RESEARCH

The static and dynamic bearing-pressure distribution in hydrodynamic bearings is determined theoretically by solving Reynolds' differential equation with the application of finite-difference or finite-volume methods or with the use of finite-element formulations or similar techniques. Modelling of the lubrication conditions in zones with a diverging gap or in regions with cavitation is complex, since the subsequent effects depend on the gas content in the lubricant and on the existing ventilation possibilities. However, the gas phase consists essentially of air, and the saturation pressure of the air dissolved in the lubricant is close to the ambient pressure. As the dissolved air emerges from the lubricant, air is drawn laterally from the surroundings into the bearing. This process is described in [5] and [6], for instance. For determining the temperature distribution and the variable viscosity in the lubricant film, the energy equation must be employed. For a more exact determination of the maximal operating temperature as well as the temperature distribution, the heat conduction must also be considered. Furthermore, the turbulence of the lubricant film must be taken into account for designing and dimensioning high-speed journal bearings, since this factor also affects the heat conduction in the lubricant film, the power loss, and the stability reserve [7-9].

On the basis of the investigations known to date, the calculation programmes ALP3T and ALP3TA (for radial and axial bearings, respectively) as well as SR3 (rotor dynamics) and also the present calculation software Combros/Combros-A (radial- and axial-bearing calculations) have been developed in the German-speaking countries. Within the scope of joint research projects by the Research Association for Combustion Engines (FVV) and the Power Transmission Engineering Research Association (FVA), these programmes have been placed at the disposal of many users for a wide range of applications. At present, the bearing characteristics of turbomachinery for high circumferential velocities and high specific loads can be reliably determined in advance with the application of existing methods of calculation, provided that the operational parameters as well as the effective lubricant-gap geometry during operation are known with sufficient accuracy. However, these prerequisites are not satisfied for many practical applications. Moreover, the availability of special test rigs which are capable of operating at a maximal circumferential velocity above 120 m/s and with specific bearing loads above 4 MPa is still very limited at present. Nevertheless, a highly exact experimental determination of the tribological and fluid-mechanical as well as rotor-dynamic processes in journal bearings under severe loads and at high to ultrahigh circumferential velocities is an essential prerequisite for calibration of the models documented in the literature. Furthermore, the availability of the highly complex technical equipment which is necessary for measuring and testing of hydrodynamic bearings is a vital requirement for the machine-construction industry. Facilities of this kind would be especially beneficial to small and medium-sized enterprises, where complex bearing systems are manufactured or installed in highly critical machinery. These companies are usually not capable of performing such elaborate tests themselves.

Experimental verification of the results obtained by the applied solution techniques is a prerequisite for the theoretical treatment of the relevant physical effects at very high circumferential velocities. Consequently, the FVV/FVA Research Group Fluid-Film Bearings has initiated the joint project, High-Performance Bearing Test Rig, with intensive participation by various industrial partners [10]. As a result of this project, a test rig has been designed and constructed at the Institute of Tribology and Energy Conversion Machinery at Clausthal University of Technology. With the use of this test rig, highly accurate and comprehensive measurements can be performed on representative journal and thrust bearings as well as combined thrust-journal bearings for turbomachinery, as demanded in practice.

3 DESCRIPTION OF THE TEST RIG

For designing the test rig, the following essential test requirements have been taken as basis:
– stationary and dynamic testing of hydrodynamically as well as hydrostatically supported radial and axial bearings (including single- and double-action axial bearings)
– determination of values in the lubrication gap (pressure, gap width, temperature, flow regime)
– measurement of the lubricant flow rate at the positions of all bearings
– determination of the power losses (from the measurement of the supplied volume flow rates and temperature differences in the inlets and outlets near the bearing)
– measurement and recording of segment motion on tilting-pad bearings
– investigation of misalignment effects (especially in the case of axial bearings).

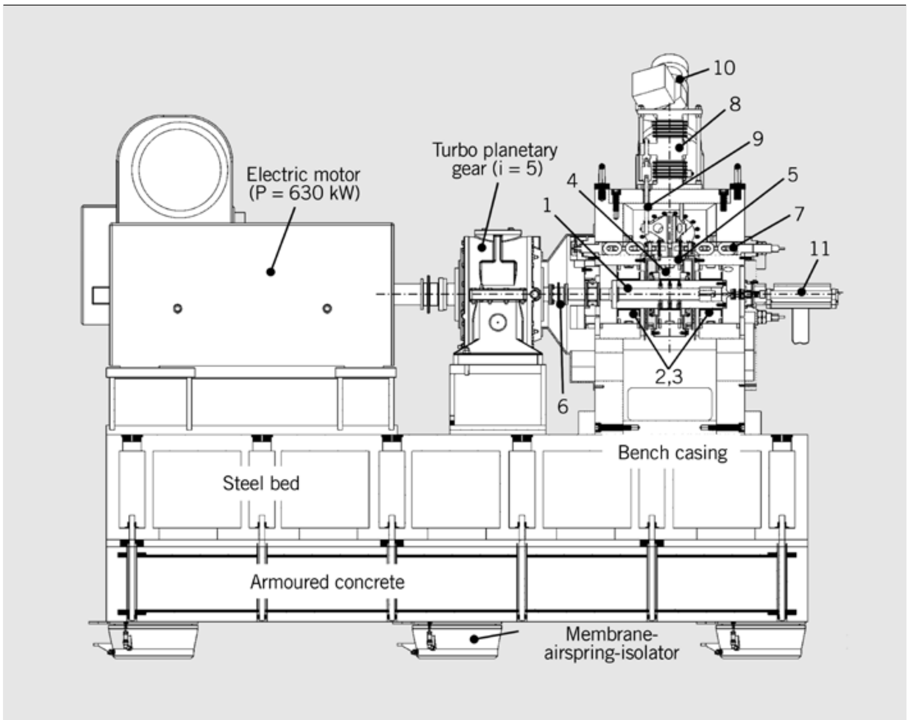

FIGURE 1 Overall view of the high-performance journal-bearing test rig (© TU Clausthal)

On the basis of the demand profile which resulted from these test requirements, as well as the results of preliminary investigations, a high-performance bearing test rig has been designed, constructed, and put into operation. The basic structure of this test rig at the design and application stage for the investigation of hydrodynamic radial bearings is illustrated in **FIGURE 1**.

The test-bearing shaft (1) is suspended in the support bearings (2, 3). The test bearing (4) is installed in the test-bearing housing

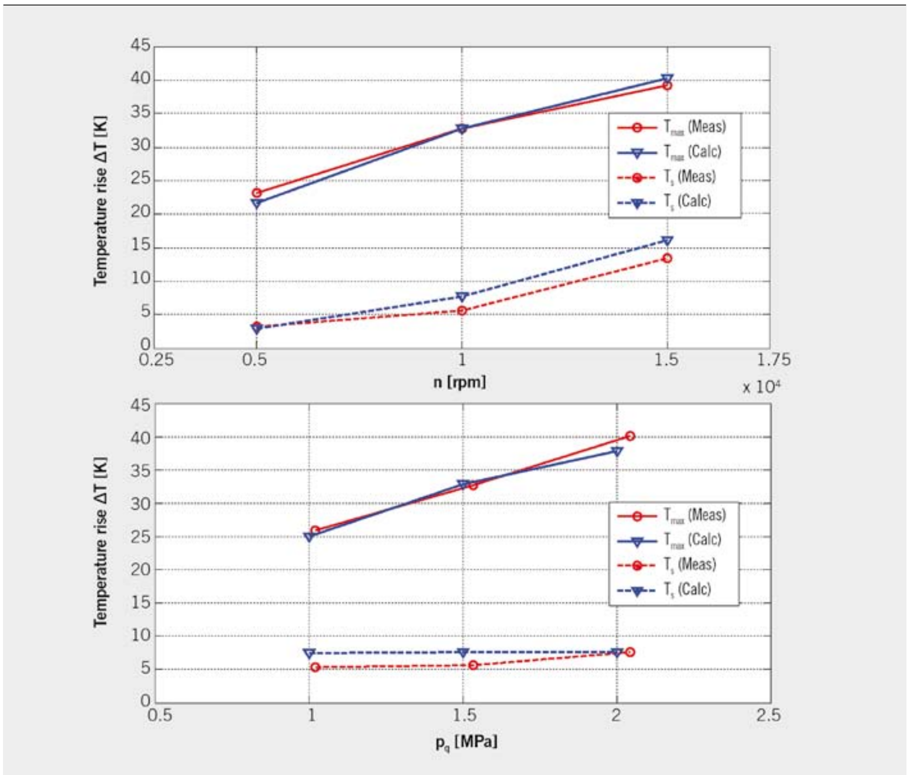

FIGURE 2 Calculated and measured temperature increase at the measuring points of an offset-halves bearing as a function of the rotational speed and load; circumferential velocity: 35 to 95 m/s (© TU Clausthal)

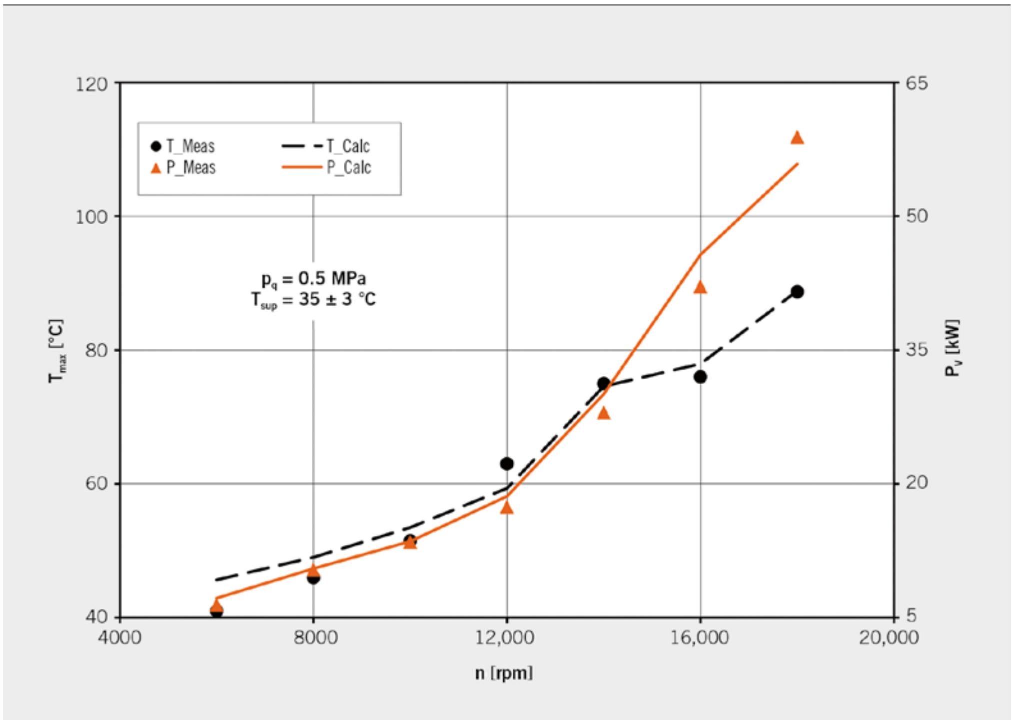

FIGURE 3 Calculated and measured maximal measuring-point temperature and power loss in an offset halves bearing; circumferential velocity: 35 to 110 m/s (© TU Clausthal)

(5). The drivetrain is completed by a compensation coupling which allows angular motion (6). The radially movable test bearing is adjusted and guided either in parallel with the axis or in a misaligned condition by a system consisting of six chains which allow displacement in the transverse direction (7). A double-action pneumatic compensator (8) is connected to the test-bearing housing by coupling rods (9) and introduces a static load in the vertical direction. By means of a further compensator set which is displaced by an angle of 90°, a horizontal load can be imposed on the test bearing. The purposes of the metal bellows are the adjustment of the angular position of the static load vectors as well as positioning and alignment of the test bearing within the range of bearing clearance. Furthermore, two hydropulse cylinders (10) are arranged at a displacement angle of 90° on the test-bearing housing. By means of transversely elastic coupling rods, the cylinders are coupled to the stator system, and the dynamic test loads are thus introduced. A rotary signal transmitter (11) is employed for wired transmission of the measured signal from the rotating gap sensors to the stationary system.

4 RESULTS

In the course of the comprehensive approval-test procedure, experimental investigations have been performed during the various progressive stages of design and application. For this purpose, different operating conditions were considered by variation of the rotational speed and load as functions of the specific properties of the test bearings. Moreover, investigations were performed with static as well as dynamic load forces. For verification of the test-rig functions, the results of these measurements were compared with the predictions obtained with the Combros/Combros-A software for hydrodynamic bearing calculations. These numerical computation programmes are based on the currently known physical models for the description of hydrodynamic lubrication conditions. Furthermore, the test results have been employed for comparison in the course of various research projects for the investigation of hydrodynamic radial and axial bearings [11-13]. Among other results, measurements performed on an offset-halves bearing were considered; in this case, the temperature distribution and rotor displacement had been determined under vertically imposed static load. In **FIGURE 2**, the measured and calculated temperature increase at the measuring points of the offset-halves bearing is plotted as a function of the load and rotational speed at a constant inlet temperature.

As can be seen from the figure, the measured and calculated values agree very well. Further investigations on the static characteristics of various journal and thrust bearings yielded equally good agreement between the measured and calculated results.

As the circumferential velocity increases, a transition from predominantly laminar flow to increasingly turbulent flow is observed. In this range, the conditions for convective heat transport through the lubricant change, and the dissipation of frictional heat improves. In the example shown in **FIGURE 3**, this transition becomes evident around n = 14,000 rpm.

In this example, the smaller initial gradient of the maximal bearing temperature is compensated by an increase in the frictional power dissipation as the circumferential velocity continues to increase. A comparison of results between measurement and calculation indicates good agreement. Consequently, the models employed for calculation with due consideration of lubricant-film turbulence are assumed to simulate the bearing conditions during operation with sufficient accuracy, even at very high circumferential velocity of the turbine bearings.

For determining the dynamic characteristics of thrust bearings, a measuring technique based on the method described in [1] has been developed and applied for the first time; for this purpose, a sinusoidal excitation has been superimposed on the static load.

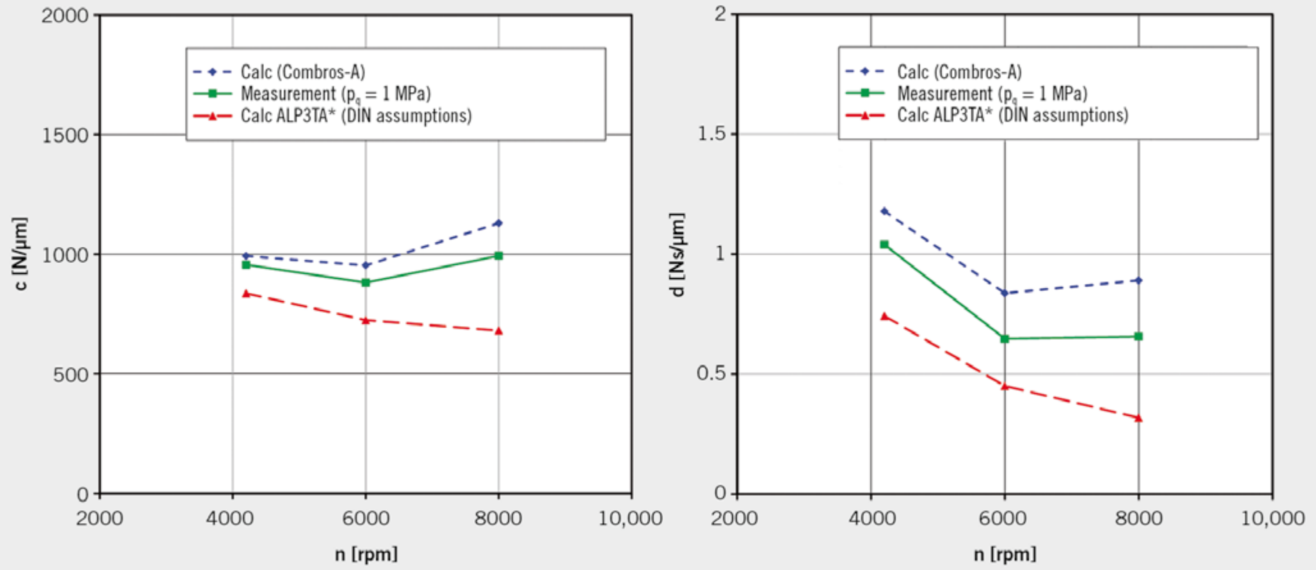

FIGURE 4 Comparison of the measured and calculated axial stiffness values c and damping d, as functions of the rotational speed; p_q = 1 MPa (© TU Clausthal)

The test results were initially evaluated with the use of dynamic characteristics, which had been determined with the application of the programme ALP3TA for axial-bearing calculations, with the application of a simplified computational model for rectangular segments. For further comparisons, calculations were performed with the Combros-A software, by means of which the geometrical shape of the annular- sector segments of the test bearing is considered more exactly in polar coordinates. Moreover, the properties of the non-isoviscous lubricant as well as the effect of the centrifugal force are considered in the calculation of the pressure variation. Furthermore, the local flow conditions within the lubricant gap and the fractional film content are employed as input parameters for the determination of dynamic coefficients. In addition, the segment deformation which occurs in the static operating point during real operation is taken into account as an approximation with the application of bending-beam theory. In **FIGURE 4**, the predictions obtained with the computational models are compared; for this purpose, the effect of elasticity in the segment support was also considered in the calculation.

As can be seen from the figure, the more detailed modelling of the geometrical shape of the segments and fluid film properties affects the prediction significantly. The dynamic axial-bearing tests therefore already yielded good overall agreement between the experimental results and the predictions from the calculations. It is expected that the consideration of ancillary effects, as for example lubricant supply conditions in the inlet zone between the segments, will lead to further enhanced predictions of the bearing properties.

As a result of changes in international standards and series of technical rules, the importance of identifying dynamic coefficients is expected to increase further in the future. In particular, increased consideration will be given to the calculation of asynchronous (tilting-pad bearing) coefficients with the use of extended journal-bearing models. For certain types of bearing geometry, as well as specific segment-suspension conditions and segment motion, the dynamic bearing properties may exhibit significant sensitivity toward the excitation frequency f_E, as considered in international publications, for instance [14], [15].

For further verification of the existing dynamic testing system at high excitation frequencies, therefore, representative reference bearings have been investigated experimentally. For this purpose, the dynamic characteristics of the test and support bearings employed have been assumed to be independent of the excitation frequency. In this case, a fixed-geometry journal bearing (offset-halves bearing) and an adequately profiled offset-pivot radial tilting-pad bearing with four segments have been employed as test bearings.

With the method of identification applied here, sinusoidal excitation forces (single frequency) are imposed on the bearings in the x and y direction, respectively, and the amplitude and phase angle of the test-component displacements are determined by performing two measurements with the use of displacement sensors. The evaluation of the relative motion between the rotor and test bearing as well as the absolute motion of the bearing in the inertial system of the test rig in the time or frequency domain then yields the dynamic coefficients. The bearing reaction forces are modelled by Eq. 1:

Eq. 1

$$\begin{pmatrix} F_x \\ F_y \end{pmatrix} = \begin{pmatrix} C_{11} & C_{12} \\ C_{21} & C_{22} \end{pmatrix} \times \begin{pmatrix} x \\ y \end{pmatrix} + \begin{pmatrix} D_{11} & D_{12} \\ D_{21} & D_{22} \end{pmatrix} \times \begin{pmatrix} \dot{x} \\ \dot{y} \end{pmatrix}$$

Where x and y are relative displacement components of the bearing with respect to the rotor, F_x and F_y are components of the bearing reaction force, C_{ik} and D_{ik} are stiffness and damping coefficients of the bearing. The dynamic coefficients are extracted from the bearing housing equations of motion and Eq. 1. Particularly the characteristics of the cross-coupled stiffness coefficients can cause rotor

instability. In **FIGURE 5** and **FIGURE 6**, measured and calculated dynamic characteristics are compared for the test bearings.

Especially in the case of the fixed-geometry journal bearing, the agreement between the identified and calculated stiffness values is excellent. The detected deviation from the predicted direct stiffness values of the tilting-pad bearing is the subject of further investigations. To a certain extent, the predicted damping coefficients are overestimated somewhat. On the whole, the identified dynamic coefficients for the reference bearings are thus largely independent of the excitation frequency in the frequency range under investigation, as expected, with due consideration of the scatter among the measured values and the sensitivity of the displacement sensors. The experimentally determined decrease in the direct damping coefficients of the tilting-pad bearing in the range of an excitation frequency f_E of about 125 Hz can be explained by deviations in the phase angle of the excitation forces. These deviations are caused by the system which is currently employed for controlling the hydraulic actuators on the test rig.

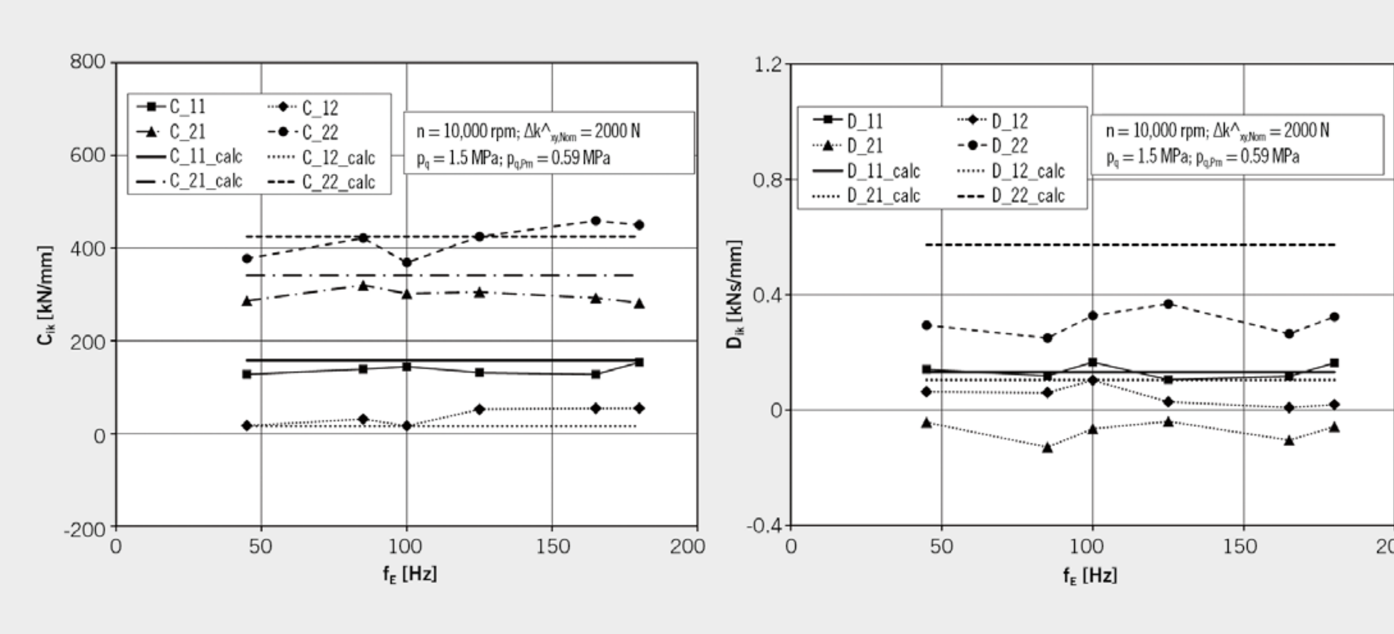

FIGURE 5 Stiffness and damping coefficients of an offset-halves bearing (comparison between measurement and calculation); frequency series at f_W = 166.7 Hz, $p_{q,\ nom}$ = 1.5 MPa (© TU Clausthal)

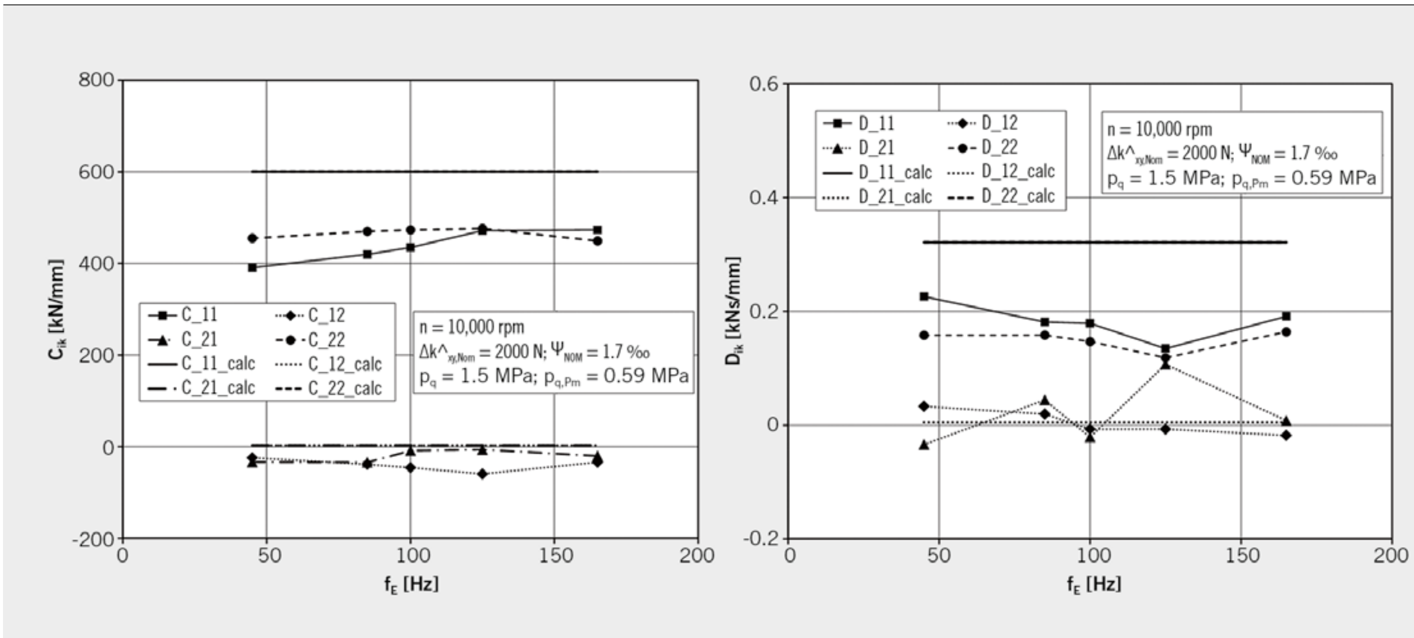

FIGURE 6 Stiffness and damping coefficients of a radial tilting-pad bearing (comparison between measurement and calculation); frequency series at f_W = 166.7 Hz, $p_{q,nom}$ = 1.5 MPa (© TU Clausthal)

Further research projects are planned for the investigation of bearing properties which depend on the excitation frequency; this work will include steps for optimising the system in the future.

5 SUMMARY

The continuing trend in the development of operationally reliable and nearly maintenance-free turbomachinery with optimised efficiency demands technical innovations and constant progress in designing, dimensioning, development, construction, and application of fluid-film bearings. With the high-performance bearing test rig as an exclusive and unique feature of the joint research effort, a highly efficient testing system can be placed at the disposal of the industry. In an international environment with numerous contenders, this development can offer special benefits to small- and medium-sized enterprises. Moreover, the predictions resulting from the use of computational software for designing hydrodynamic bearing systems are expected to receive increased international acceptance.

REFERENCES

[1] Glienicke, J.: Feder- und Dämpfungskonstanten von Gleitlagern für Turbomaschinen und deren Einfluss auf das Schwingungsverhalten eines einfachen Rotors. Dissertation, TH Karlsruhe, 1966

[2] Glienicke, J.; Han, D.-C.; Leonhard, M.: Practical Determination and Use of Bearing Dynamic Coefficients. Tribology International, Dec. 1980, pp. 297-309

[3] Rückert, A.: Experimentelle Überprüfung der Berechnungsgrundlagen für die Radialgleitlager von Turbomaschinen. Fortschr.-Ber. VDI, Reihe 1 Nr. 214, Düsseldorf, VDI-Verlag, 1992

[4] Schüler, D.: Berechnung der Feder- und Dämpfungszahlen von Mehrflächengleitlagern und das Schwingungsverhalten eines einfachen Rotors unter Berücksichtigung des Schmiermittelzuführdrucks. Dissertation, Ruhr-Universität Bochum, 1975

[5] Elrod, H. G., A Cavitation Algorithm. Trans. ASME, J. of Lubr. Tech., Vol. 103, 1981, No. 3, pp. 350-354

[6] Jakobsson, B.; Floberg, L.: The Finite Journal Bearing, Considering Vaporization. Trans. Chalmers Univ. Tech. Gothenburg, Göteborg, 1957

[7] Hopf, G.: Experimentelle Untersuchungen an großen Radialgleitlagern für Turbomaschinen. Dissertation, Ruhr-Universität Bochum, 1989

[8] Mittwollen, N.; Schmitz, A.; Rückert, A.; Reinhardt, W. D.: Verbesserung der Berechnungsgrundlagen für schnelllaufende, hochbelastete Mehrgleitflächen- und Radialkippsegmentlager. Abschlussbericht des BMFT-Verbundprojekts 03T0012A, Braunschweig, 1991

[9] Odermatt, R.: Stationär belastete Radial-Gleitlagersegmente mit und ohne Randleisten. Mitt. aus d. Inst. f. Grundl. d. Masch. Konstr. Nr. 11, ETH Zürich (Verlag), 1981

[10] Blumenthal, H.; Schwarze, H.: Hochleistungs-Gleitlagerprüfstand. Aufbau eines Hochleistungs-Gleitlagerprüfstandes zur Ermittlung von tribologischen Kenngrößen bei hohen Lasten und höchsten Umfangsgeschwindigkeiten. FVV-Berichte, Heft Nr. 1033, FVV Frankfurt/M., 2013

[11] Kraft, C.; Schwarze, H.: Verbesserte Axialgleitlagerberechnung. Hochbelastete, schnelllaufende Axialgleitlager in einfacher und doppeltwirkender Anordnung unter Berücksichtigung statischer Spurscheibenverkantung. FVV-Berichte, Heft Nr. 1019, FVV Frankfurt/M., 2013

[12] Friedrich, S.; Blumenthal, H.; Esderts, A.; Schwarze, H.: Gleitlager-Lebensdauer. Lebensdauerkriterien innovativer Werkstoffe für hochtourige und hochbelastete Gleitlager. FVA-Berichte, Heft Nr. 1010, FVA Frankfurt/M., 2012

[13] Hagemann, T.; Schwarze, H.: Verbesserte Radialgleitlagerberechnung. Stationär und instationär hoch belastete Radialgleitlager für schnell laufende Rotoren bei Berücksichtigung der Lagerdeformationen. FVA-Berichte, Heft Nr. 996, FVA Frankfurt/M., 2011

[14] Carter, C. R.; Childs, D.: Measurements Versus Predictions for the Rotordynamic Characteristics of a Five-Pad Rocker-Pivot Tilting-Pad Bearing in Load-Between-Pad Configuration, Journal of Engineering for Gas Turbines and Power, Vol. 131, Article ID 012507, 2009

[15] Al-Ghasem, A. M.; Childs, D.: Rotordynamic Coefficients Measurements versus Predictions of a High-Speed Flexure-Pivot Tilting-Pad Bearing (Load-Between-Pad Configuration), Journal of Engineering for Gas Turbines and Power, Vol. 128, No. 4, pp. 896-906, 2006

THANKS

The results presented here constitute a part of the joint research project, High-Performance Bearing Test Rig (FVV-No. 924, FVA-No. 531 I). The authors wish to thank the Research Association for Combustion Engines e.V. (FVV, Frankfurt) and the Power Transmission Engineering Research Association e.V. (FVA, Frankfurt) for co-financing of the project. These research associations in turn wish to express their thanks to the participating industrial partners for financial promotion of the project.

AUTHORS

Dr.-Ing. Helge Dageförde
is Development Engineer in System Development for Gasoline Combustion Process at the Robert Bosch GmbH in Schwieberdingen (Germany).

Dipl.-Ing. Markus Bertsch
is Research Assistant at the Institute of Internal Combustion Engines at the Karlsruhe Institute of Technology (KIT) (Germany).

Dr.-Ing. Heiko Kubach
is Head of Combustion Process Research at the Institute of Internal Combustion Engines at the Karlsruhe Institute of Technology (KIT) (Germany).

Prof. Dr. sc. techn. Thomas Koch
is Head of the Institute of Internal Combustion Engines at the Karlsruhe Institute of Technology (KIT) (Germany).

Reduction in Particle Emissions with Gasoline Engines with Direct Injection

Within a FVV research at the Institute of Internal Combustion Engines (IFKM) at the KIT, investigations were carried out on a rapid compression machine and single cylinder engine, in order to identify the cause of particle emissions and the influencing parameters. Both test carriers were equipped with a gasoline direct injection with central injector position. Through the combination of comprehensive optical, thermodynamic and exhaust gas analysis measuring equipment and numerous applicative degrees of freedom on the test carriers, it was possible to examine individual engine-internal influential variables on an isolated basis and consider these in relation to the measured particle emissions.

THE SEAL OF APPROVAL FOR SCIENTIFIC ARTICLES IN MTZ.
MTZ
PEER REVIEW
RECEIVED 2015-02-10
REVIEWED 2015-02-20
ACCEPTED 2015-06-08
REVIEWED BY EXPERTS FROM RESEARCH AND INDUSTRY.

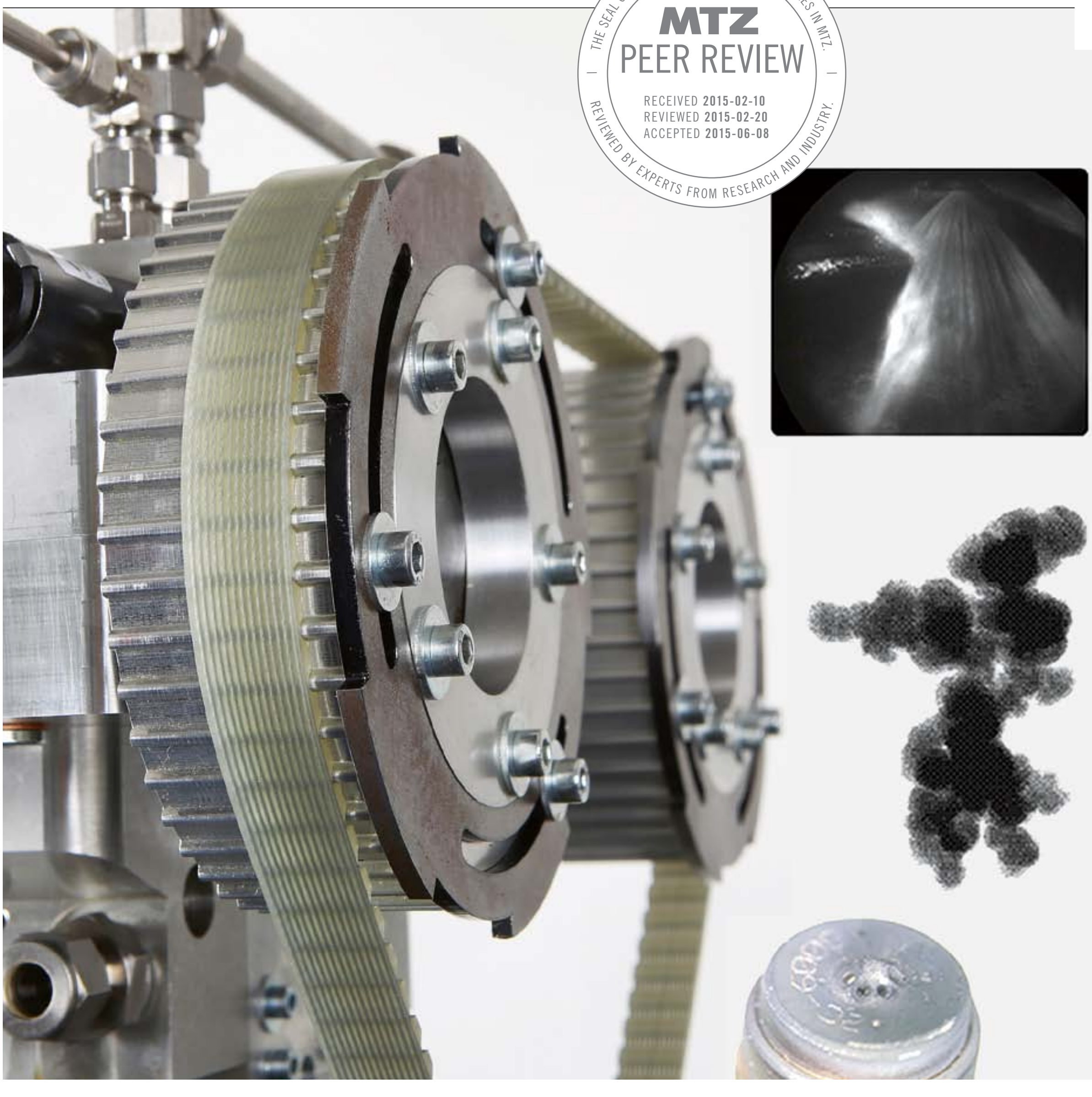

1 MOTIVATION
2 TEST CARRIERS
3 PARTICLE MEASURING EQUIPMENT
4 RESULTS
5 SUMMARY AND OUTLOOK

1 MOTIVATION

Reducing harmful emissions and enhancing efficiency are the primary targets of engine development. The gasoline engine with direct injection and exhaust gas turbocharging has established itself as a key technology in recent years. However, internal mixture formation is accompanied by an increase in the emission of particles, which are largely classified as harmful to health.

The aim of the research project was therefore to identify the engine-internal causes of particle emissions in gasoline engines with direct injection for automotive application, and to investigate the extent to which these can be reduced through engine-internal measures. To this end it was necessary to establish a comprehensive understanding of the engine-related influential factors pertinent to particle generation, oxidation, characteristics and emission. For this purpose, optical measuring methods were used to analyse the mixture formation and combustion, measure the particle concentration and size distribution, and examine the emitted soot with the aid of electron microscopy with respect to morphology and chemical composition.

2 TEST CARRIERS

The engine tests were conducted on a single-cylinder engine with central injection position. The fundamental engine data is summarised in **TABLE 1**. For optical investigations in the combustion chamber, two accesses were used for light source and camera, and equipped with endoscopes with an 8 mm outer diameter and 70° opening angle. The set-up is shown in **FIGURE 1** (left). **FIGURE 1** (right) shows the observation space in the combustion chamber accessible with this configuration.

3 PARTICLE MEASURING EQUIPMENT

An AVL 489 Particle Counter Advanced (APC, certified according to PMP specifications) was used in order to determine the particle concentration in the exhaust gas, and partly also a TSI 3090 Engine Exhaust Particle Sizer (EEPS). The systems were mutually operated on the sampling system of the AVL measuring system here, **FIGURE 2**. In order to keep the particle concentration in the diluted exhaust gas behind the Volatile Particle Remover (VPR) within a range suitable for the downstream measuring systems, dilution took place by a factor of 100 to 2000.

4 RESULTS

The following section presents the results of the three-year project in abridged form. The experimental investigations were conducted at three NEFZ-relevant operating points:
- 50 km/h constant travel: 2 bar indicated mean effective pressure, 2000 rpm engine speed
- end point of acceleration at 120 km/h: 8 bar indicated mean effective pressure, 2000 rpm engine speed
- catalyst heating operation: 1.8 bar indicated mean effective pressure, 1200 rpm, 50 % mass fraction burnt ≥ 75 °CA a. TDC, the operating point is additionally described by the respective exhaust gas enthalpy flow in kW/l displacement volume.

The expelled particle emissions are the fundamental result of a multitude of mutually interactive influencing variables, which have an effect on the one hand on the formation and on the other hand

Engine type	Single cylinder, direct injection (central injector), water cooled, four-valve
Working process	Otto four-stroke
Mixture	Homogeneous
Compression ratio [-]	12:1
Stroke [mm]	90
Bore [mm]	84
Displacement [cm³]	498
Valvetrain	Cam phaser (intake and exhaust) variable intake valve lift
Layout of injector and spark plug position	Longitudinal arrangement (parallel to crank shaft), central injector

TABLE 1 Engine data (© IFKM)

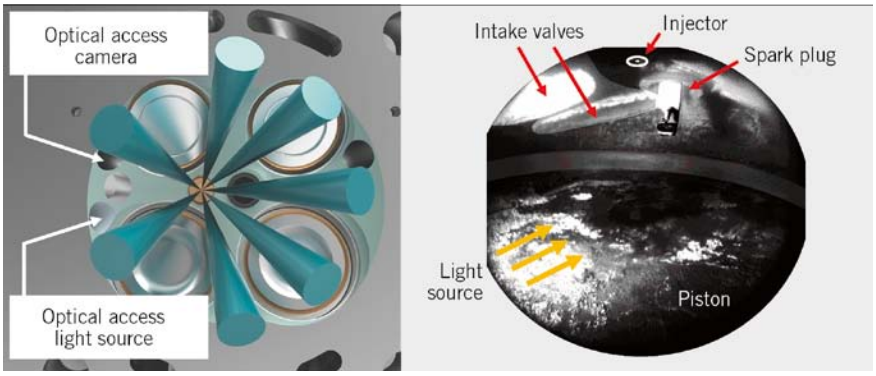

FIGURE 1 Set-up of the optical accesses (left) and observation space (high speed) visualisation of single-cylinder engine (right) (© IFKM)

on the oxidation. The following section discusses a number of parameters that influence the formation. Because the particles themselves largely consist of carbon, the fuel system, that is to say the injector nozzle geometry and the injection pressure, as well as the injection strategy and the resulting air-fuel ratio, play a decisive role. More detailed investigations into the fuel influence itself were presented at the 2013 SAE Conference in Seoul [1].

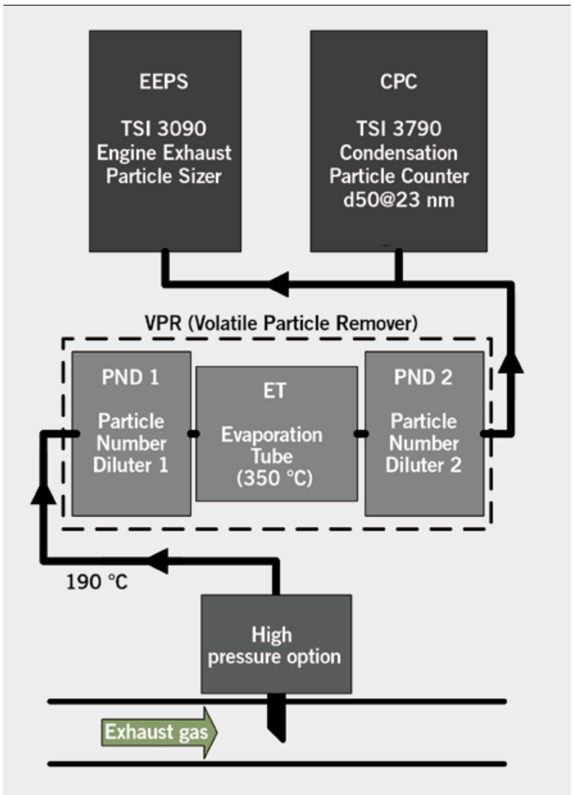

FIGURE 2 Particle measuring system set-up with mutual sampling and dilution system (© IFKM)

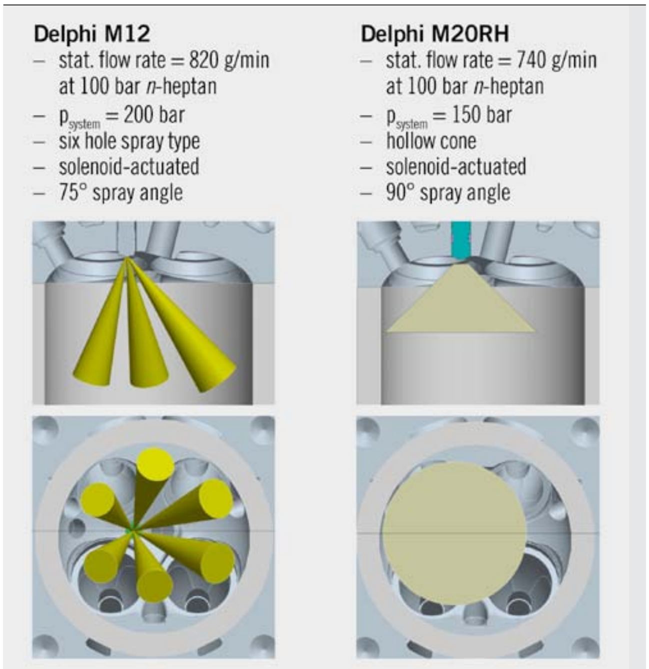

FIGURE 3 Injector overview (© IFKM)

4.1 NOZZLE TYPE

In order to analyse the influence of the fuel injection on the occurrence of particle emissions, multiple injectors were provided for the research project, which differ in terms of throughput, nozzle geometry, spray angle and actuation, **FIGURE 3**. During the first half of the project, comprehensive parameter variations were implemented with all injection valves [2]. In the second half of the project, two injectors were selected on the basis of the results: A multi-hole nozzle with suitable spray targeting (Delphi M12 injector) and an outwardly opening nozzle (Delphi M20 injector). The wide spray of the outwardly opening nozzle results in an exposed jet length of just 45 mm right to the cylinder wall. With an exposed jet length of 81 mm, the spray from the multi-hole nozzle offers considerably more favourable conditions with respect to the spray-wall interaction. During operation with the outwardly opening nozzle and individual injection quantities of over 25 mg in the intake stroke, it was no longer possible to avoid coating the inlet valve. In addition to fuel deposits, an increased proportion of oil in the exhaust gas was also observed due to flushing effects. With the multi-hole nozzle it was possible to avoid part interaction through the suitable selection of the injection start.

In order to investigate the effects of the spray characteristics (individual jets versus hollow cone) and the opening angle (multi-hole nozzle: 75° versus outwardly opening nozzle: 90°) on the particle emissions, long main injection (> 25 mg) was used in the catalyst heating operation in the intake stroke on the one hand, whilst short injection was applied in the ballistic operating range (≈ 0.3 mg) shortly before the ignition time point on the other.

During catalyst heating operation, the provision of a large exhaust gas enthalpy flow is of primary importance. The engine is driven almost de-throttled, with very late mfb50. Severe cyclical fluctuations arise due to the late combustion position with low turbulence level. With near-ignition small-quantity injection, enrichment and an increase in the turbulence level may be attained at the spark plug, and thereby also a stabilising of the combustion. In this way the engine can be operated with a globally light, lean mixture for the avoidance of excessively high HC emissions. However, considerable particle emissions can arise due to the rich mixture at the spark plug or any fuel that has not been fully vaporised.

FIGURE 4 shows the spray spread of the small-quantity injection in the ballistic operating range for both injectors. It is clear that the fuel preparation with the outwardly opening nozzle is significantly superior to that of the multi-hole nozzle. As such, no individual droplets are apparent with the outwardly opening nozzle and faster fuel preparation is also observed. In contrast, with the multi-hole valve – in particular in the area around the spark plug – individual droplets can be seen, which arise in particular towards the end of injection, that is to say when the injector needle is closed. The cause of this can be found in the better spray disintegration of the hollow cone spray, in comparison to the multi-hole nozzle. Whilst the fuel with the hollow cone spray is distributed evenly over the ring gap and even the smallest injection quantities are injected in the ballistic operating range at nominal pressure (150 bar), with the multi-hole nozzle the injection pressure does not yet reflect the rail pressure during the valve opening process due to the internal throttling points (needle, spray holes). Due to

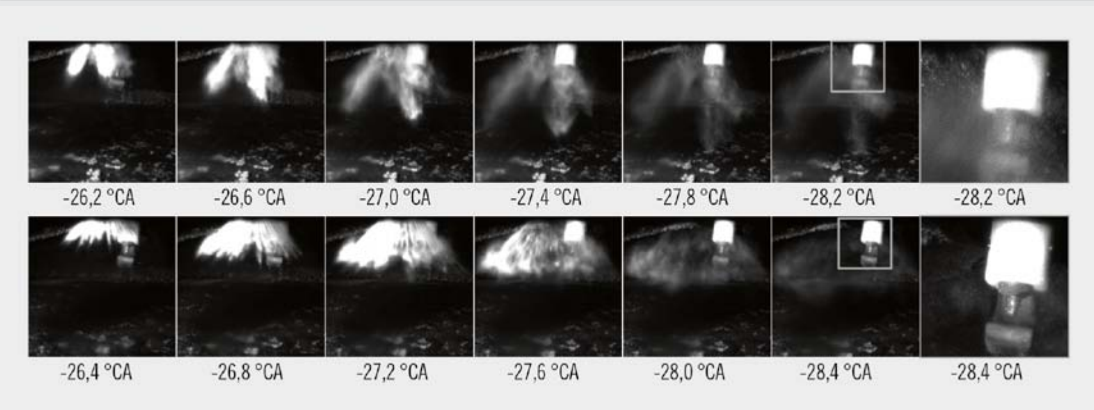

FIGURE 4 Spray spread of small-quantity injection (≈ 0.3 mg) (top: Multi-hole nozzle (M12); bottom: outwardly opening nozzle (M20)) (© IFKM)

the incomplete opening in ballistic operation, the valve is already closed again before the nominal pressure is present in the injection holes. The likelihood of fuel residues in the spray holes and so-called dripping effects is therefore also increased by the lower spray pulse. All of these effects, in combination with the very short time between injection and ignition, lead to a poorer preparation of thenear-ignition injection of the multi-hole nozzle in comparison to theoutwardly opening nozzle (multi-hole nozzle greater than 1.5 × 10^6 p/cm³; outwardly opening nozzle less than 0.5 × 10^6 p/cm³).

4.2 INJECTION STRATEGY AND AIR-FUEL RATIO

The correct timing and spatial placement of the near-ignition injection is of great significance for the aforementioned reasons, both in achieving minimal combustion fluctuations as well as low particle emissions. In order to examine this more closely, the LaVision ICOS fuel (SP for optical determination of the fuel concentration in the area of the electrodes) was used to examine the effect of near-ignition injection on the fuel concentration close to the ignition gap and this was discussed in the context of particle emissions and combustion fluctuations. For this purpose the engine was operated with global lambda of 1.05, a specific exhaust gas enthalpy flow of 6 KW/l, two injections in the intake stroke, a third shortly before the ignition time point, and a multi-hole nozzle (M12) and an outwardly opening nozzle (M20) in alternation. The influence of the timed placement of the near-ignition injection can be seen in **FIGURE 5**. The top two diagrams in **FIGURE 5** show the measured values with the multi-hole nozzle, the two bottom figures show the outwardly opening nozzle values. The left column shows the λ-course for the various injection time points of the third injection (SOI 3) around the ignition time point (IGN). The right column shows the associated values of the particle emissions

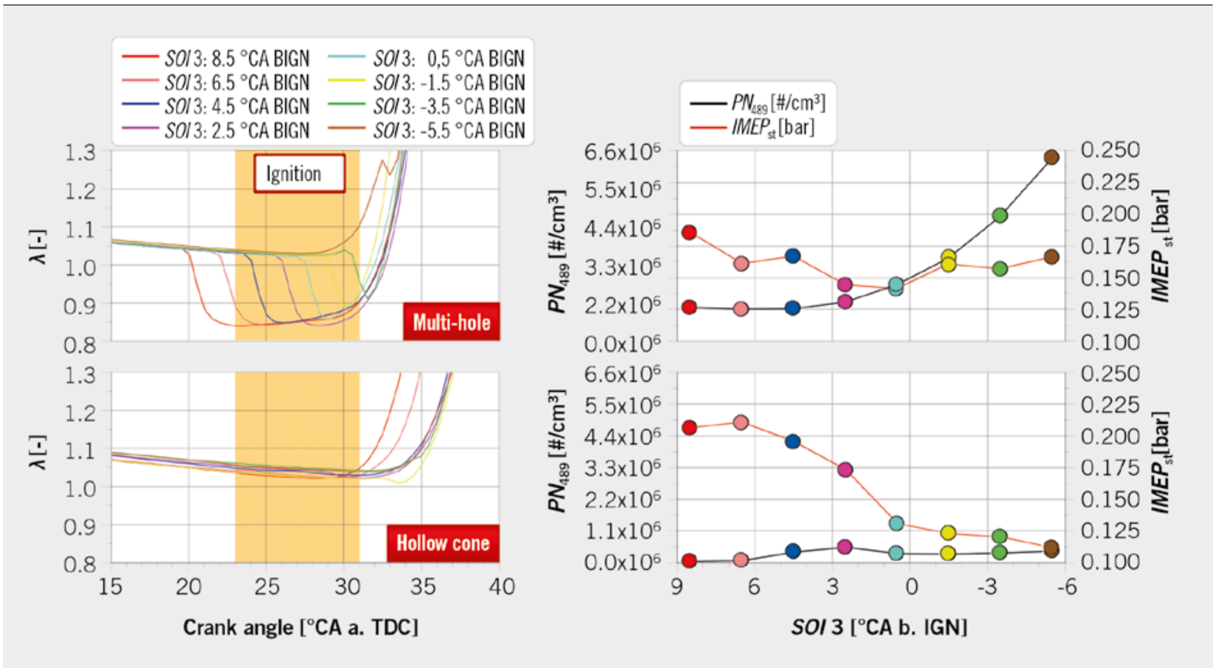

FIGURE 5 Influence of the near-ignition third injection (λ = air ratio at the spark plug, SOI 3 = start of the 3rd injection, vZZP = before ignition, PN489 = particle number measured with AVL Particle Counter 489, Pmi, st = standard deviation of the indicated mean effective pressure) (© IFKM)

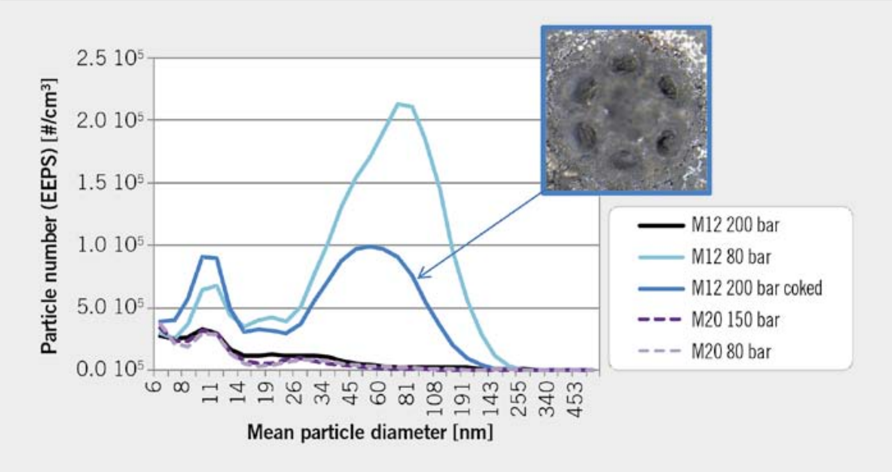

FIGURE 6 Influence of the injection pressure and injector state on the particle size (© IFKM)

(black line) and combustion fluctuation (grey line). Both injectors were operated with the third injection with the minimum actuation period of 0.22 ms. The resultant near-ignition injected quantities were approximate 0.3 mg (1.3 % of total fuel mass) with the multi-hole nozzle and approximate 0.9 mg (3.9 % of total fuel mass) with the outwardly opening nozzle. With the multi-hole nozzle, significant enrichment is observed at the spark plug across the entire variation range, which only decreases with injection after the ignition time point. In equal measure, low combustion fluctuations (IMEPst) can be observed, which constantly lie below the value without near-ignition injection (0.2 bar). On the other side, the particle emissions are at a higher level and increase constantly with a reduction in the period of time between injection and ignition. The measurements with the outwardly opening nozzle exhibit distinctly different behaviour. Irrespective of the SOI 3, almost no enrichment is apparent at the ignition gap, equally the particle emissions lie at a consistently lower level in comparison to the multi-hole nozzle, even if this is above the operating strategy without near-ignition injection. Unlike operation with the multi-hole nozzle, the combustion fluctuations initially increase with an SOI 3 > 0.5 °KW before IGN in comparison to operation without near-ignition injection, although these assume very low values across the remaining range. The comparison of the λ-measurement between both injectors clearly shows the considerably better mix-

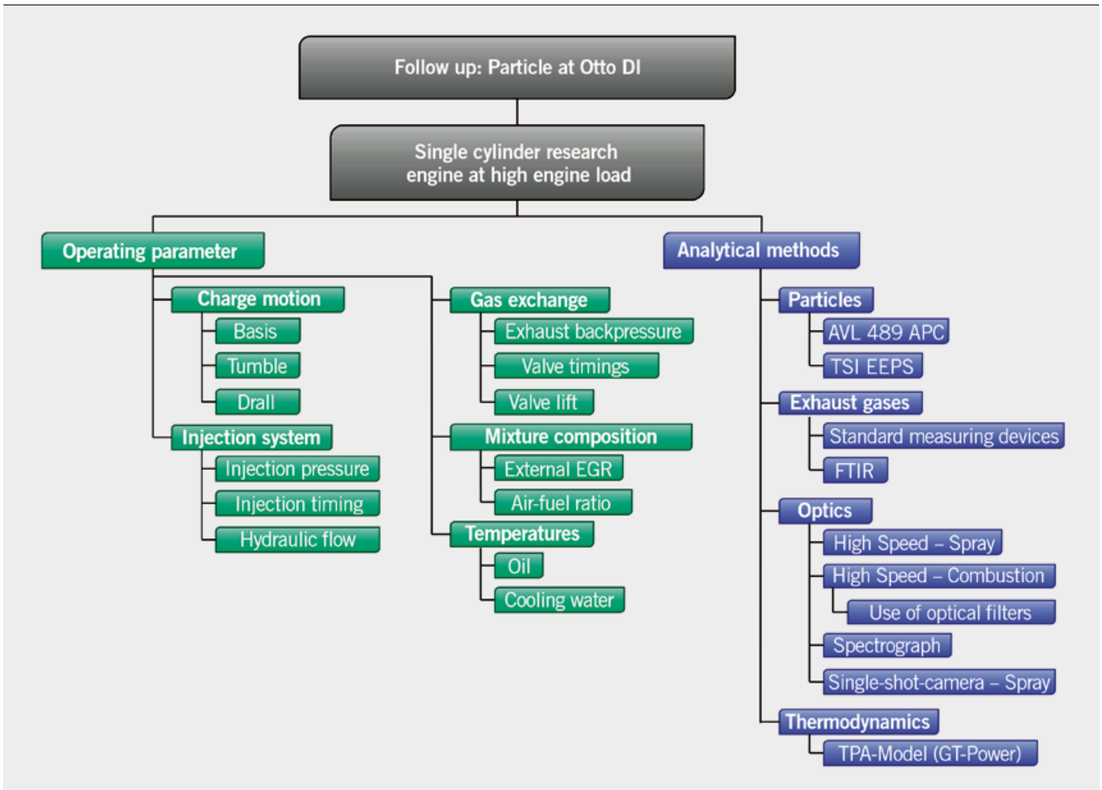

FIGURE 7 Main topics of the follow-up project (© IFKM)

ture preparation of the outwardly opening nozzle, in particular in the ballistic range. Whilst the full injection pressure is not yet present with the multi-hole nozzle due to throttling losses in the injector and the spray spread and jet disintegration are therefore negatively influenced and result in larger fuel droplets with a comparatively low pulse. With the outwardly opening nozzle the full injection pressure is also available in the ballistic operating range, so that even the smallest quantities are distributed with a high pulse and unlimited spray disintegration.

This injector-related characteristic explains the course of the λ-measurement in **FIGURE 5**. The correlation with the particle emissions and quiet running shows that localised enrichment at the ignition time point stabilises combustion, but also leads or can lead to increased particle emissions, in particular with a reduction in time between SOI 3 and the ignition time point. However, in order to definitively establish stabilisation without a significant increase in the particle emissions, it is necessary to avoid extensive enrichment in the area well below $\lambda = 1$ and achieve stabilisation insofar as possible exclusively through the turbulence generated with injection. For this purpose, a precise spatial and time-based positioning of the near-ignition injection is necessary, as well as the use of a mixture controller that is also able to inject small quantities with a high pulse.

4.3 INJECTION PRESSURE

The fundamentally positive influence of an increased injection pressure on the mixture formation and the reduction in particle emissions has already been discussed in numerous publications [2, 3]. However, it is also apparent that a reduction in the injection pressure to 80 bar with operation with an outwardly opening nozzle through alignment of the injection strategy must not necessarily lead to a noteworthy increase in particle emissions. For example, it has been possible to show a particle emission level of less than 1.0×10^5 particles/cm³, at an operating point with 8 bar indicated mean effective pressure, 2000 rpm engine speed and the outwardly opening nozzle. With the multi-hole nozzle it was not possible to reduce the particle concentration below 1.5×10^6 particles/cm³ with this injection pressure. However, this was not due exclusively to the poorer mixture preparation resulting from the lower injection pressure. Instead, the weaker injection pulse led to an incomplete vaporisation of the residual liquid fuel at the injector tip and therefore also to carbonisation, which is not fully removed with a renewed raising of the injection pressure to 200 bar. In this way, the particle emissions at 200 bar injection pressure increased tenfold from around 7.1×10^4 particles/cm³, due to the deposits forming at the injector tip. **FIGURE 6** shows the particle size distribution at the specified operating point for both injectors. The black line shows the reference measurement, the light blue line represents operation at 80 bar injection pressure optimised through applicative measures, and the dark blue line with the M12 multi-hole injector plots the course at 200 bar injection pressure and a carbonised injector tip due to previous operation at 80 bar injection pressure. The measurement of the size distribution also clearly shows that a reduction in the injection pressure is accompanied by an increase in the mean particle diameter in agglomeration mode. From this, it is possible to deduce that the reduction in the injection pressure results in a disproportionate increase in the emitted particle mass in comparison to the number of particles. This was also observed in other investigations [4].

5 SUMMARY AND OUTLOOK

Within the framework of the FVV research project, a combination of engine-internal investigation methods and measuring equipment for determining the number and size distribution of particles in the exhaust gas was used to examine the influence of various engine and operating parameters on particle formation, oxidation and morphology.

In the associated second part, which has been in progress since August 2013, the investigation scope was expanded to include higher loads (maximum 14 bar IMEP). In particular in turbocharged operation, the preparation of large injected fuel quantities poses a challenge for low-particle operation. Various charge movements and an increase in the injection pressure are under investigation as variation parameters for the improvement of the mixture formation. The exhaust gas counter-pressure can be adjusted on the single cylinder engine irrespective of the charge pressure. With this degree of freedom and the variable valve control times it is possible to set various thermodynamic framework conditions. Furthermore, it is also possible to influence the calorifics via an additional external EGR. **FIGURE 7** shows the various variation parameters, as well as the measuring equipment used in order to assess the particle formation and oxidation. In addition to conventional exhaust gas analyses and the previously applied optical and particle measuring equipment, an FTIR is also used to analyse the gaseous emissions.

The findings of this project generate a more detailed understanding of the influencing parameters, the interaction and mechanisms of particulate formation in gasoline engines. With this know-how the particle emissions of future engines can be reduced by means of selective optimisation of components and engine operating parameters.

REFERENCES

[1] Dageförde, H.; Koch, T.; Beck, K.; Spicher, U.: Influence of Fuel Composition on Exhaust Emissions of a DISI Engine during Catalyst Heating Operation. In: SAE Technical Paper 2013-01-2571, 2013

[2] Dageförde, H.; Kubach, H.; Spicher, U.: Untersuchung von Maßnahmen zur Reduktion der Partikel-Anzahlemissionen bei Otto-DI-Motoren. [Investigation into measures for a reduction in the particle emissions with gasoline DI engines. In: Interim report on project no. 1046, FVV issue R558, 2012

[3] Schumann, F.; Kubach, H.; Spicher, U.: The Influence of Injection Pressures of up to 800 bar on Catalyst Heating Operation in Gasoline Direct Injection Engines. In: COMODIA Proceedings (2012), pp. 305-310

[4] Matousek, T.; Dageförde, H.; Bertsch, M.: Influence of Injection Pressures up to 300 bar on Particle Emissions in a GDI-Engine. In: Proceedings of 17th ETH-Conference on Combustion Generated Nanoparticles, Zurich, 2013

THANKS

The results were obtained within the framework of the research project no. 1046 Investigation into measures for a reduction in the particle emissions with gasoline DI engines which was funded by the FVV. The authors wish to thank the FVV, the working committee and the chairmen Dr. Herwig Richter and Dr. Daniel Sabathil for their support.